COMPARING MEASURED AND THEORETICAL TARGET REGISTRATION ERROR OF AN OPTICAL TRACKING SYSTEM

NILOOFAR BANIVAHEB

A THESIS SUBMITTED TO THE FACULTY OF GRADUATE STUDIES
IN PARTIAL FULFILLMENT OF THE REQUIREMENTS FOR THE DEGREE OF
MASTER OF SCIENCE

GRADUATE PROGRAMME IN COMPUTER SCIENCE AND ENGINEERING
YORK UNIVERSITY
TORONTO, ONTARIO

FEBRUARY 2015

ABSTRACT

The goal of this thesis is to experimentally measure the accuracy of an optical tracking system used in commercial surgical navigation systems. We measure accuracy by constructing a mechanism that allows a tracked target to move with spherical motion (i.e., there exists a single point on the mechanism—the center of the sphere—that does not change position when the tracked target is moved). We imagine that the center of the sphere is the tip of a surgical tool rigidly attached to the tracked target. The location of the tool tip cannot be measured directly by the tracking system (because it is impossible to attach a tracking marker to the tool tip) and must be calculated using the measured location and orientation of the tracking target. Any measurement error in the tracking system will cause the calculated position of the tool tip to change as the target is moved; the spread of the calculated tool tip positions is a measurement of tracking error called the target registration error (TRE). The observed TRE will be compared to an analytic model of TRE to assess the predictions of the analytic model.

ACKNOWLEDGEMENTS

I am using this opportunity to express my sincerest gratitude to my supervisor, Dr. Burton Ma, for his knowledge, guidance, and support. I am thankful for his generous funding, invaluably constructive criticism and friendly advice during this research work.

I would like express my warm thanks to my committee members for taking time out of their busy schedules to serve on my thesis examination committee.

Most importantly, I would like to thank my parents and my sister for their love, encouragement, and support.

TABLE OF CONTENTS

LIST OF FIGURES

LIST OF APPENDIX FIGURES

LIST OF EQUATIONS

Chapter 1
Introduction

Image-guided surgery is a type of surgery where surgeons employ tracked surgical instruments and preoperative or intraoperative medical images to obtain navigational information. Contemporary image-guided surgical systems consist of a tracking system linked to a computer workstation. The tracking system is capable of real-time measurement of the position and orientation, or pose, of specially instrumented surgical tools. The pose of the tracked tools is used to compute and display navigational information to the surgeon using the computer workstation. An image-guided surgical system for knee replacement surgery is shown in Figure 1-1. In the figure, the surgeon is using a surgical drill to which is attached a tracking target. A second target, not visible in the figure, is rigidly attached to the femur of the patient. The tracking system cameras, just visible in the upper-right corner of the figure, measure in real time the pose of the drill and the patient's femur. By computing the relative pose of the drill and femur, navigational information can be shown to the surgeon on a computer monitor. In this case, the axis of the drill bit relative to the femur is being shown to the surgeon. For this particular knee replacement procedure, the axis of the drill bit determines the final orientation of the implanted prosthesis, and the placement of the prosthesis is one of the main factors that determine the outcome of the procedure.

Figure 1-1: A contemporary image-guided surgical navigation system. A surgeon holds a surgical drill that is tracked by an optical tracking system (just visible in the upper right corner). The monitor displays real-time navigational information (in this case, the axis of the drill relative to the femur of the patient).

1.1 Early Forms of Image-guided Surgery

It was originally introduced for assistance in brain surgery and brain tumor treatment; however, it has since been used in most other surgical specialties. Early concepts of image-guided surgery dates back to 1908 when Horsley and Clark (Horsley & Clarke, 1908) invented a device that uses a set of three coordinates (*x*, *y* and *z*) in an orthogonal

frame of reference affixed to a subject's head (a monkey in their experiment) and allowed electrodes to be directed to a specific location into the skull within a Cartesian space defined by the frame. Because their device precedes the invention of tomographic imaging, they could not acquire an image of a specific patient's brain. Therefore, they relied on the assumption that one's brain is the same as another in order to locate a certain structure within the patient's head.

The invention of the computed tomography (CT) in 1973 (Hounsfield, 1973) enabled researchers to acquire the three-dimensional images of an internal structure of the body. This was a significant invention in the history of image-guided surgery because it allowed the surgeon to see the structure and position of an internal body structure without cutting it open. Consequently, being able to track a surgical instrument within the body and associate it with the acquired medical images could provide surgeons with valuable navigational information during the surgery. In the 1980s, several groups of researchers studied the design of surgical navigation systems (e.g., (Roberts, Strohbehn, Hatch, Murray, & Kettenberger, 1986), (Kosugi, et al., 1988) and (Friets, Strohbehn, Hatch, & Roberts, 1989)) but an articulated arm designed by a group of researchers from Vanderbilt (Galloway, Edwards, Lewis, & Maciumas, 1993) was the first system that has most of the concepts of a modern surgical navigation system. Their system was designed for neurosurgery and had the ability to simultaneously display the position of the surgical instrument attached to the articulated arm on three orthogonal planes. One of the major issues of the Vanderbilt group's system and in general any surgical navigation system

based on articulated arms, is the weight and cumbersomeness of the system. Moreover, the arms could not be accurate and flexible enough at the same time; therefore, it was not convenient to use them for real-world operations. Systems based on articulated arms were not able to track multiple devices at the same time. In addition, it was relatively difficult to sterilize the arm. These restrictions motivated the need for employing free-hand localizers in surgical navigation systems.

1.2 3D Free-Hand Localization

As we discussed earlier, articulated arms were one of the localization methods that was adopted in early image-guided surgery systems. Basically, articulated arms measure the position and orientation of the end of the arm by measuring changes in the arm joint angles and lengths from an initial zero point. But the medical community soon realized that handheld localizers are more practical and convenient to use for image-guided surgery applications. Freehand localizers (i.e., localizers other than articulated arms) were available for decades prior to their use for surgical navigation, but sonic localizers were the first systems that were used in surgery (e.g., (Barnett, Kormos, Steiner, & Weisenberger, 19930) and (Reinhardt, Horstmann, & Gratzl, 1993)). In sonic localizers, an emitter transmits a sound pulse beyond human audible frequency range. The system measures the time taken for the pulse to reaches the receivers, which are placed at known locations in a fixed geometry, and calculates the distances between the receivers and emitters. The location of the emitter can be determined from these distances.

Sonic localizers have some problems that restrict their usage in surgical applications. First, the accuracy of these systems depends on the speed of sound in air. The design of sonic localizers is based on the speed of sound at a standard temperature and pressure in air. However, variations in temperature and humidity can cause variations that are significant enough to cause notable localization errors. Second, sonic systems require noticeable latencies (e.g., about 45 *ms* for a configuration of five non-collinear emitters when receivers are a meter from the patient) between each time that they localize an instrument; but the tracked instrument should not be moved during each frame of localization. These problems motivated researchers to seek a more feasible solution for localization and tracking of instruments during surgery.

1.3 Tracking Systems

In general, different industries use tracking systems for variety of applications. In the field of virtual and augmented reality, tracking systems are used for measuring the user's viewpoint by reporting the pose and orientation of the user's head and interacting with virtual objects by tracking the user's hand (or other parts of the body). Tracking systems are also used for industrial measurements such as measuring the position of tools in variety of industries. Medicine is another field that benefits from tracking systems used mainly for clinical guidance systems.

Localizing and tracking surgical instruments is one of the most important parts of an image-guided intervention process. Therefore, tracking systems are an essential part of an image-guided surgery system. Tracking devices are responsible for tracking the

position of the surgical instruments relative to the patient anatomy. Although articulated arms and sonic localizers were used in early surgical navigation system, the limitation of these systems prompted the field to move toward a more efficient and practical approaches for tracking. Strobe-based 3D tracking was the approach that replaced sonic localizers in image-guided surgery applications.

1.3.1 Optical Tracking Systems

Optical tracking, which is the dominant tracking technology for surgical guidance applications, is based on strobe-based 3D tracking. Optical tracking is the means of determining the real-time position of an object within a tracking volume, by tracking a group of markers attached to the object using the tracking system's cameras. Optical tracking systems proved to be a feasible tracking solution for clinical applications mainly because of their high accuracy and large working volume (i.e., the area in which a tacking object can be tracked).

Applications of optical tracking systems are not limited to clinical systems. In fact, optical tracking systems are used in wide variety of industries that ranges from motion capture to automotive industry. The broad use of optical tracking has led to introduction of variety of optical tracking systems from different manufacturers. These systems are based on variants of optical tracking technologies with different specifications.

Videometric tracking systems are one of the variants of optical tracking systems that track objects by capturing video images and identifying the known marker patterns.

The markers patterns are captured with one or more calibrated video cameras during the calibration process. Videometric tracking systems are mainly used for virtual and augmented reality applications but they are also available in some clinical guidance systems. For instance, MicronTracker manufactured by Claron Technology Inc., Toronto, Ontario, Canada, is a commercially available tracking system that can be used in a variety of medical guidance applications. It works based on videometric tracking technology and uses visible light to capture standard video images and detect marker patterns by processing the images.

Another type of tracking systems that works based on optical tracking technology is laser tracking systems. In these systems, an array of photosensors is attached rigidly to a carrier. At least two conventional semiconductor lasers emits fan-shaped laser beam and sweep the tracking volume. The position of the tracking object is determined by real-time sampling of the position of the laser emitting system relative to at least three known points and obtaining the position of the photosensors with respect to the laser system, which can be calculated when the photosensors receive the laser beam. An example of such a tracking system is the laserBIRD2 manufactured by Ascension Technology of Burlington, Vermont, USA that is mainly used for object tracking in simulators and virtual reality systems. Laser tracking systems have not found widespread use in clinical applications.

The third type of optical tracking systems are IR-based tracking systems. As the name suggests, these systems use infrared light (IR) to track objects. A camera module

that consists of at least two planar or three linear charge-coupled device (CCD) units receive IR light from the markers attached to a tracking object and determines the position of the object by combining the images captured by the CCDs. The CCDs should only capture IR light from the markers to reliably identify the markers; so a filter which eliminates all ambient light of other wavelength, is placed in front of each CCD. The markers, which are also referred to as fiducial markers or fiducials, are objects that are placed in the field of view of an optical tracking system and are used as points of reference.

As we can see in Figure 1-1, which shows an IR-based optical tracking system, each CCD captures a 2D image of the markers attached to a tracking object. The CCDs only capture the reflected IR from the markers; therefore the images are simple greyscale images that only show the markers from the point of view of each CCD. Then, these images are sent to a control computer and combined by software to report the position of the tracking object. In the rest of this document, we use the term optical tracking to refer to IR-base optical tracking.

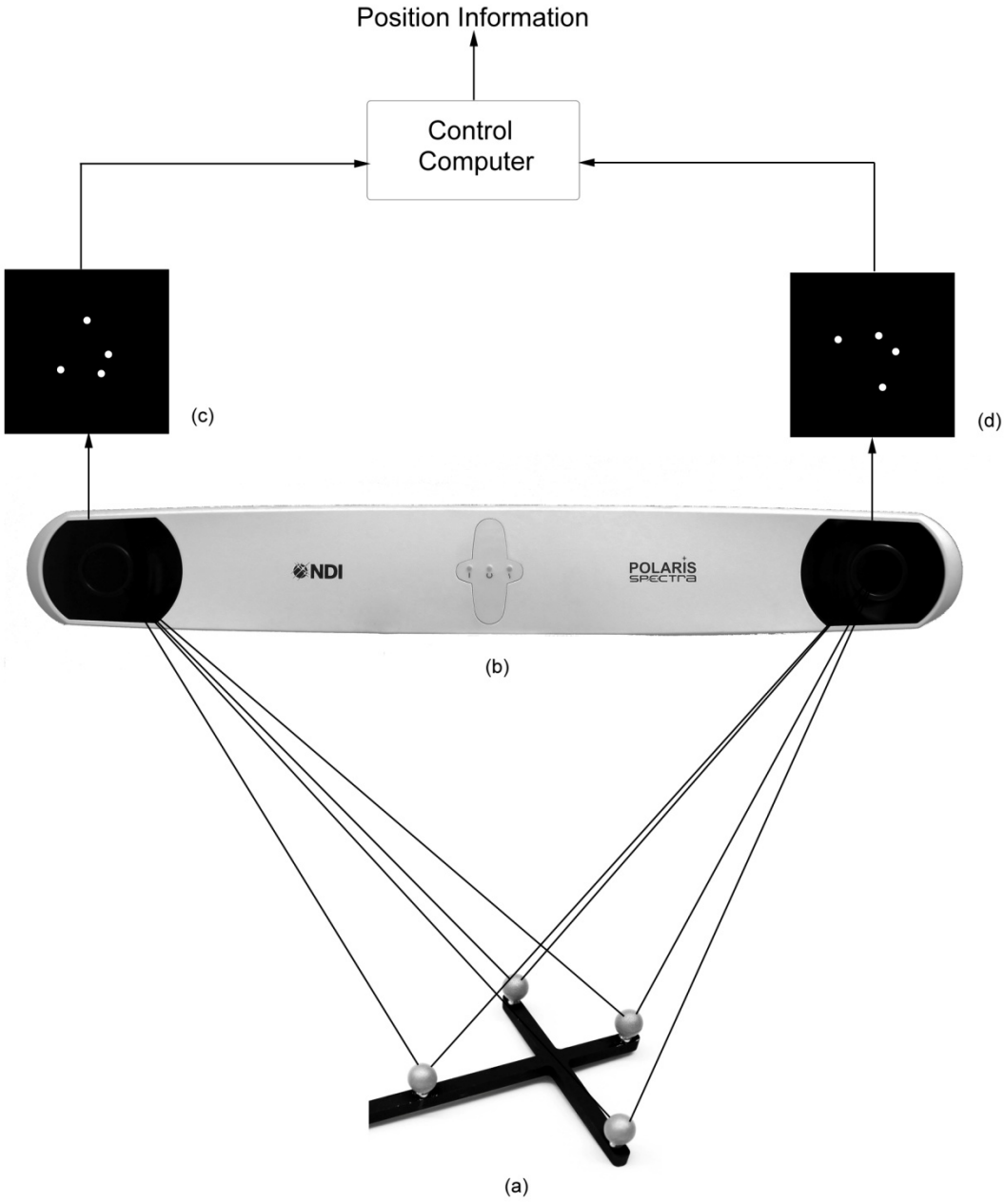

Figure 1-2: An IR-base optical tracking system. (a) Tracking markers. (b) Tracking system's camera. (c) 2D greyscale image of left CCD. (d) 2D greyscale image of right CCD.

In optical tracking systems, the camera should receive emitted or reflected IR from the markers. Markers of these systems are usually categorized based on the source of IR. Currently, two types of markers for optical tracking systems exist:

- *Active markers*: Optical tracking systems were initially designed to use active markers. An active marker is a light-emitting diode (LED) that can emit IR light. The LEDs are usually wired to the system and controlled by a control unit that fires them sequentially. Then, the CCDs of the tracking system's cameras detect the markers and locate them based on the known fixed distance between the CCD units, the known geometric configuration of the markers and the firing sequence of the LEDs. There are minimum configuration requirements for the markers in order to be tracked properly. For instance, at least three non-collinear LEDs are required for detecting the six degree of freedom position of a tracking object. The LEDs must be powered during the tracking therefore active markers must always be wired to the system or a battery.
- *Passive markers:* Another approach for optical tracking markers is the passive marker technology. In this approach, markers are spheres with retro-reflective coating that can reflect IR. The camera emits IR light in the tracking volume. The markers reflect the illuminated IR light, so the system can detect the markers by receiving the reflected IR. The tracking system determines the position of an object by detecting the pattern of the

markers attached to it. This pattern must be unique for each tracking object so the system can localize and track each object reliably. Passive markers do not need to be powered therefore no wires are needed between the tracking system and a tracking object.

Each of the aforementioned technologies of optical tracking markers has their own advantages and disadvantages. Active markers were the initial approach for building optical tracking systems and were adopted in early optical tracking systems. The Optotrak 3020 (Northern Digital Inc., Waterloo, Ontario, Canada) was one of the first commercial optical tracking system that was designed to use active markers. FlashPoint 5000 (Image Guided Technologies Inc., Boulder, Colorado, USA) was another tracking systems that worked based on active markers technology. The active markers that are used in the tracking systems are sterilizable LEDs that are wired to the systems. But dealing with these wires in a busy operating room with a lot of equipment is challenging.

In general, optical tracking systems can track active markers more accurately compared to passive markers. More active tools (compared with passive tools) can be tracked at the same time. The biggest disadvantage of active markers is their need to be wired to the system all the time. The wires might not be fully sterilizable and are hard to work with in an operating room. Active markers are also more expensive than passive markers. Considering the fact that surgeons usually prefer to replace the markers after each operation to ensure their full sterility, active markers higher cost is also a

disadvantage. These drawbacks make active markers not a very efficient and practical choice for surgical navigation systems.

Passive markers were employed in optical tracking systems shortly after active markers. The Polaris tracking system (Northern Digital Inc., Waterloo, Ontario, Canada) was a smaller and less expensive tracking system compared to the Optotrak 3020 that was able to track passive markers. Passive markers need not to be wired to the system, so it is easier to use them in operating rooms. Although passive markers can be sterilized, they are commonly replaced with new markers after each surgery. In fact, these markers are not very expensive and usually surgeons prefer to replace them after a surgery to ensure safety and sterility. The biggest advantage of passive markers over the active ones is being wire free. This characteristic is what makes them the dominant type of marker for image-guided surgery applications. Currently passive markers are the preferred type of optical markers for clinical guidance applications because of their ease of use and cost efficiency.

Optical tracking systems are currently the dominant tracking systems in the medical field that are most widely used in clinical guidance applications. The underlying reasons for quick and wide adaption of these systems for clinical applications are mainly their relatively high accuracy and reliability. Moreover, the low cost of optical markers (i.e., passive markers) is another contributing factor to the dominance of optical trackers. Another advantage of optical tracking systems is the low probability of interference with other devices in the room. Optical trackers use IR light for tracking which is less likely to

interfere with other IR devices in the operating room. There have been a few reported instances where the emitted IR from optical makers interferes with other IR devices during a clinical practice, but these cases are rare.

Despite the advantages of optical trackers, these systems also suffer from some restrictions. All optical trackers must maintain a direct line-of-sight between the tracker's camera and the markers to maintain tracking. This is the major limitation of these systems because the line-of-sight can be easily blocked during the tracking with surgical instruments and operating room equipments. Moreover, optical tracking is not an optimal solution for tracking a flexible tool. This is because the markers are usually placed away from the tip of the tool; therefore, the tool must be rigid to reliably extract the tool tip location from the markers location with an optical tracker. Despite all of these limitations, optical tracking is the standard tracking technology in today's clinical applications. Currently, NDI Polaris tracing systems is the de-facto standard for research studies and some clinical applications.

There are also other tracking technologies that are less common for medical practices. Electromagnetic tracking is another tracking technology that can be used in surgical guidance systems. Electromagnetic tracking systems measure fields generated by small electromagnetic field emitters, which are attached to a tracking object, to localize the emitters and determine the direction and orientation of the object. The main advantage of these systems is that they do not have a direct line-of sight requirement.

Electromagnetic tracking systems are also suitable for tracking flexible tools because the emitters can be placed at the tip of the tool and the tip can be tracked directly.

The main disadvantage of electromagnetic trackers is that the magnetic field can be distorted by nearby metal objects or the magnetic fields from the other surrounding equipment. This can interfere with the tracking and decrease the tracking accuracy. The main underlying reason for the limited adoption of electromagnetic trackers in clinical guidance application is their lower accuracy comparing with optical tracking systems.

1.4 Data Digitization and Representation

The next step after tracking the surgical tools with a tracker is transferring data to a control computer. The method of data transfer and the type of interface to the computer varies for different tracking systems. Commonly tracking systems are connected to the control computer using a serial RS 232 or USB interface. Another important factor in designing an image-guided surgery system is the way that the tracking system formats and communicates tracking data.

Tracking systems report the translation and rotations from the global coordinate system (i.e., coordinate system of the tracking system's camera) to the tracking object's coordinate system. This information can be simply transmitted in form of rotation and translation matrices. However, generally the quaternion representation of the rotational components is preferred over a full rotation matrix. This is mainly because the transmission of nine matrix components of a full rotational matrix is not very efficient and requires more bandwidth. Quaternions consist of a scalar component q_w and a vector

component $[q_x \ q_y \ q_z]^T$. Most modern tracking systems, such a NDI Polaris, report transformations in form of quaternions and translations.

Registering the tracking volume with the preoperative or intraoperative images and showing the position of the tracking instruments on the medical images are other key steps in a surgical navigation system. Registration in image-guided navigation systems is the process of aligning the physical intraoperative data with the preoperative or intraoperative medical images. There are different registration methods that are used in both medical and non-medical applications. The main criteria of a registration algorithm that should be assessed for its adoption in clinical guidance application are the accuracy and reliability of an algorithm. Image-guided surgery systems commonly rely on point-based registration algorithms for the alignment of acquired data with preoperative and intraoperative images. Accuracy of registration algorithms has been studied for decades and it is still an active area of research.

1.5 Accuracy

Clinical data exists that suggests image-guided techniques have a positive impact in certain medical procedures such as pedicle screw implantation in the cervical and lumbar spine, total knee arthroplasty, and total hip arthroplasty (Baethis, et al., 2010), (Bejek, et al., 2007) and (Sugano, 2013). Accuracy is one of the most crucial issues in image-guided surgery systems. Researchers have studied the sources and types of are error in surgical guidance systems for more than a decade. As discussed in this chapter, generally an image-guided intervention process includes the following steps:

1. Acquire preoperative medical images (usually CT or MRI images).
2. Track and localize the surgical instrument with a tracking system.
3. Register the patient's anatomy with the preoperative and intraoperative images.
4. Display the position of the surgical tool (usually tip of the surgical instrument) on the preoperative and/or intraoperative images.

Performing the above steps without any error would lead to a reliable and robust image-guided intervention process. However, it is known that errors can be introduced in each step of the process. As mentioned earlier, tracking systems are responsible for localizing the surgical tools and returning their measured 3D positions or transformations that are used to calculate the tool tip 3D position. Obviously, accurate positioning of surgical tools is a requirement for a reliable image-guided surgical system that can play an important role in the overall accuracy of an image-guided intervention process. The topic of this thesis is measuring the tracking accuracy of an optical tracking system.

In the next chapter, an in-depth review of the related technical work on tracking accuracy in medical field is presented. First, the accuracy measures that are commonly used for optical tracking systems are described. Then, we present a survey of existing literature on tracking accuracy of optical trackers in the field of image-guided interventions.

In this thesis, we have compared empirically measured values of error at the tip of a tracking tool (i.e., TRE that is described in the next chapter) with the theoretical

estimations of this type of error when using an optical tracking system. For this purpose, we designed a variety of experiments that are described in chapter 3. First, the method for calculating the target location from the measured markers locations is presented. Then, we explain the experimental setup including hardware, software and the apparatus. Finally, the experiment methodology including the method of data collection is described.

In chapter 4, we present the results of the performed experiments. Plots that are generated from the collected data and used for analysis are included in this chapter. To visualize the measured locations of the markers, their 3D locations are plotted for each set of data collection. The spread of the calculated target location using the method that is described in chapter 3, are also plotted and presented in chapter 4. In addition, the root-mean-square (rms) values of TRE for each set of data are calculated and presented. Finally in chapter 5, we analyze the results and present our conclusions from the performed experiments.

Chapter 2
Related Work

Researchers have been studying the field of image-guided interventions (IGI) for about 20 years (Peters & Clearly, 2008). As discussed in the previous chapter, there are different types of surgical guidance systems that have been a subject of interest for many years. These systems commonly rely on point-based registration for the alignment between preoperative or intraoperative medical images and the physical patient anatomy. Point-based registration is the process of finding the rotation and translation that matches corresponding fiducial points with least-squares distances fit. Registration in surgical guidance systems is described as the problem of finding the rigid transformation that best relates two different coordinate systems by finding the best match of a set of fiducial marker locations known in both systems (i.e., surgical instrument coordinate system and tracking system physical coordinate system). A crucial property of registration that plays an important role in the usability of surgical guidance systems is the registration accuracy. This chapter presents an in-depth review of the related work in the area of surgical guidance systems accuracy.

2.1 Accuracy Measures

Accuracy of point-based registration, which is the main underlying factor in surgical guidance systems accuracy, has been an active research field since the early 1990s (Maurer, McCrory, & Fitzpatrick, 1993). Three useful measures of error for estimating

the accuracy of point-based registration methods were introduced by (Maurer, McCrory, & Fitzpatrick, 1993) and have been used extensively used in the literature.

- *Fiducial Localization Error* (FLE) is the distance between the true position of a fiducial marker and its measured position. For optical tracking system, FLE is described as the error of optical tracking system in locating a fiducial marker attached to a surgical instrument.
- *Fiducial Registration Error* (FRE) is the root-mean squared distance between the measured position of a fiducial marker in one coordinate system and its corresponding position in the other system after the registration process. For optical tracking systems, the tracking system uses the known position of the fiducial markers (from the calibration process) in the surgical instrument coordinate system, to find the measured position of the fiducials in the tracking system coordinate system. FRE is the distance between corresponding fiducials after this process.
- *Target Registration Error* (TRE) is the distance between corresponding points other than fiducial points after registration. For optical tracking systems, the tracking system uses the transformations found from aligning the measured fiducial positions and their known (from calibration) positions, to obtain the instrument tip position in the tracking system coordinate system from the tip position in the instrument coordinate system. Therefore, TRE is defined as tip locating error after this process.

Figure 2-1 demonstrates the three discussed error measures for an optically tracked surgical instrument.

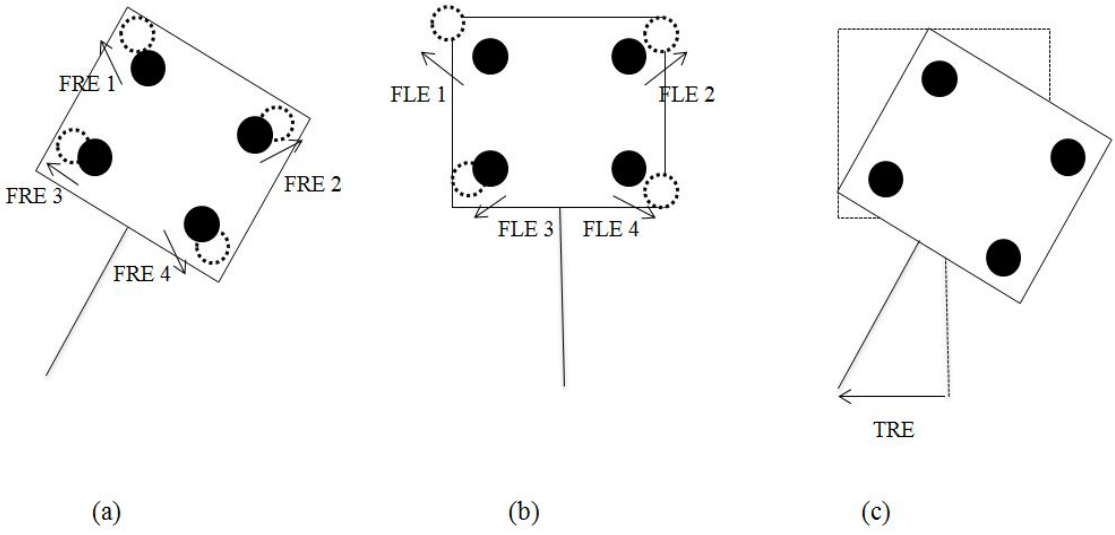

Figure 2-1: Types of errors in point-based registration. (a) FRE is the error between the registered positions of a fiducials in two coordinate systems. (b) FLE is the distance between true position (solid circles) and measured position (dotted circles) of fiducials. (c) TRE is the distance between the registered position of points other that fiducial in two coordinate systems.

Despite the fact that FLE, FRE and TRE are vector values, they are commonly discussed as scalar values in the literature. In fact, the scalar values that are usually reported for these errors are actually the length of the error vector. Generally tracking systems provide feedback on the registration accuracy based on the error in aligning the fiducials (FRE), which arises from error in measuring the position of these fiducial points (FLE). However, surgeons are most interested in the accuracy of the system in

positioning of the tool tip location (TRE). TRE cannot be measured directly because targets are usually inside the patients' body. Therefore, some methods are needed to estimate TRE from other measurable factors such as FLE and FRE. Researchers have studied the properties of and proposed ways to estimate TRE based on other available error measurements such as FLE. A review of existing literature in estimating target registration error is presented in the next section.

2.2 Literature Review of Registration Accuracy

In early 1990s, researchers mostly tried to investigate the properties of TRE by performing numerical simulations (e.g. (Hill, et al., 1994) and (Maurer, Fitzpatrick, Wang, Galloway, Maciunas, & Allen, 1997)) because there were no analytical expressions for estimating TRE. These simulations were useful to understand the overall behaviour of TRE but they were time-consuming and costly to be performed. Moreover, it was also difficult to conclude error patterns from simulations without having an explicit error expression. TRE was expected to depend on the configuration of the fiducials, the magnitude of FLE, and the position of the target point (Fitzpatrick, West, & Maurer, 1998). However, absence of an analytical expression for TRE prevented researchers from gaining a more in-depth understanding of the error behaviour.

In 1979, Sibson presented an equation (Equation 2-1) for FRE (Sibson, 1979). Sibson suggested that the expected value of FRE depends on the expected value of FLE.

$$(FRE)^2 = \frac{N-2}{N} \left(FLE^2 \right)$$

Equation 2-1: Equation for the expected value of FRE^2.

Based on the Equation (2-1), FRE^2 depends on FLE^2 and the number of fiducials N. This is important because it shows that the expected value of FRE is independent of the fiducials configuration (i.e., spatial distribution).

In 1998, Fitzpatrick *et al.* derived an equation to approximate the root-mean-square (rms) value of TRE (Fitzpatrick, West, & Maurer, 1998). Their approximation equation (Equation 2-2) was the first analytical expression for TRE^2 which paved the way for further investigation of registration accuracy at the surgical instrument tip. Their work also demonstrated the dependency of target registration error on the relative position of fiducial points.

$$(TRE)^2 \approx \frac{(FLE)^2}{N} \left(1 + \frac{1}{3} \sum_{k=1}^{3} \frac{d_k^2}{f_k^2} \right)$$

Equation 2-2: Equation for the expected value of TRE^2.

In Equation 2-2, f_k is the rms distance of the fiducials from principal axis k, d_k is the distance of the target (i.e., any desired point that is not one of the fiducial) from principal axis k and N is the number of fiducials. This equation shows that TRE^2 is proportional on FLE^2 but it also depends on the fiducial configuration (i.e., number and spatial distribution). From Equation 2-2, it can be concluded that a collinear fiducial configuration will increase TRE when the target is distant from the line of fiducials.

Moreover, Equation 2-2 shows that TRE^2 would have an ellipsoidal shape centered at the centroid of the fiducials. In order to validate their approximation equation, they performed numerical simulations and showed that the results agreed closely with their theoretical expression. Also their presented expression for TRE^2 agrees with the results from Maurer's (Maurer, Fitzpatrick, Wang, Galloway, Maciunas, & Allen, 1997) and Hill's (Hill, et al., 1994) simulations.

(Fitzpatrick, West, & Maurer, 1998) also provided an expression for the expected squared fiducial registration error (FRE^2) which was exactly equivalent to the one presented by Sibson (Sibson, 1979). Both of the proposed equations for FRE suggested that FRE^2 is proportional to FLE^2 but independent of the fiducial configuration. They concluded that the independence of FRE from the fiducial configuration makes it a poor indicator of the target registration accuracy. This was a valuable result because it was common in 1990s to use FRE to provide feedback on the target registration accuracy of a point-based registration tracking system. On the other hand, the dependency of TRE on the fiducial configuration makes it a better estimator of system registration accuracy than FRE. This is even more important considering the fact that TRE is expected to be worst when the fiducials are registered more accurately. Following their work, West *et al.* provided an approximation expression for TRE distribution in a study aimed to evaluate the accuracy of retrospective image registration methods (West, et al., 1999). However, they ignored anisotropy of the rotational error distribution in their presented expression for TRE distribution.

One basic assumption in Fitzpatrick's work (Fitzpatrick, West, & Maurer, 1998) and other works based on it was that the error in localizing the fiducials (FLE) is isotropic; that is the error along each of the *x*, y and *z* Cartesian axes are equivalent. Although this assumption might be valid in some point-based registration applications, it may not be an appropriate assumption in the case of medical navigation systems. In general, FLE is known to have an anisotropic distribution because medical images have different spatial resolution in each coordinate direction. In the case optical tracking systems, FLE is not distributed isotropically.

In order to accommodate the assumption of noise anisotropy, Fitzpatrick and West extended their previous work (Fitzpatrick, West, & Maurer, 1998) and presented an approximation for TRE when FLE is distributed anisotropically (Fitzpatrick & West, 2001). In the same work, they also presented an approximate expression for the distribution of TRE for the first time. In addition they also provided the expressions for the root-mean-square (rms) value for any arbitrary directional component of TRE. They validated the presented expression of TRE distribution with numerical simulations and suggested that their approximation expression is a valid indicator of TRE as long as the assumptions which they used to derive their expression remain valid. They derived their TRE distribution expression under the assumption of independent fiducial localization error with zero mean normal distribution. Moreover, they also suggested that the presented expression would be more reliable with non-collinear fiducial configurations.

One of the factors that influence TRE is the configuration of fiducial markers. Different groups of researchers studied the effect of fiducial configuration on TRE and proposed guidelines to minimize TRE. In 2004, West and Maurer studied the effect of fiducial configuration on tool tip position tracking error for the case of optical tracking systems (West & Maurer, 2004). They suggested that TRE not only depends on FLE (generally reported by systems manufacturers), but also on the fiducial configuration and tip location relative to the fiducials. This was not new and other researchers suggested such dependency (Fitzpatrick, West, & Maurer, 1998). Also some works had been done to measure the accuracy of different optical tracking systems (e.g., (Chassat & Lavallee, 1998) and (Khadem, et al., 2000)) but most of those studies were performed with a fixed fiducial configuration. West and Maurer was one of the first groups who evaluated TRE with different fiducial configurations. They simulated cases with different number and spatial configurations of fiducials and compared the simulation results with the theoretical expression of Fitzpatrick *et al.* (Fitzpatrick, West, & Maurer, 1998) for approximating the TRE^2 in each case. They also derived a formula for the case of collinear fiducials. In addition, they extend their theory for the case where a composition of transformations is performed (i.e., instrument is tracking relative to a coordinate reference frame) and computed the target registration error for different positions of the instrument relative to a coordinate reference system (CRF). In order to validate their theory, they also performed numerical simulations and found negligible difference between the results.

Based on West and Maurer's results, decreasing the distance between the tool tip and the tracking fiducials would decrease tool tip tracking error. Moreover, increasing the distance between the planar fiducials would also decrease tip positioning error. Relative to a CRF, tip tracking error decreases by decreasing the distance between the instrument tip and CRF fiducials. In terms of the effect of the number of fiducials in tool tip tracking error, adding fiducials could decrease the expected TRE if the added fiducials were configured in a way that did not change its rms distance to the three principal axes. This agrees with the expected expression of TRE from Fitzpatrick *et al.* (Fitzpatrick, West, & Maurer, 1998) which suggests that TRE is inversely proportional to number of fiducials. It should be should be noted that adding a fiducial at the centroid of the fiducials would have the smallest effect in decreasing TRE because it only improves the translational component of TRE, and it is known that the rotational component is the dominant TRE component. These results are useful for designing more accurate optical tracking systems but it should be noted that the proposed theories are based on the assumption of independent, identical, zero-mean and isotropic FLE distribution. However, it is known that in optical tracking systems FLE is not distributed isotropically. Basically, the error along axis orthogonal to the optical tracking system sensor (usually the *z* axis) is three to five times larger than the error along the other axes (West & Maurer, 2004). Therefore, consideration should be made before applying the aforementioned results and theories to the design of optical tracking systems.

The approximation of TRE distribution that was proposed by Fitzpatrick and West (Fitzpatrick & West, 2001) estimates TRE with the accuracy of a first-order approximation and was derived with Monte-Carlo simulations. Moghari and Abulmaesumi presented a closed-form approximation of TRE distribution with the accuracy of up to the second-order Taylor series approximation based on the Unscented Kalman Filter (UKF) (Moghari & Abolmaesumi, 2006). In addition, they also derived an equation for the mean squared value of TRE. They suggested that the previously presented first-order approximation of TRE does not accurately estimate TRE in the case where datasets have different moments about each axis. They used numerical simulation to validate their theoretical results and showed that their proposed method for estimating the TRE distribution is more accurate than previous TRE distribution approximation (Fitzpatrick & West, 2001) in the case of data sets with different structure (data sets with different moments about each axis).

Ma and Ellis used a novel approach to estimate TRE for both fiducial-based and surface-based registration problem (Ma & Ellis, 2006). Their method was based on the behavior of a passive, elastic mechanism and behaves the registration fiducial points as elastic mechanisms that are suspended by linear springs. Small displacements of mechanisms (registration fiducials) can be analysed using the concept of spatial stiffness, which is a widely used and studied concept in the fields of mechanics and robotics. In 2003, Ma and Ellis applied the concept of spatial stiffness analysis to estimate the maximum TRE in fiducial-based registration under the assumption of an identical,

isotropic Gaussian distribution for FLE (Ma & Ellis, A spatial-stiffness analysis of fiducial registration accuracy, 2003). Following that, they extended their spatial-stiffness model of fiducial registration for surface based registration and derived the spatial-stiffness matrix in the case of surface-based registration under the assumption of FLE having an identical, isotropic Gaussian distribution (Ma & Ellis, Spatial-stiffness analysis of surface-based registration, 2004).

Later in 2006, Ma and Ellis derived equations for expected root-mean-square value of TRE for both fiducial-based and surface-based registration (points are selected from a surface and aligned to a surface model) based on their spatial-stiffness model under the same assumptions (i.e., identical, isotropic Gaussian FLE distribution) (Ma & Ellis, Analytic expressions for fiducial and surface target registration error, 2006). Their presented approximation expression of TRE for fiducial-based registration was shown to be identical to Fitzpatrick *et al.* TRE expression (Fitzpatrick, West, & Maurer, 1998). Their equation for expected value of TRE in case of surface based registration was unique and agrees closely with their simulation results.

Most of the research works that we discussed above, assume that the error in localizing the fiducials has isotropic, independent and identical distribution. As discussed earlier, optical tracking systems, which are the most common systems in surgical navigation, are known to have lower measurement precision in the viewing direction of the camera. It is known that in the case of optical tracking systems, the error along axis orthogonal to the optical tracking system sensor (usually the z axis) is three to five times

larger than the error along the other axes (Khadem, et al., 2000). In general, all of analytical models for TRE estimation have two requirements: a model of FLE distribution and a registration algorithm. Basically the error distribution in fiducial localization can have the following characteristics:

- *Isotropic* or *anisotropic***:** If FLE has identical magnitude in all directions it has isotropic distribution; otherwise the FLE distribution is anisotropic.
- *Homogeneous* or *heterogeneous*: If FLE has the same distribution for all fiducial points it has homogeneous (identical) distribution; otherwise FLE distribution is heterogeneous (non-identical or inhomogeneous).
- *Unbiased* or *biased*: If the expected value of FLE is zero its distribution is unbiased; otherwise FLE has biased distribution.

Different registration algorithms are developed based on the characteristics of the distribution of FLE. Closed-form solutions such as Horn's (Horn, 1987) and Maurer's (Maurer, Aboutanos, Dawant, Maciunas, & Fitzpatrick, 1996) for registration of two data sets are based on the assumption of identical or heterogeneous and isotropic FLE distribution. Other iteration-based registration methods such as Balachandran's (Balachandran, Fitzpatrick, & Labadie, 2005) can accommodate the assumption of identical or heterogeneous and anisotropic distribution of FLE. Matei and Meer proposed a solution for aligning two data sets in the presence of heterogeneous (inhomogeneous) anisotropic noise (Matei & Meer, 1999) that is provably optimal in a least-squares sense.

Ma *et al.* studied the effect of anisotropic noise on TRE and derived an equation for estimation the expected root-mean-square (rms) value of TRE in presence of anisotropic FLE (Ma, Moghari, Ellis, & Abolmaesumi, 2007). They also presented a registration algorithm based on the Unscented Kalman Filter (UKF) that produces results which agree with the predicted TRE from their theoretical derived equation. In addition, they studied the performance of the different fiducial registration algorithms in presence of identical, anisotropic FLE. Based on their simulation results, TRE was worst when coordinate reference frame (CRF) of the instrument was directly facing the system's camera. On the other hand, the expected TRE was the smallest when the instrument's CRF was perpendicular to the viewing direction of the tracking system. Obviously, this situation is not practical since fiducials would not be visible to the camera in this orientation. For the registration algorithms comparison, they showed that Horn's method (Horn, 1987), least mean squares (LMS) registration algorithm with the assumption of isotropic noise, had the worst performance and their UKF-based registration algorithm produced the most accurate results. Ohta and Kanatani's algorithm (Ohta & Kanatani, 1998), which is a registration algorithm with the assumption of anisotropic, inhomogeneous Gaussian error distribution, performed better than Horn's method but not as well as the presented UKF-based algorithm.

In 2008, Wiles *et al.* described a closed-form solution to calculate the expected value of TRE when error in localizing the fiducials has an anisotropic normal distribution (Wiles, Likholyot, Frantz, & Peters, 2008). Their solution was based on a least mean

squares registration algorithm and presented expressions for mean, covariance and root mean square (rms) value of TRE under the assumption of anisotropic FLE. They also verified their theoretical expressions with Monte Carlo simulation. Their derived expression for expected TRE generalized the previous error model of Fitzpatrick *et al*, (Fitzpatrick, West, & Maurer, 1998), which was limited to the case of isotropic FLE, to accommodate the case of anisotropic and correlated FLE.

The solution proposed by Wiles *et al.* (Wiles, Likholyot, Frantz, & Peters, 2008) was based on an ordinary least squares registration algorithm but Moghari and Abolmaesumi suggested that applying a weighted least squares method could produce more accurate estimation of the mean squared value of TRE when FLE has an identical anisotropic distribution (Moghari & Abolmaesumi, Maximum likelihood estimation of the distribution of target registration error, 2008). Since 2008, there was no solution for estimating the distribution of TRE in the presence of isotropic or anisotropic and inhomogeneous FLE. Mogahri and Abolmaesumi proposed a solution for this situation that was based on Maximum Likelihood (ML) estimation (Moghari & Abolmaesumi, Maximum likelihood estimation of the distribution of target registration error, 2008). The Maximum Likelihood (ML) principal was used to estimate the variances of the registration parameters that were then utilized to derive the equation of TRE distribution. In order to evaluate their proposed algorithm, Mogahri and Abolmaesumi implemented the TRE distribution equations presented by Fitzpatrick and West (Fitzpatrick & West, 2001) and Wiles *et al.* (Wiles, Likholyot, Frantz, & Peters, 2008) and compared the

results with the estimated TRE distribution from their algorithm under the assumption of FLE with different distributions. They showed that when FLE has an isotropic, identical and zero-mean Gaussian (unbiased) distribution, the results from their proposed algorithm were nearly the same compared to Fitzpatrick and West's (Fitzpatrick & West, 2001) and Wiles' *et al.* (Wiles, Likholyot, Frantz, & Peters, 2008) results and all agreed closely with the simulations. Their proposed method predicted the distribution of TRE more accurately when FLE distribution was anisotropic and inhomogeneous. In the case of anisotropic and identical FLE, the ML-based algorithm outperformed the other two implemented algorithms and followed the results from numerical simulations more closely. Finally, when FLE had an anisotropic and inhomogeneous (heterogeneous) distribution, their suggested algorithm estimated the TRE distribution more accurately compared with the other two algorithms and showed better agreement with the simulation results.

Later in 2009, Moghari and Abolmaesumi extended their previous work (Moghari & Abolmaesumi, Maximum likelihood estimation of the distribution of target registration error, 2008) and proposed a general solution based on the Maximum Likelihood (ML) algorithm for estimating the distribution of TRE in the presence of FLE having independent, heterosgeneous, zero-mean Gaussian distribution (Mogahri & Abolmaesumi, 2009). In their previous work, they indicated that their suggested solution agrees with the results from the implemented expression of Fitzpatrick and West for TRE distribution (Fitzpatrick & West, 2001) in the case of independent, isotropic and identical

FLE distribution. Their follow-up work in 2009 (Mogahri & Abolmaesumi, 2009), mathematically showed that their suggested ML-based algorithm simplifies to the Fitzpatrick and West's algorithm under the same assumptions. They also indicated that when FLE has independent, isotropic, identical, zero-mean, Gaussian distribution, their suggested ML-based algorithm extends the method proposed by Ma *et al.* (Ma, Moghari, Ellis, & Abolmaesumi, 2007). Moreover, they also performed numerical simulations to verify their proposed algorithm under the assumption of any arbitrary independent and zero-mean Gaussian distribution. However, it should be noted that their proposed approximate expressions for the mean square value and distribution of TRE were derived for the cases where FLE has independent and zero-mean Gaussian distributions and are only valid as long as these assumptions remain valid.

Ma *et al.* derived an equation to predict the root mean square value of TRE when FLE has independent, heterosgeneous, zero-mean Gaussian distribution (Ma, Moghari, Ellis, & Abolmaesumi, Estimation of optimal fiducial target registration error in the presence of heteroscedastic noise, 2010). Their proposed method is based on the concept of spatial-stiffness of mechanisms that was described and used in their previous works (Ma & Ellis, A spatial-stiffness analysis of fiducial registration accuracy, 2003), (Ma & Ellis, Spatial-stiffness analysis of surface-based registration, 2004) and (Ma & Ellis, Analytic expressions for fiducial and surface target registration error, 2006). They indicated that for using the presented equation for estimation of root mean square TRE in case of heteroscedastic noise, an optimal registration algorithms is required (ordinary

least-squares registration algorithms are not optimal when error is heteroscedastic). In addition, they compared the predicted root mean square TRE from their theoretical expression with the simulation results from two registration algorithms (Horn's method (Horn, 1987) and HEIV algorithm (Matei & Meer, 1999)). They showed that the predicted root mean square TRE values from their proposed equation were similar to the simulated root mean square TRE values using the HEIV algorithm. This is because HEIV algorithm is an optimal registration algorithm under the assumption of heteroscedastic error. The predicted TRE values from the proposed equation followed the simulated results except for the cases when tracking fiducials were arranged in a nearly co-linear fashion. In these cases, the proposed method overestimated the root mean square value of TRE. Based on their presented results, Horn's method, an ordinary least-squares registration algorithm, performs worst than HEIV algorithm. Therefore, it was suggested that root mean square values of TRE can be predicted more accurately in the presence of anisotropic error by using an optimal registration algorithms.

In 2009, Fitzpatrick studied the relation of fiducial registration error (FRE) and target registration error (TRE) (Fitzpatrick J. M., 2009). The study was basically aimed at providing a mathematical proof for the results observed earlier by Steinmeier *et al.* (Steinmeier, Rachinger, Kaus, Ganslandt, Huk, & Fahlbusch, 2000) and Woerdeman *et al.* (Woerdeman, Willems, Noordmans, Tulleken, & van der Sprenkel, 2007). In 2000, Steinmeier *et al.* studied the registration accuracy of several fiducial-based neurosurgery navigation systems and found no correlation between the reported accuracy of systems

and their actual accuracy. This means that having a surgical guidance system which reports high registration accuracy does not mean that the actual accuracy is also high. Later in 2007, Woerdeman *et al.* presented a comparison of three different registration methods (patient-to-image registration using anatomical landmarks, adhesive markers and surface matching) by performing preoperative registration with each of the registration methods on fifty patients and concluded that registration when using adhesive markers is the most accurate non-invasive registration method. Besides, they also indicated that they found negligible coloration between FRE and TRE.

Surgical navigation systems usually report the measured FRE value or an estimation of TRE based on the measured FRE as the indicator of the tracking accuracy. Therefore, surgeons commonly consider the system's reported accuracy as its actual accuracy. Fitzpatrick's work (Fitzpatrick J. M., 2009) showed that this assumption is wrong in the case of fiducial-based registration when FLE is isotropic and identical. He suggested that FRE and TRE are uncorrelated and therefore assuming that the deviation of predicted FRE value is an indicator of the actual system accuracy is wrong. In order to prove this, a new method of statistical analysis of FRE was developed and used to show that FRE and TRE are completely independent to the first order in FLE. In other words, it was proved that for a given registration, a smaller or larger predicted value of FRE does not cause smaller or larger value of TRE comparing to its predicted value. Numerical simulations were performed to verify the proposed analytical results and showed that FRE and TRE are merely uncorrelated. However, their mathematical proof analytically

proved that FRE and TRE are completely uncorrelated. A surprising result based on the Fitzpatrick work (Fitzpatrick J. M., 2009) is that values that are usually displayed by surgical navigation systems as an indicator accuracy does not give any information about the systems actual accuracy and are not reliable. Fitzpatrick suggested that surgeons should not rely on the surgical guidance systems reported accuracy measurements and new accuracy indicators should be developed and used in these systems.

In 2009, Fitzpatrick (Fitzpatrick J. M., 2009) only studied the relation of FRE and TRE in the case where the error in localizing the fiducials (FLE) has isotropic and identical distribution. Danilchenko and Fitzpatrick extended Fitzpatrick's previous work (Fitzpatrick J. M., 2009) and investigated this problem in the presence of inhomogeneous and anisotropic FLE when arbitrary weighing is employed in the registration algorithm (Danilchenko & Fitzpatrick, 2010). They calculated the cross-covariance matrices of FRE and TRE and used them to provide new analytical expressions for FRE^2 and TRE^2. To generalize the previous results (Fitzpatrick J. M., 2009), Danilchenko and Fitzpatrick (Danilchenko & Fitzpatrick, 2010) employed ideal weighting for each fiducial and showed that FRE and TRE are independent in the presence of inhomogeneous and/or anisotropic FLE. They also validated their results by comparing them with the previously published expressions of FRE and TRE and performing simulations. Their suggested FRE^2 expression proven to be equivalent to the one proposed by Sibson in 1979 (Sibson, 1979). Furthermore, they showed that their presented expression for TRE^2 agrees with the Moghari's (Mogahri & Abolmaesumi, 2009) and Wiles' (Wiles, Likholyot, Frantz, &

Peters, 2008) formulas for TRE. Based on their simulation results, when ideal weighting is used neither correlation nor dependence was found between FRE and TRE. In the case of uniform weighting (i.e., no weighting), a negligible correlation and dependence was observed. This agrees exactly with the Steinmeier (Steinmeier, Rachinger, Kaus, Ganslandt, Huk, & Fahlbusch, 2000) and Woerdeman (Woerdeman, Willems, Noordmans, Tulleken, & van der Sprenkel, 2007) experiments results that employed uniform weighting in their studies. The simulation results verified their theoretical results and agree closely with their presented expressions. As a result, they suggested that TRE are FRE are independent for any distribution of FLE (homogeneous or inhomogeneous, isotropic or anisotropic) using an optimal registration algorithm and therefore FRE is an unreliable measure of registration accuracy.

As discussed earlier, TRE is expected to depend on the fiducials configuration. It is known that the placement and spatial distribution of fiducial markers, influence target registration error directly (West J. B., Fitzpatrick, Toms, Maurer, & Maciunas, 2001). Because the actual TRE is not known, researchers commonly use an analytical expression of TRE to study the effect of fiducials placement on TRE and to find optimized fiducial configurations. In 2001, West *et al.* investigated the importance of the fiducial markers configuration in target registration accuracy of point-based registration (West J. B., Fitzpatrick, Toms, Maurer, & Maciunas, 2001). They concluded that the placement of fiducial markers is an in important factor that affects TRE. They used Fitzpatrick's *et al.* analytical expression of TRE (Fitzpatrick, West, & Maurer, 1998) to calculate the

expected squared TRE at a desired target for different fiducial configurations. Based on their results, TRE can be minimized by using as many fiducial markers as possible, placing the fiducials centroid as close as possible to the target location and avoid collinear configurations of fiducial markers. Following these proposed guidelines can minimize TRE; however they are not always practical and easy to follow.

Shamir *et al.* studied the effect of fiducials configuration on TRE and proposed a method to improve target localizing accuracy of image-guided optical tracking systems (Shamir, Joskowicz, & Shoshan, 2012). Their suggested method calculates optimal fiducial marker placements to that minimize the expected TRE which is calculated based on physical FLE model computed from previous localization data. Then the surgeon can interactively select fiducials placement and override system selection based on the software visualization of the expected TRE for each fiducial configuration. In their calculations, they modeled FLE as isotropic, independent and inhomogeneous noise with normal distribution. Basically, the proposed method used patients' diagnostics medical images to automatically compute fiducials placements and selection of the anatomical landmarks. This step was performed before preoperative imaging and did not require additional patients scanning. They preformed neurosurgery clinical experiments with the proposed method on five patients who underwent brain surgery with a surgical navigation system.

Based on Shamir's *et al.* results, optimizing the placement of a single fiducial marker can reduce TRE by 25% on average. Moreover, they also suggested that having

more fiducials would not always reduce TRE. This result is in contrast to West *et al.* proposed guideline (West J. B., Fitzpatrick, Toms, Maurer, & Maciunas, 2001) that increasing the number of fiducials decreases TRE. They suggested that this contrast might be the result of the assumed FLE distribution model. West *et al.* study assumed FLE has isotropic, independent, homogeneous and normal distribution. In contrast, Shamir *et al.* modeled FLE with anisotropic, independent, inhomogeneous and normal distribution. They also mentioned that using a different registration algorithm that can accommodate a more realistic FLE model can possibly lead to being able to reduce the actual TRE by using more fiducial markers.

All of the research works that we discussed previously, assume that fiducial markers are fully visible all the time. But this assumption is not always true in surgical optical tracking systems applications. Actually occlusion of fiducial markers or the camera's line of sight is not uncommon during surgeries. It is known that one of the influential factors on the accuracy of optical tracking systems is the geometry of the tracking setup which includes the number of visible fiducials, spatial distribution of the fiducials and the pose of the tracking cameras. Therefore, a reliable method for estimating optical tracking system accuracy should account for fiducials visibility and tracking setup geometry. Sielhorst *et al.* presented a method for real-time estimation of TRE based on the visibility and geometry of a tracking configuration (Sielhorst, Bauer, Wenisch, Klinker, & Navab, 2007). Their suggested method is based on the expected TRE formula described by Fitzpatrick *et al.* (Fitzpatrick, West, & Maurer, 1998) and

TRE model presented by Hoff *et al.* (Hoff & Vincent, 2000). In order to estimate TRE, Sielhorst *et al.* modeled the error in the tracking system's camera plane and then calculated tracking error at target location by accounting for fiducials setup geometry, fiducials visibility and the camera and target pose. To model the tracking system error, in addition to FLE and TRE they used two other error measurements which were defined as follows:

- *Image Plane Error* (IPE) is the measured error in the tracking system's camera.
- *Mean Target Error* (MTE) is the error of tracking the target when it placed in the centroid of the fiducials. This error depends on the error in localizing the fiducials and the spatial placement of the tracking target.

They first modeled IPE as a 2D error in the plane of the camera censor and created covariance matrices for each camera. Then they derived FLE from IPE and made covariance matrices for each fiducial. In the next step, FLE was propagated to calculate MTE for each target. Finally, TRE was calculated based on MTE. In case of isotropic and uniform distribution the suggested model of Sielhorst *et al.* mathematically agrees with the results of Fitzpatrick *et al.* (Fitzpatrick, West, & Maurer, 1998) and Hoff *et al.* (Hoff & Vincent, 2000). However, they argued that these assumptions are not always reliable and modelling FLE with anisotropic and non-uniform distribution is more realistic. Based on their results, the assumption of anisotropic and non-uniform FLE distribution shows it benefits in case of one or more fiducials or cameras occlusion. Their proposed method

can provide real-time feedback on tracking accuracy that would be valuable to surgeons because they could estimate the accuracy of the optical tracking system at any time during the operation. Moreover, online estimation of registration accuracy based on fiducials visibility paves the way for designing and using multiple camera tracking systems because it can assure certain level of accuracy in such systems.

Chapter 3
Measuring Target Registration Error

Almost all of the discussed research works in Chapter 2, analyzed registration accuracy of optical tracking systems by providing analytical expressions that estimate TRE. The accuracy of the theoretical models has been validated using computer simulations. To the best of our knowledge there are few research studies that are focused on carefully measuring TRE using an actual optical tracking system and comparing the measured TRE to the theoretical models. We propose a method to measure TRE through a variety of experiments and compare the measured values with theoretical estimations of TRE. In this chapter, our proposed method for measuring TRE is presented. First, the theoretical calculation of TRE is discussed in the next section. Then, we describe the design of the experiments including the hardware, software and apparatus. Finally, we discuss the experiments methodology and describe how the experiments are performed.

3.1 Finding the Target Location

The approach we used to find the target location is based on the method described by Thompson *et al.* (Thompson, Penney, Dasgupta, & Hawkes, 2013). They presented a method to derive the target location during the calibration process in both the instrument's and the global coordinate systems using the transformations reported by the tracking system. For each frame of data the transformations is obtained from the optical tracking system. This gives us a 3×3 rotation matrix (R_i) and a 3-dimensional translation

vector(T_i). During the calibration process (and also in all of our experiments) the target (i.e., the tip of the instrument) is fixed and would not move. If we let q be the target location in the global coordinate system (i.e., tracking system's coordinate system) and p be the target location in the tool's coordinate system, for each frame of data we have the Equation (3-1).

$$q \approx \{R_i]p + T_i$$

Equation 3-1: Target location in the global coordinate system for each frame of data.

Rearranging the Equation (3-1) gives us Equation (3-2).

$$p = R_i^{-1}(q - T_i) = R_i^{-1}q - R_i^{-1}T_i$$

Equation 3-2: Target location in the tool's coordinate system.

For the full data set including n frames of data, there are n Equations (3-1) and by adding those n equations we have Equation (3-3).

$$nq = \left(\sum_{i=1}^{n} R_i\right)p + \sum_{i=1}^{n} T_i$$

Equation 3-3: Target location in the global coordinate system for the full data set.

Similarly, we have n Equations (3-2) that adding them give us Equations (3-4).

$$np = \left(\sum_{i=1}^{n} R_i^{-1}\right)q - \sum_{i=1}^{n}(R_i^{-1}T_i)$$

Equation 3-4: Target location in the tool's coordinate system for the full data set.

Equations (3-3) and (3-4) can be rearranged to yield Equations (3-5) and (3-6).

$$nq - (\sum_{i=1}^{n} R_i)p = \sum_{i=1}^{n} T_i$$

Equation 3-5: Equation (3-3) after rearranging.

$$np - \left(\sum_{i=1}^{n} R_i^{-1}\right)q = -\sum_{i=1}^{n} (R_i^{-1}T_i)$$

Equation 3-6: Equation (3-4) after rearranging.

Equations (3-5) and (3-6) can be written in form of a matrix equation (Equation (3-7)).

$$\begin{bmatrix} nI_3 & -\sum_{i=1}^{n} R_i \\ -\sum_{i=1}^{n} [R_i]^T & n[I_3] \end{bmatrix} \begin{bmatrix} q \\ p \end{bmatrix} = \begin{bmatrix} \sum_{i=1}^{n} T_i \\ \sum_{i=1}^{n} (R_i^{-1}T_i) \end{bmatrix}$$

Equation 3-7: Linear Equations (3-5) and (3-6) in form of a matrix equation.

Finally, q and p can be found by solving the linear system represented by Equation (3-7):

$$\begin{bmatrix} q \\ p \end{bmatrix} = \begin{bmatrix} nI_3 & -\sum_{i=1}^{n} R_i \\ -\sum_{i=1}^{n} [R_i]^T & n[I_3] \end{bmatrix}^{-1} \begin{bmatrix} \sum_{i=1}^{n} T_i \\ \sum_{i=1}^{n} (R_i^{-1}T_i) \end{bmatrix}$$

Equation 3-8: Matrix equation for finding q and p.

In our experiments, we use Equation (3-8) to find q which is the target location in the global coordinate system and subsequently we analyse the calculated target locations to understand the behaviour of TRE. The design of the experiments is discussed in the next section.

3.2 Experimental Setup

3.2.1 Hardware

The experiments are performed using a Polaris Spectra optical tracking system manufactured by Northern Digital Inc. (NDI) of Waterloo, Ontario, Canada. The Polaris Spectra (Figure 3-1) has a large pyramid shaped tracking volume and supports claimed measurement accuracy up to 0.3mm RMS throughout the volume. It supports a maximum sampling rate of 60 (Hz); however, the sampling rate depends on the number and type of the tools that are being tracked.

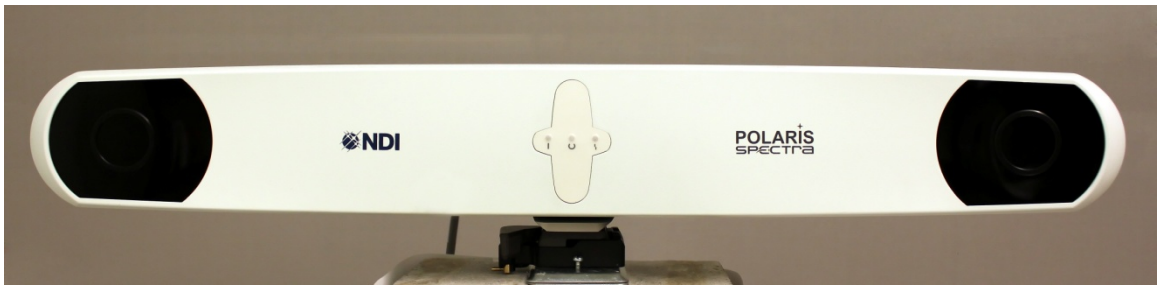

Figure 3-1: NDI Polaris Spectra tracking system.

The Polaris Spectra can track both active and passive markers and it also supports hybrid configurations (i.e., tracking a combination of passive, active wireless and active

tools). It uses a global coordinate system with an origin located somewhere within its position sensor (as it is shown in Figure 3-2). The global coordinate system cannot be changed and is defined in the manufacturing process.

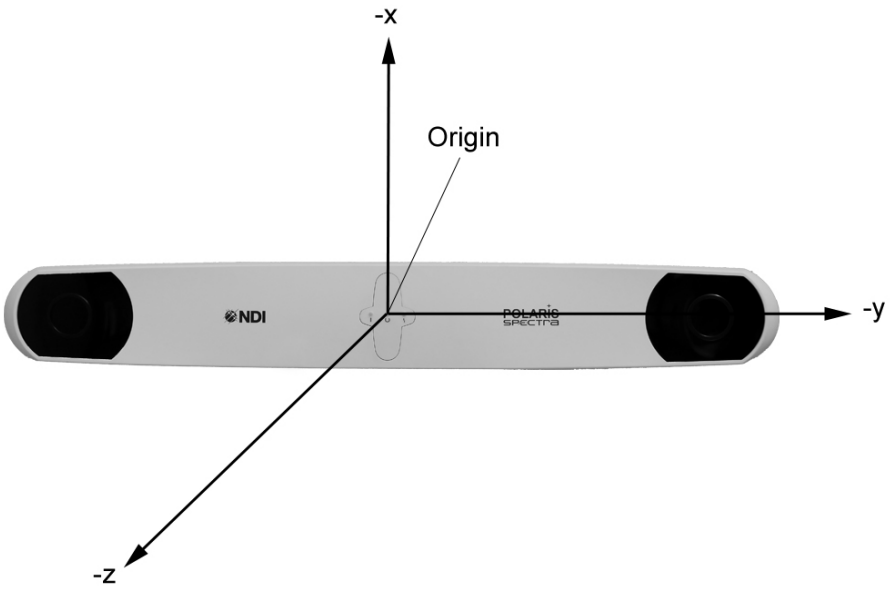

Figure 3-2: Global coordinate system.

For the experiments, we designed and built different tools with different types of markers. Basically, a tool is a rigid structure which has at least three markers mounted on it where the markers are fixed and have no relative movement between them. Two different tools with different marker configurations were designed and built with each type of marker. We built the tools using passive, radix and active markers on them; the various marker types are shown in Figure 3-3 and are described in greater detail below. For designing the tools, we followed all of the constraints and guidelines provided by NDI such as marker geometry constraints and tool compatibility constraints.

NDI passive sphere markers (Figure 3-3 (a)), which are used on passive tools, have a retro-reflective coating that reflects IR from the tracking system's position sensor to its source so the system can report the position of each passive marker. Figure 3-4 shows the passive tools that we built for the experiments. Another type of markers that we used to build passive tools is the NDI Radix Lens (Figure 3-3 (b)). Radix Lens markers are a new passive technology from NDI that are more robust to tissue and liquid contamination and can be easily cleaned to recover tracking. A Radix Lens has a retro-reflective coating on the back and a plastic surface on the front. Figure 3-5 shows the passive tools with Radix Lens markers that we use in the experiments. We also made two active tools with two different configurations of active markers. Basically, an active marker (Figure 3-3 (c)) is an infrared light emitting diode (IRED) that is mounted on a ceramic base. The tracking system's position sensor detects the emitted IR and reports the position of the marker. The active tools that are used in the experiments can be seen in Figure 3-6.

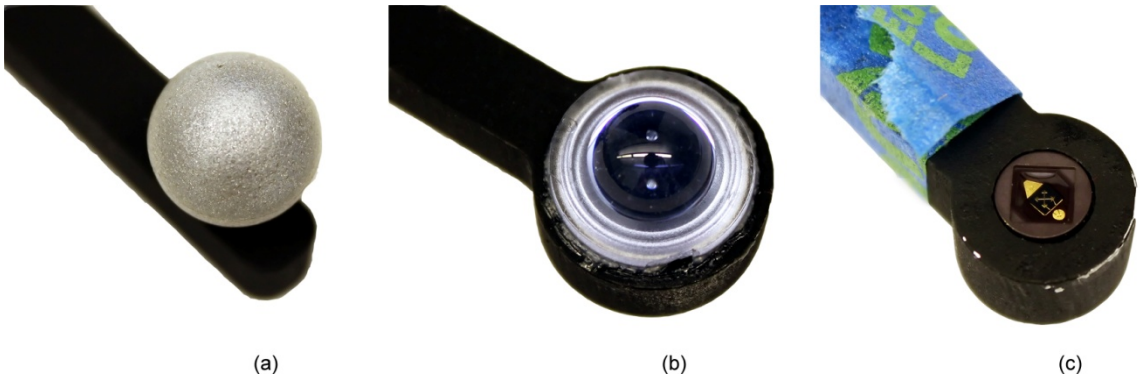

Figure 3-3: Different types of makers. (a) Passive sphere marker. (b) Radix lens marker. (c) Active marker.

Figure 3-4: Passive tools. (a) Passive tool with V-shaped configuration of markers. (b) Passive tool with T-shaped configuration of markers.

Figure 3-5: Radix tools. (a) Radix tool with v-shaped configuration of markers. (b) Radix tool with T-shaped configuration of markers.

Figure 3-6: Active tools. (a) Active tool with v-shaped configuration of markers. (b) Active tool with T-shaped configuration of markers.

The Polaris Spectra needs to know some information such as the placement of the tool's markers, the location of its origin, and its manufacturing data to track the tools and accurately interpret the collected data. A tool definition file, which is associated with each tool, is a file that includes this information and must be loaded into the system before the system can track the specific tool. One of the steps in the procedure of making a tool definition file is to define the origin and the tool's coordinate system. In Figure 3-7 the defined coordinate system and the origin for Radix tools is shown. We defined the coordinate system and origin for the passive and active tools in the same way.

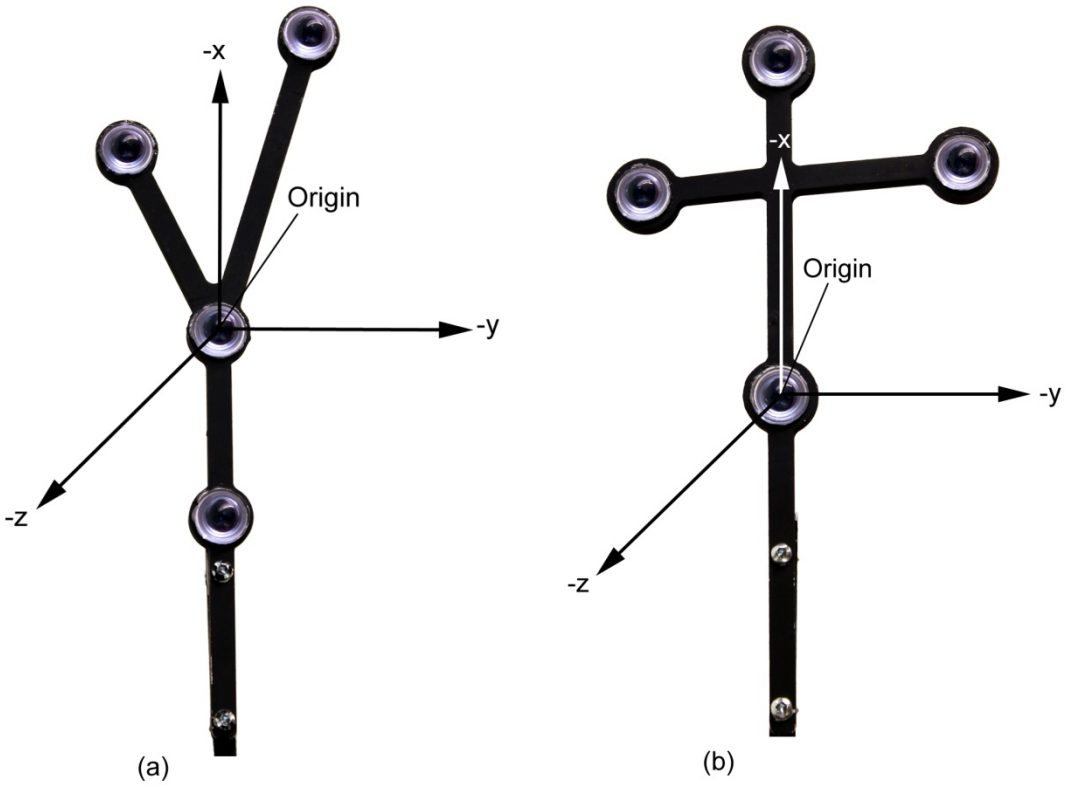

Figure 3-7: Defined coordinate systems for the tools. (a) Coordinate system of the Radix V-shaped tool. (b) Coordinate system of the Radix T-shaped tool.

One of the factors that can affect the accuracy of the measurements is any movement of the tracking system during an experiment. In order to avoid the effect of unwanted ground vibrations, the tracking system is rigidly mounted to an optical table which had passive vibration-damping support manufactured by Thorlabs Inc. of Newton, New Jersey, USA. This helps us to be more confident about the accuracy of the performed experiments since it enables us to control the effect of an unwanted variable (environment vibrations) that could influence the experiments negatively.

3.2.2 Software

During the experiments, the 3D position of each fiducial marker that was attached to the tracking targets (i.e., tools) needed to be recorded so that we could calculate the position of the target. We developed software based on the Polaris application program interface (API) to acquire the positions of the fiducial markers and record the position information. The software also has the feature to save the recorded position information in a text file. To save the position information, we have the options to either saving the markers positions as long as the tools are being tracked, or specify the number of the frames that we want to save. Figure 3-8 shows structure of the output file when six frames of data are saved for two tools each with four markers.

	X	Y	Z	X	Y	Z	X	Y	Z	X	Y	Z
Tool 1	x_{m1}	x_{m1}	z_{m1}	x_{m2}	y_{m2}	z_{m2}	x_{m3}	y_{m3}	z_{m3}	x_{m4}	y_{m4}	z_{m4}
Tool 2	x_{m1}	x_{m1}	z_{m1}	x_{m2}	y_{m2}	z_{m2}	x_{m3}	y_{m3}	z_{m3}	x_{m4}	y_{m4}	z_{m4}
Tool 1	x_{m1}	x_{m1}	z_{m1}	x_{m2}	y_{m2}	z_{m2}	x_{m3}	y_{m3}	z_{m3}	x_{m4}	y_{m4}	z_{m4}
Tool 2	x_{m1}	x_{m1}	z_{m1}	x_{m2}	y_{m2}	z_{m2}	x_{m3}	y_{m3}	z_{m3}	x_{m4}	y_{m4}	z_{m4}
Tool 1	x_{m1}	x_{m1}	z_{m1}	x_{m2}	y_{m2}	z_{m2}	x_{m3}	y_{m3}	z_{m3}	x_{m4}	y_{m4}	z_{m4}
Tool 2	x_{m1}	x_{m1}	z_{m1}	x_{m2}	y_{m2}	z_{m2}	x_{m3}	y_{m3}	z_{m3}	x_{m4}	y_{m4}	z_{m4}

Figure 3-8: Structure of the tracking software output file including the recorded marker locations of two tools when six frames of data are recorded,

Moreover, the software also reports the transformations (in form of translations and quaternions) for each handle that is used to calculate the 3D position of the target. Basically, the software records the 3D position of each marker on the tracking targets and also the transformation for each tracking target in each data frame and saves this information as text files. It also gives us the option to set the number of the frames that we want to save or it will save the 3D positions and transformations as long as the targets are being tracked. Figure 3-9 shows the structure the software output file when six frames of data is recorded for two tools.

	T_X	T_y	T_z	Q_0	Q_x	Q_y	Q_z
Tool 1	t_x	t_y	t_1	q_0	q_x	q_y	q_z
Tool 2	t_x	t_y	t_1	q_0	q_x	q_y	q_z
Tool 1	t_x	t_y	t_1	q_0	q_x	q_y	q_z
Tool 2	t_x	t_y	t_1	q_0	q_x	q_y	q_z
Tool 1	t_x	t_y	t_1	q_0	q_x	q_y	q_z
Tool 2	t_x	t_y	t_1	q_0	q_x	q_y	q_z

Figure 3-9: Structure of the tracking software output file including the recorded transformations for two tools when six frames of data are recorded,

We also need to analyze the extracted information from the software. So we developed Matlab functions to analyze and visualize the collected data from the experiments. We developed a Matlab function that plots the 3D distribution of the markers locations for each handle for a whole data set. We also implemented a Matlab function that uses Equation 3-8 to calculate the target location (i.e., q in Equation 3-8) from the recorded transformations. Then, another Matlab function uses the calculated target locations to plot the spread of the target locations with different colors for each handle orientation (i.e., tilt angle).

To visualize the markers locations and calculate the expected target location, we used a Matlab function that fits a sphere to a set of collected data for each marker on a

tracking target (in each set of data collection, each markers move on a sphere, see Section 3.2.4 on the methodology of the experiments). The function calculates the center and radius of the recorded marker's locations for each marker on a tracking target using a least squared sense. The calculated radius for each marker is the calculated target location-based on the set of data for that specific marker. The function also plots a sphere that fits a set of data.

3.2.3 Apparatus

The experiments are designed to study and observe TRE fluctuations when the experiment setup is configured in way that the target is guaranteed to stay in a fixed location in each set of data collection. In order to make sure the target location is fixed and would not move, we designed and built an apparatus that gives us the flexibility to rotate the tracking targets for a full 360 degrees in the plane parallel to the tracking system's camera plane. The handles could also be tilted with 60 degree variation along the axis perpendicular to the tracking system's camera; at the same time, the target is guaranteed to stay exactly at the same location. This was done by attaching the tracking targets to a 1 inch diameter steel precision ball that was placed on three smaller ¼ inch diameter steel precision balls forming a kinematic mount. All balls were hardened, bearing quality E52100 steel with a diameter tolerance of 0.0001 inch. The apparatus can be seen in Figure 3-10. Using the precision balls guarantees the full spherical motion of the handles, so we can be confident that the target is located at the center of the base precision ball (to within the diameter tolerance of the ball). The apparatus has a guide that

restricts the handles motion to the plane parallel to the tracking system's camera plane; so handles cannot be rotated around their *x* axis.

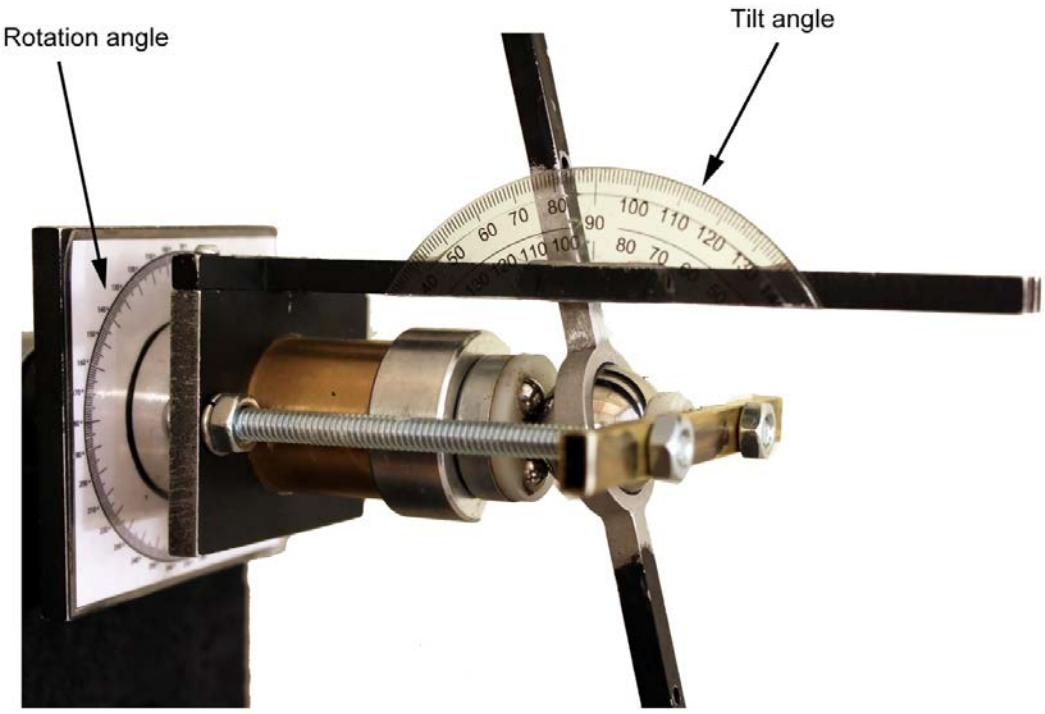

Figure 3-10: Apparatus.

As mentioned earlier, we want to avoid any vibration of the experimental setup during the experiments because any vibration of the apparatus or the tracking system would result in a movement in the target location which should be fixed during each set of data collection. Therefore, the apparatus was mounted rigidly on the same vibration-damping optical table which the tracking system was also mounted on. Figure 3-11 shows

the experimental setup. This setup enables us to perform a variety of experiments which are discussed in the following section.

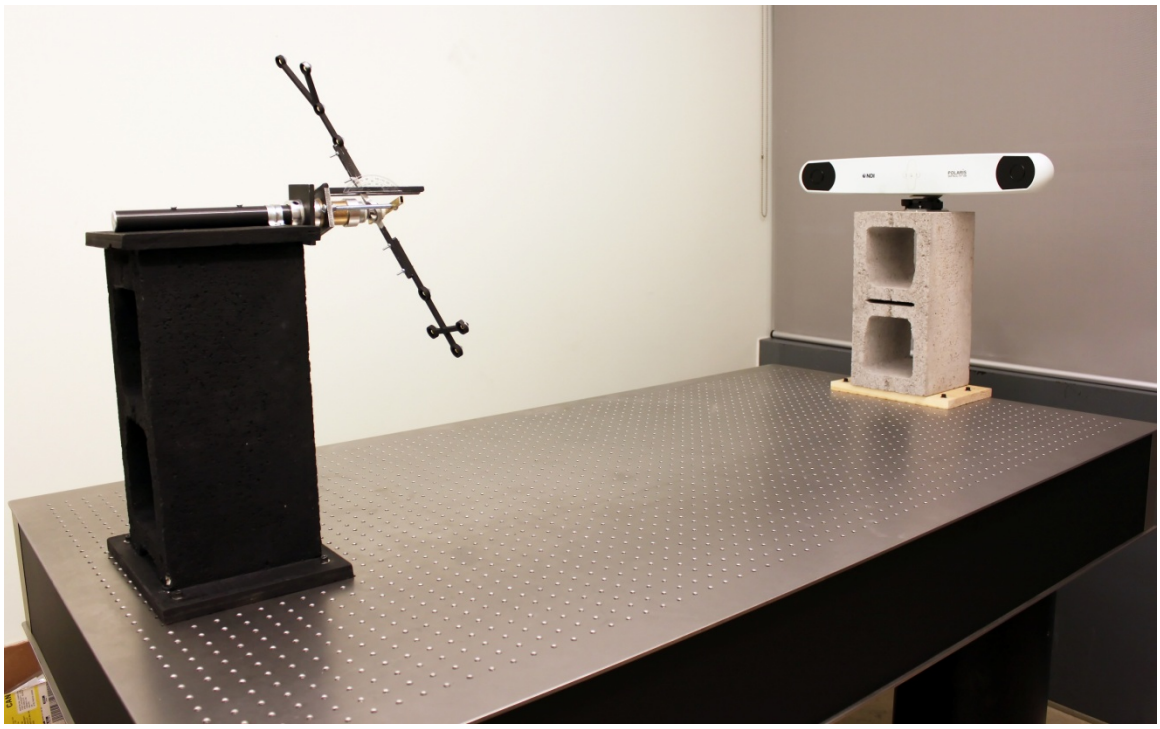

Figure 3-11: Experimental setup.

3.2.4 Method

In the experiments, we aim to measure target locations with different handle orientations and study the effect of handle pose on the measured target location. At each set of data collection, we attach two tracking targets, with each having a different configuration of fiducial markers, to the bar that is mounted on the base precision ball. Next, for each tilt angle (see Figure 3-10) we rotate the handles from 0 to 360 degrees and record each

fiducial marker's 3D position and each handle's transformation every five degrees. As we can see in figure 3-10, the design of the apparatus limits the range of tilt to 60 degrees. Initially, for the first set of data collection the tilt angel is -30º and is increased by 10 degrees for each set of data collection. Therefore, in each experiment we collect data for 7 different tilt angels. As it can be seen in Figures 3-3, 3-4 and 3-5, the fiducial markers are in the same plane (planar configuration) in both configurations of the markers. We perform this experiment with the two passive handles, the two Radix handles and the two active handles that we built. For all of the experiments, the tracking system was set to collect data at sampling rate of 60 frames-per-second.

Since it is thought that the measurement accuracy of the optical tracking system varies within the tracking volume, we repeated these experiments when the apparatus was moved from its original location. First, we moved the apparatus 9 inches to the right from its original middle position and repeated the experiments with all six handles. Then, we moved the apparatus 9 inches to the left from the original middle position and repeated the experiments using all of the handles. It should be noted that the tracking system location was fixed in all of the experiments.

One of the factors that can affect the accuracy of tracking is the number of the fiducial markers of a tracking target that are visible to the tracking system camera. We wanted to avoid the effect of the visibility of the markers in our experiments. Therefore, we made sure that all of the fiducial markers were within the tracking volume and were fully visible to the tracking system camera during each set of the experiments.

Chapter 4
Results

The results of the performed experiments, which were described in Chapter 3, are presented in this chapter. In the next section, the plots of the measured 3D locations of the markers in each set of data collection are provided. Next, we have plotted the calculated target locations for each tool using the method that was discussed in the previous chapter. Finally, the root-mean-squared value of TRE for each tilt angle per tool is calculated and plotted.

4.1. Marker Locations Plots

We used the software that we developed for data collection (see Section 3.2.2) to record the 3D positions of the fiducial markers. In the experiments, for each tilt angle, we rotated the tools for a full 360 degrees and recorded the 3D locations of the markers. Then, we plotted the recorded locations of the markers for each tool. These plots are shown in Figures 4-1 to 4-6. As mentioned in Section 3.2.4, we performed the experiments with the apparatus placed in three different locations within the tracking volume. However, for the sake of brevity, in this chapter we only present the plots for the set of experiments in which the apparatus is place in the middle location. The plots for the other experiments are provided in the Appendix.

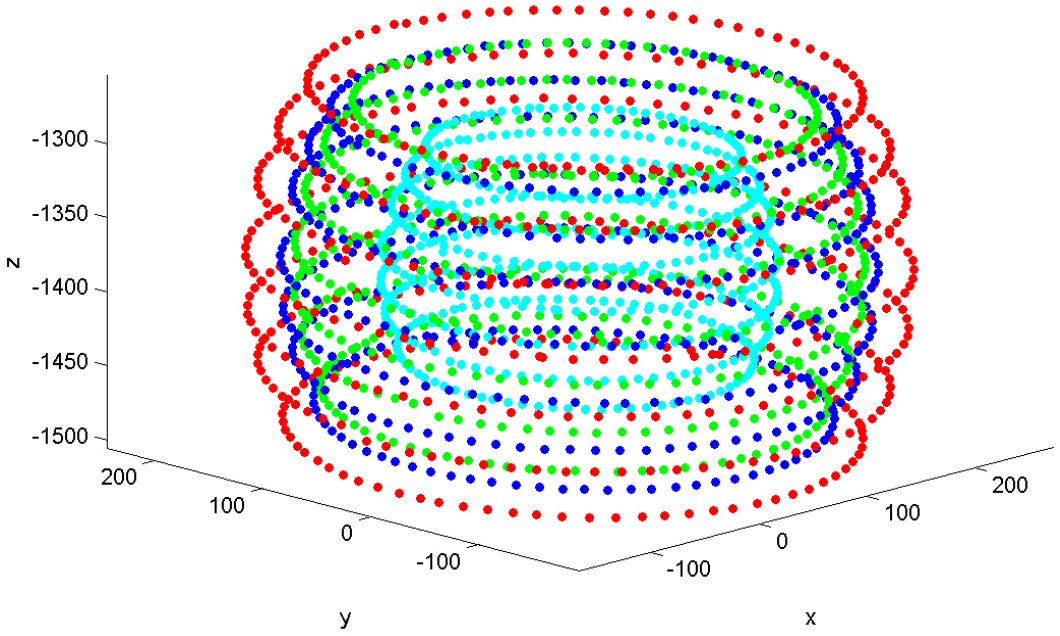

Figure 4-1: Markers locations of the T-shaped passive tool.

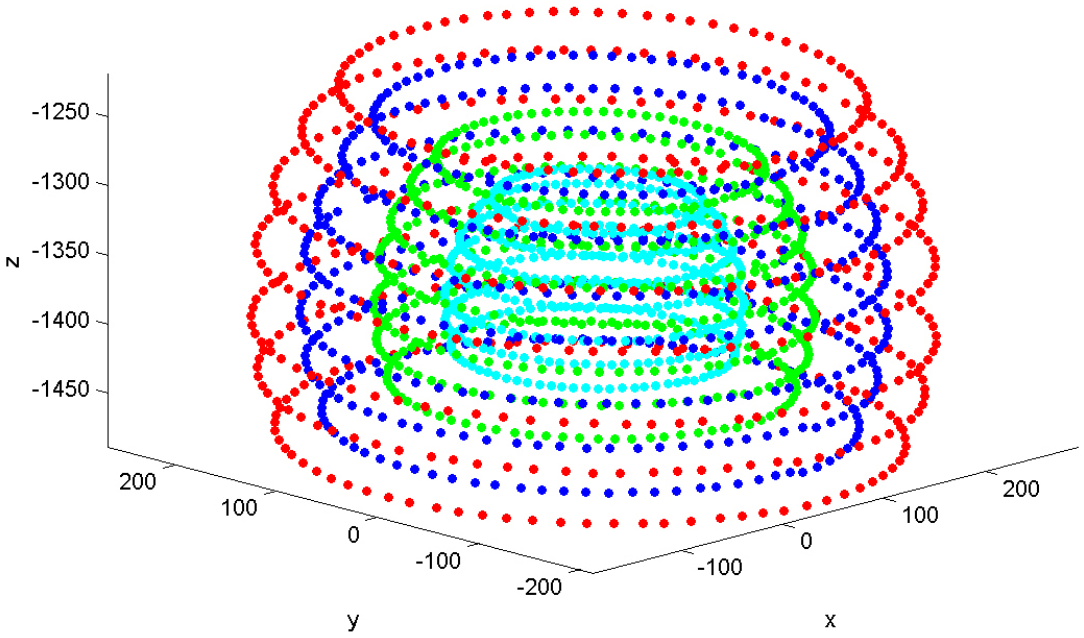

Figure 4-2: Markers locations of the V-shaped passive tool.

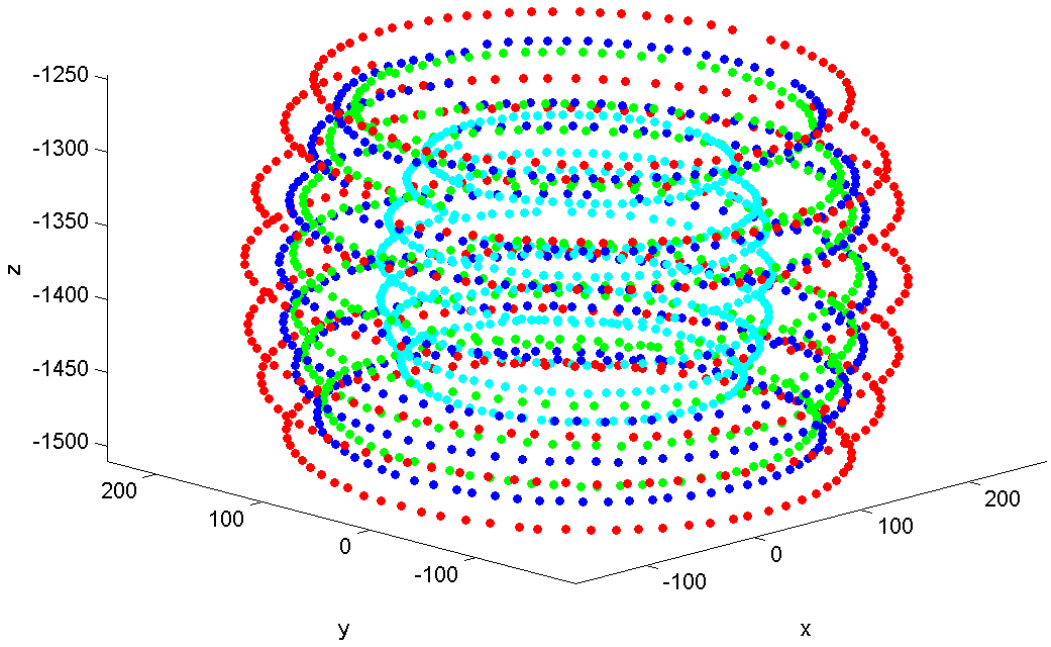

Figure 4-3: Markers locations of the T-shaped radix tool.

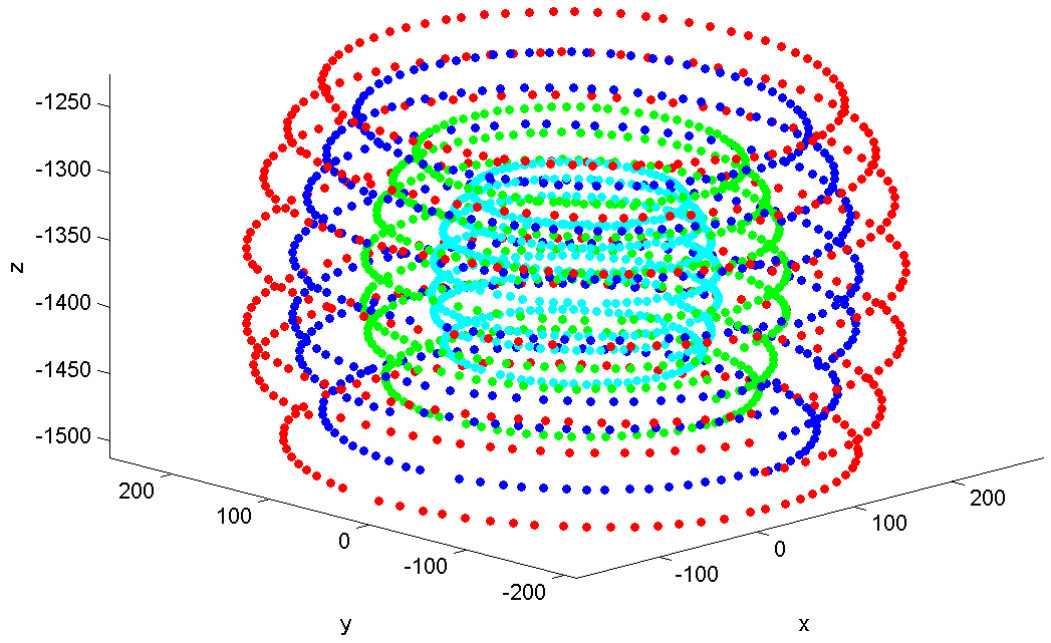

Figure 4-4: Markers locations of the V-shaped radix tool.

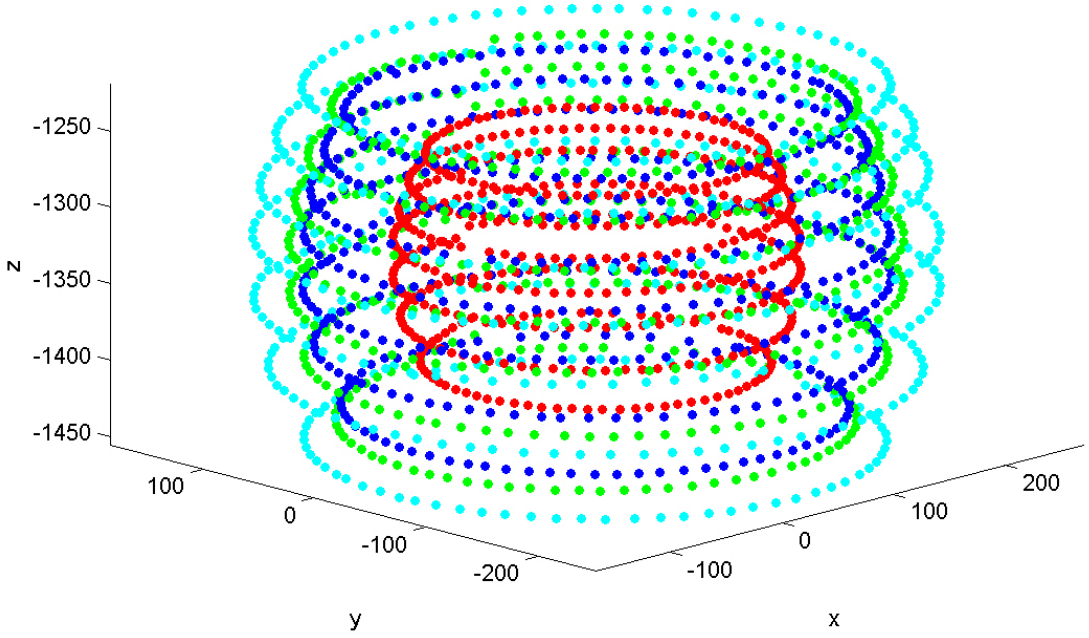

Figure 4-5: Markers locations of the T-shaped active tool.

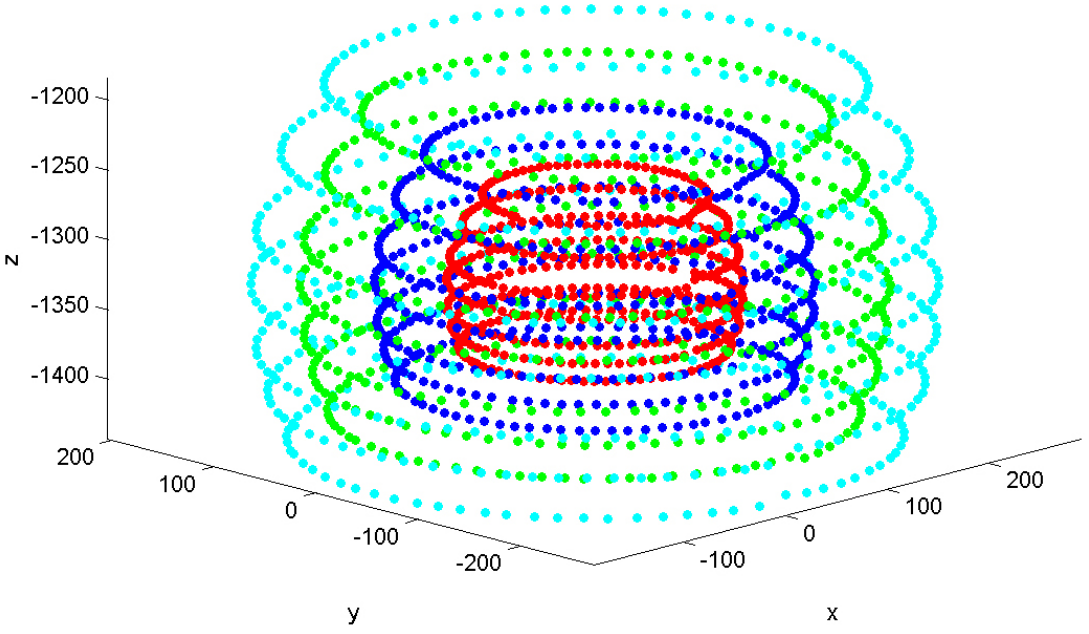

Figure 4-6: Markers locations of the V-shaped active tool.

In the Figures 4-1 to 4-6, each circle of points parallel to the *xy* plane shows a marker's locations for a tilt angle. As it can be seen in the figures, all markers had a spherical motion and moved on circles that were centered at a fixed target location. The inner circles represent the markers that were closer to the target locations and the outer ones are for the markers which located further from the target. The locations of markers are plotted with different colors. Therefore, each color in a plot represents a specific marker on a tool. With this coloring, it is easier to see and track the movement of a marker in a data set.

4.2. Target Location Plots

In our experiments, we aimed to measure TRE in order to compare it to the theoretical models of TRE. For this purpose, we needed to find the target location by using the transformations that were reported by the tracking system. Therefore, we used the method that was explained in Section 3.1 to calculate the target location of each tool. Then, we plotted the calculated target location for each tilt angle. Figures 4-7 to 4-12 presents the plotted target locations for the tools.

The plots show the spread of the calculated values of target location for each tool. Based on the design of the experimental apparatus, which was discussed in the previous chapter in Section 3.2.3, we were confident that the target was fixed while collecting each set of data. However, we can clearly see from the plots that the calculated values of target location change as the orientation of the tool changes.

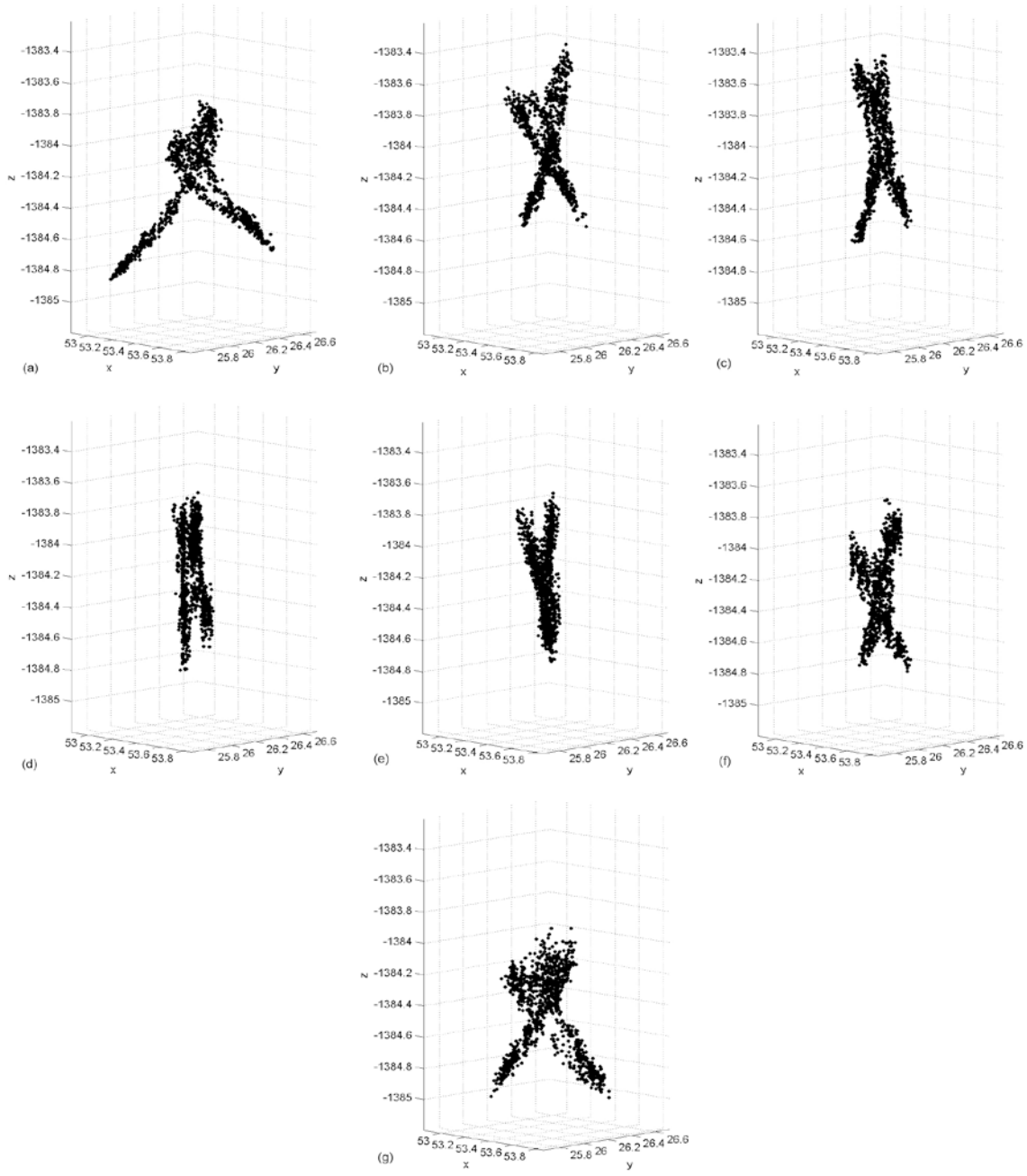

Figure 4-7: Calculated target locations of the T-shaped passive tool for each tool orientation. (a) -30º tilt angle. (b) -20º tilt angle. (c) -10º tilt angle. (d) 0º tilt angle. (e) 10º tilt angle. (f) 20º tilt angle. (g) 30º tilt angle.

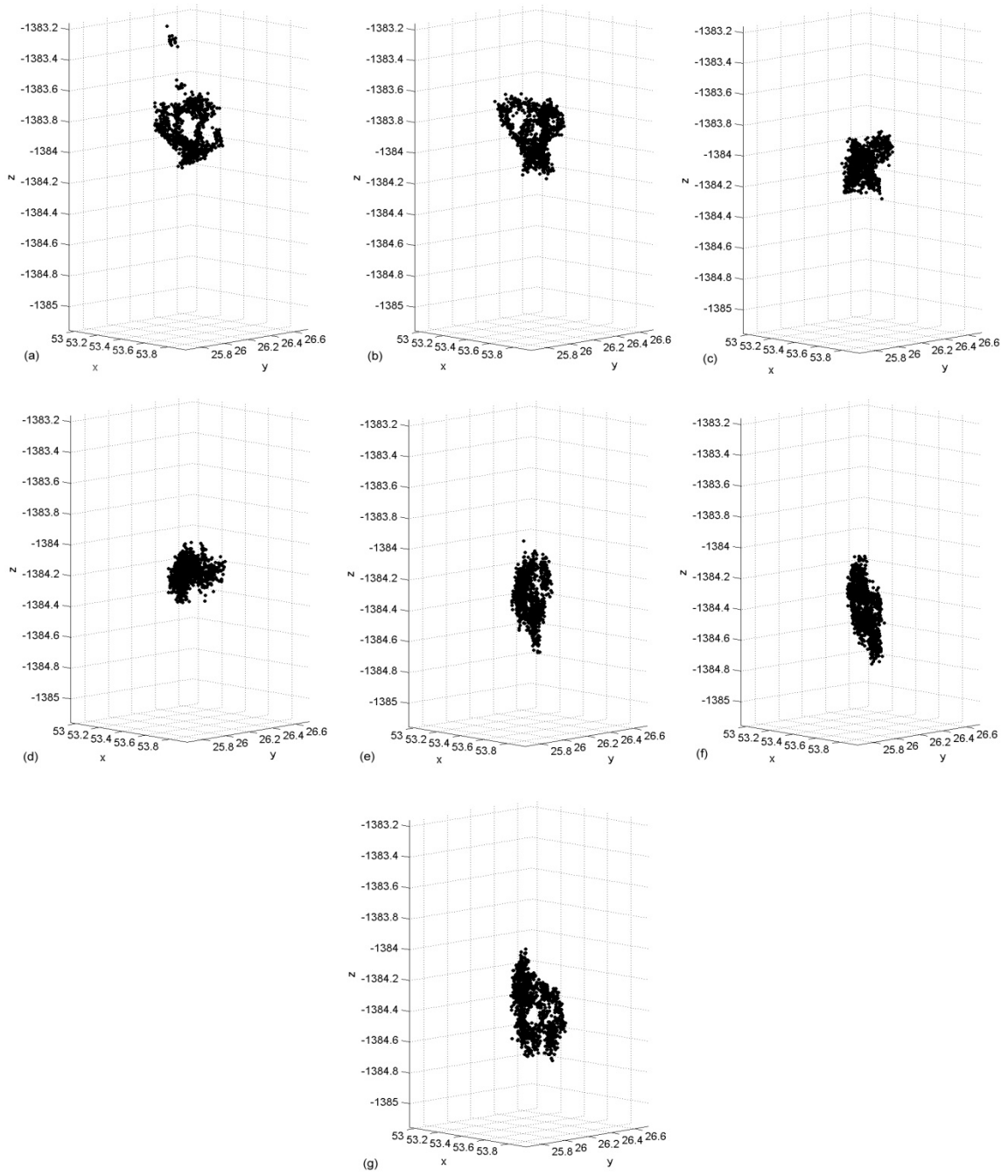

Figure 4-8: Calculated target locations of the V-shaped passive tool for each tool orientation. (a) -30º tilt angle. (b) -20º tilt angle. (c) -10º tilt angle. (d) 0º tilt angle. (e) 10º tilt angle. (f) 20º tilt angle. (g) 30º tilt angle.

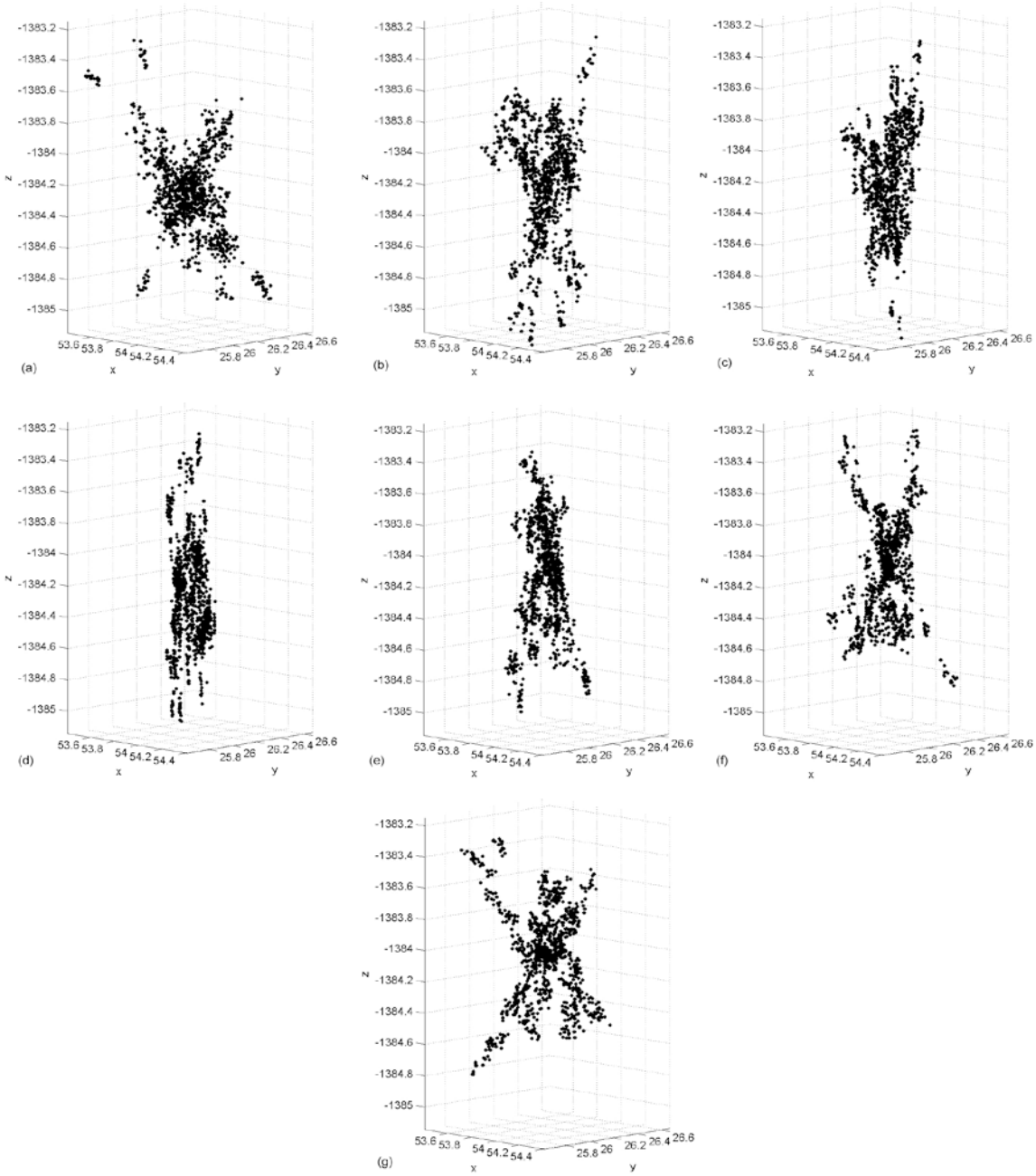

Figure 4-9: Calculated target locations of the T-shaped radix tool for each tool orientation. (a) -30º tilt angle. (b) -20º tilt angle. (c) -10º tilt angle. (d) 0º tilt angle. (e) 10º tilt angle. (f) 20º tilt angle. (g) 30º tilt angle.

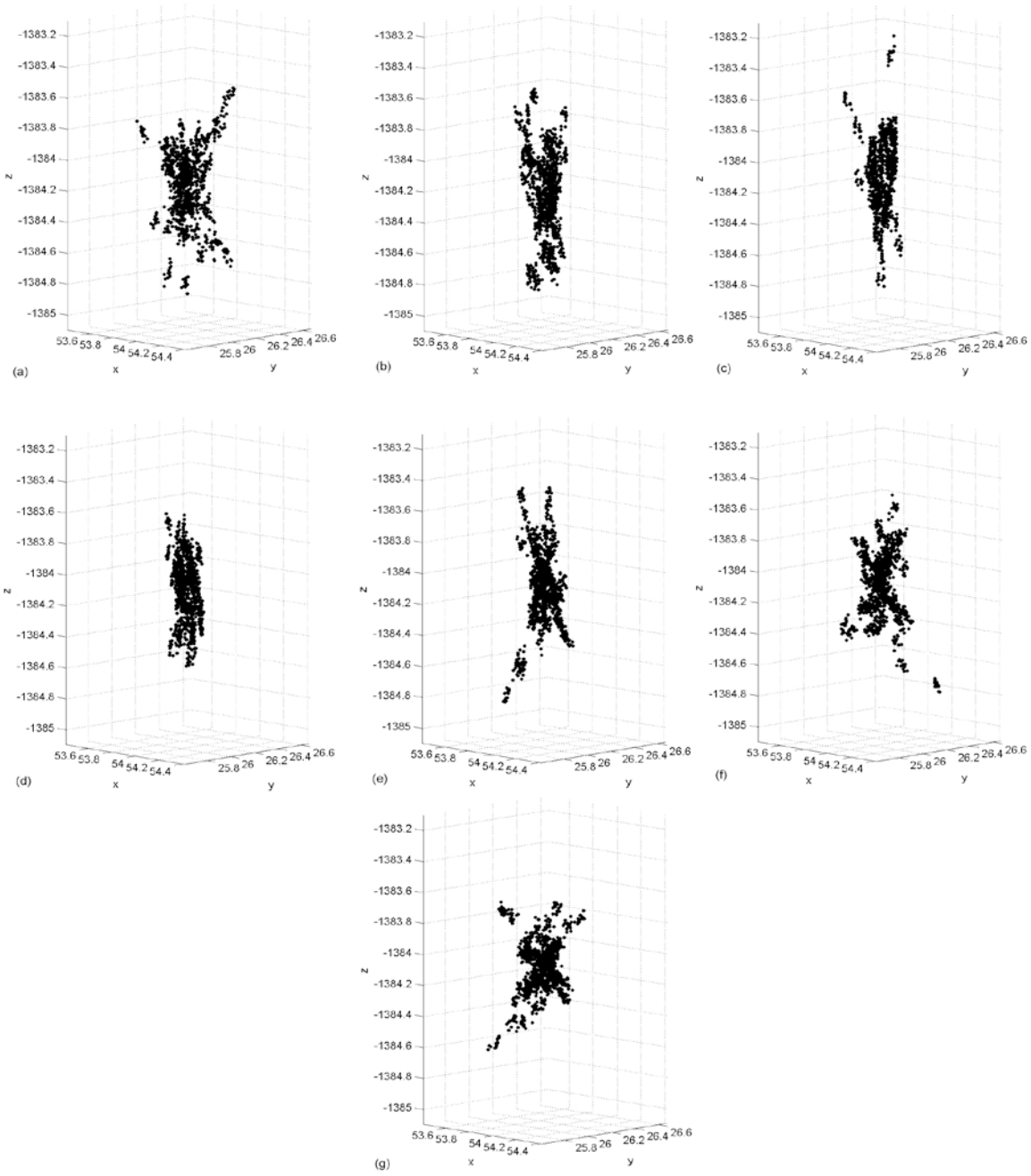

Figure 4-10: Calculated target locations of the V-shaped radix tool for each tool orientation. (a) -30º tilt angle. (b) -20º tilt angle. (c) -10º tilt angle. (d) 0º tilt angle. (e) 10º tilt angle. (f) 20º tilt angle. (g) 30º tilt angle.

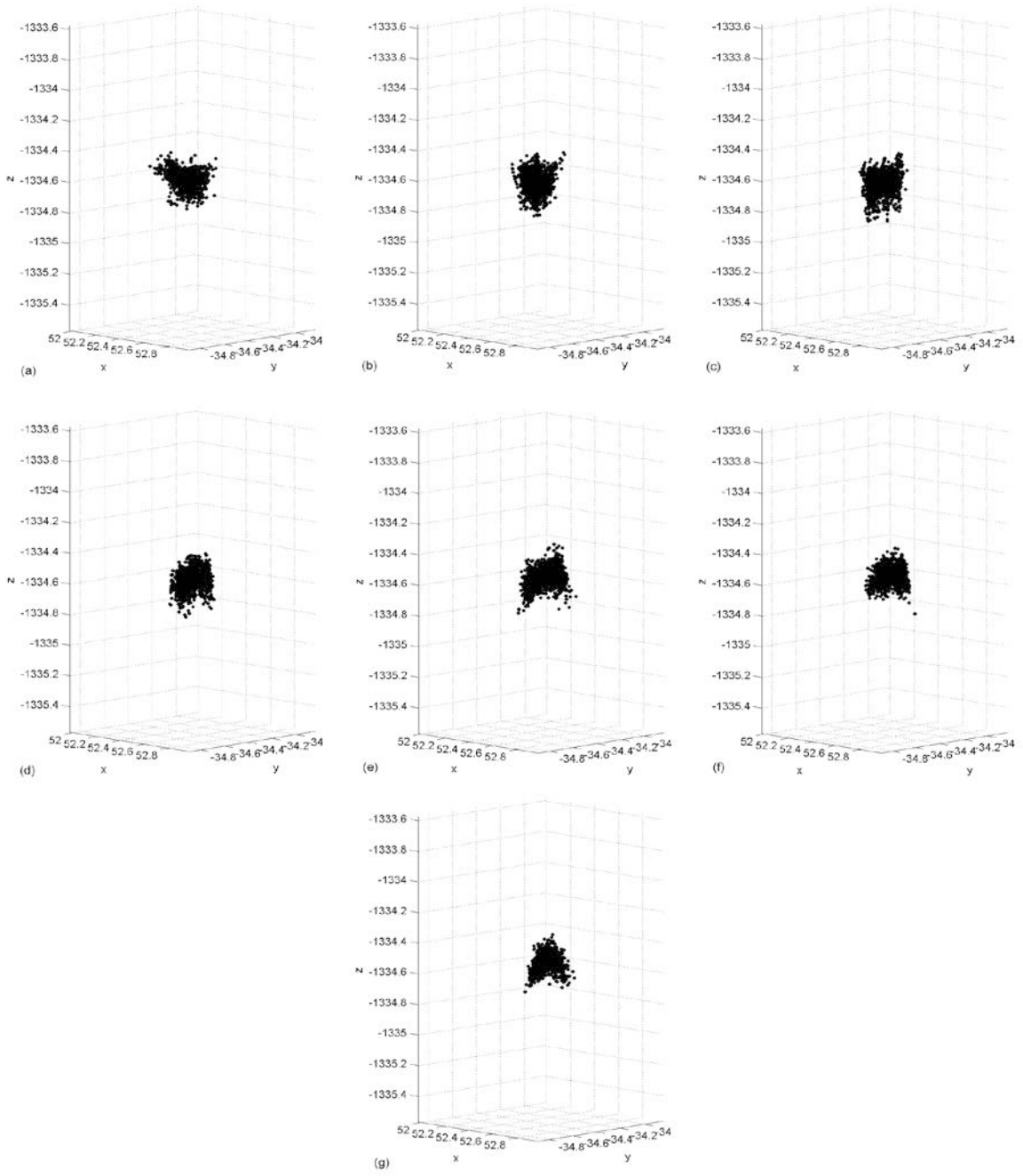

Figure 4-11: Calculated target locations of the T-shaped active tool for each tool orientation. (a) -30º tilt angle. (b) -20º tilt angle. (c) -10º tilt angle. (d) 0º tilt angle. (e) 10º tilt angle. (f) 20º tilt angle. (g) 30º tilt angle.

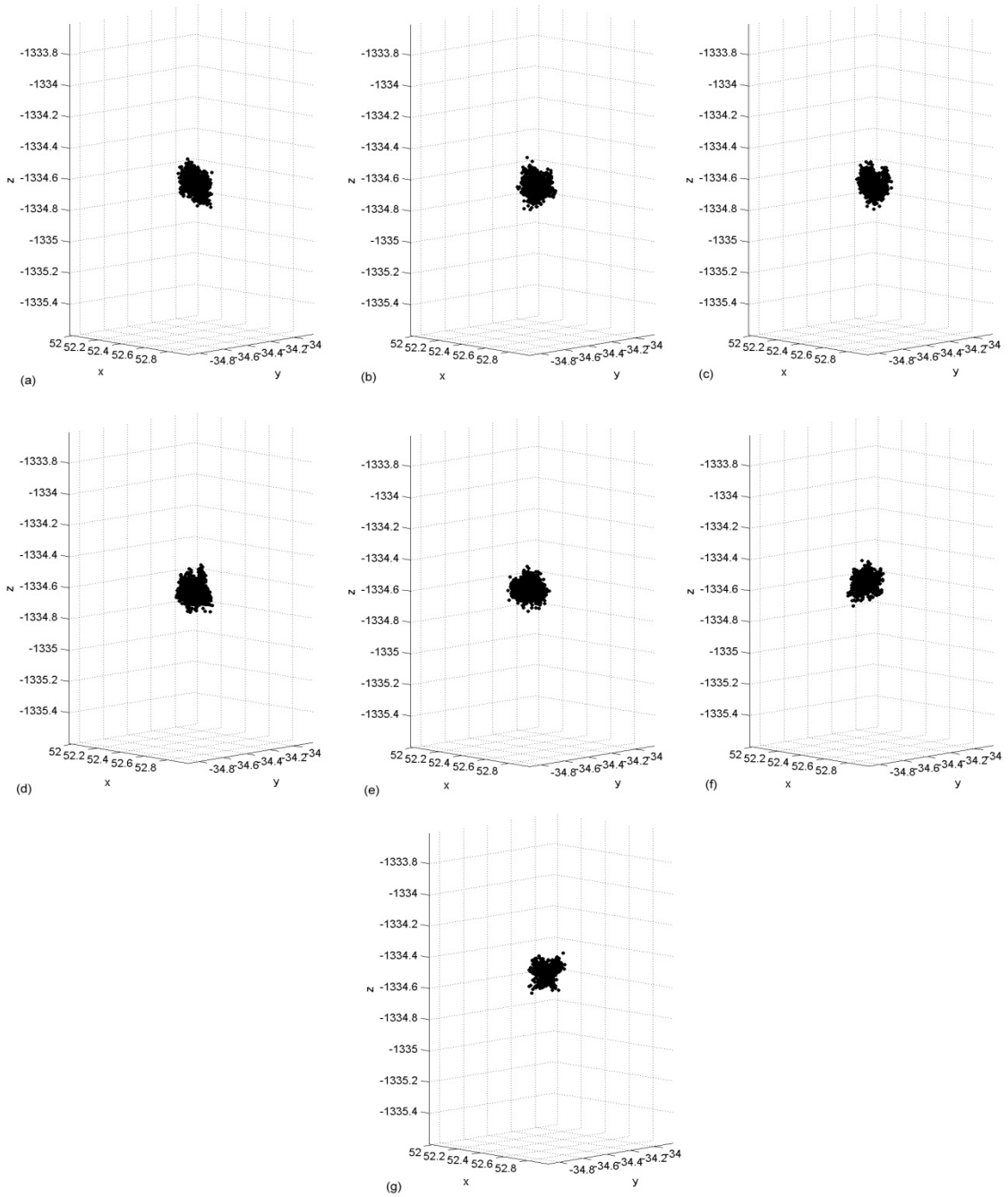

Figure 4-12: Calculated target locations of the V-shaped active tool for each tool orientation. (a) -30º tilt angle. (b) -20º tilt angle. (c) -10º tilt angle. (d) 0º tilt angle. (e) 10º tilt angle. (f) 20º tilt angle. (g) 30º tilt angle.

4.3. Root-Mean-Squared TRE

In order to see the differences between TRE measurements, we calculated the root-mean-squared (RMS) value of TRE for each tool orientation. This enabled us to analyze the effect of handle orientation on TRE. To visualize the calculated RMS TRE values and compare them, we plotted the RMS TRE values versus the tilt angle for each tool. Figures 4-13 to 4-18 show these plots for all six tools that were used in the experiments. Essentially, a smaller RMS TRE of a tilt angle shows that the tracking system can track the target more accurately when the tool is tilted at that angle.

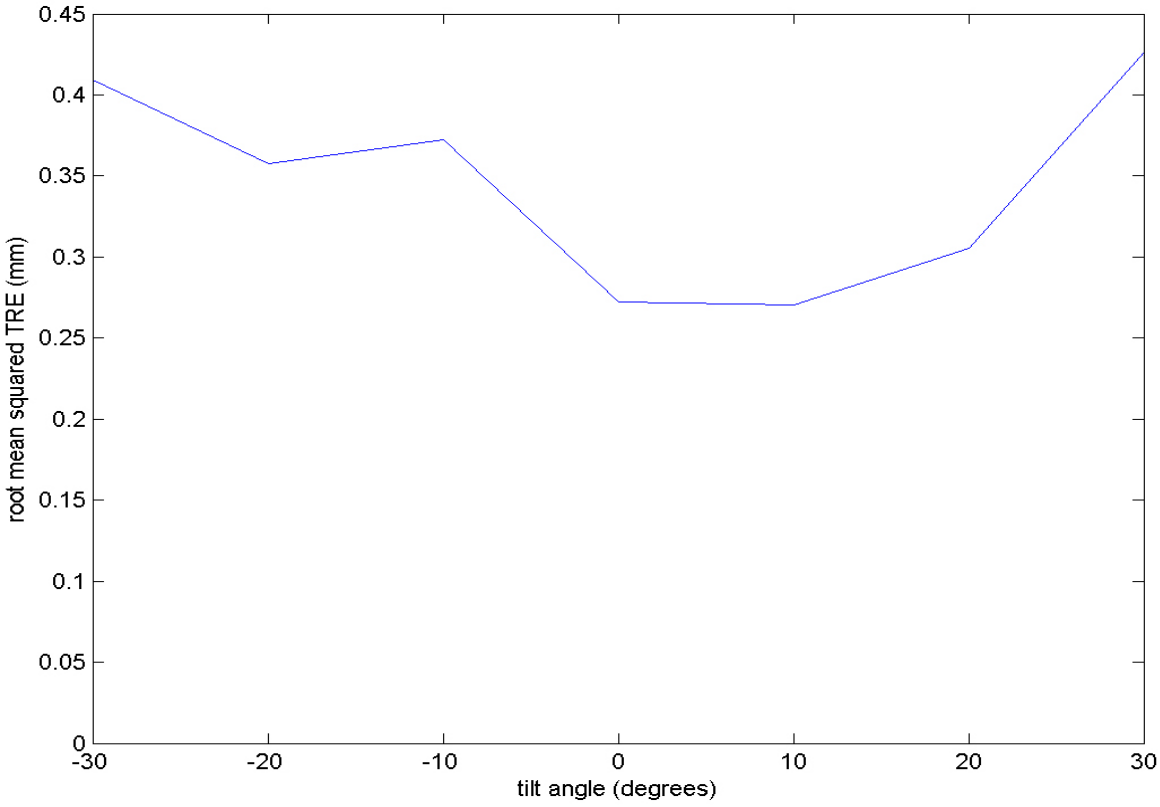

Figure 4-13: RMS TRE versus tilt angle for the T-shaped passive tool.

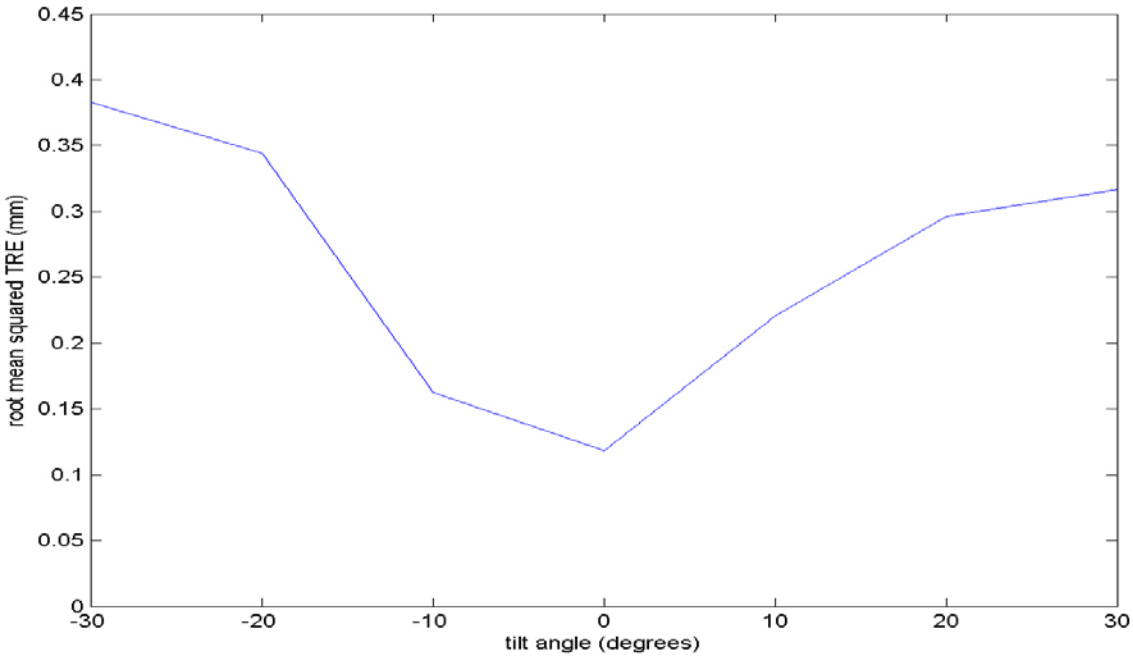

Figure 4-14: RMS TRE versus tilt angle for the V-shaped passive tool.

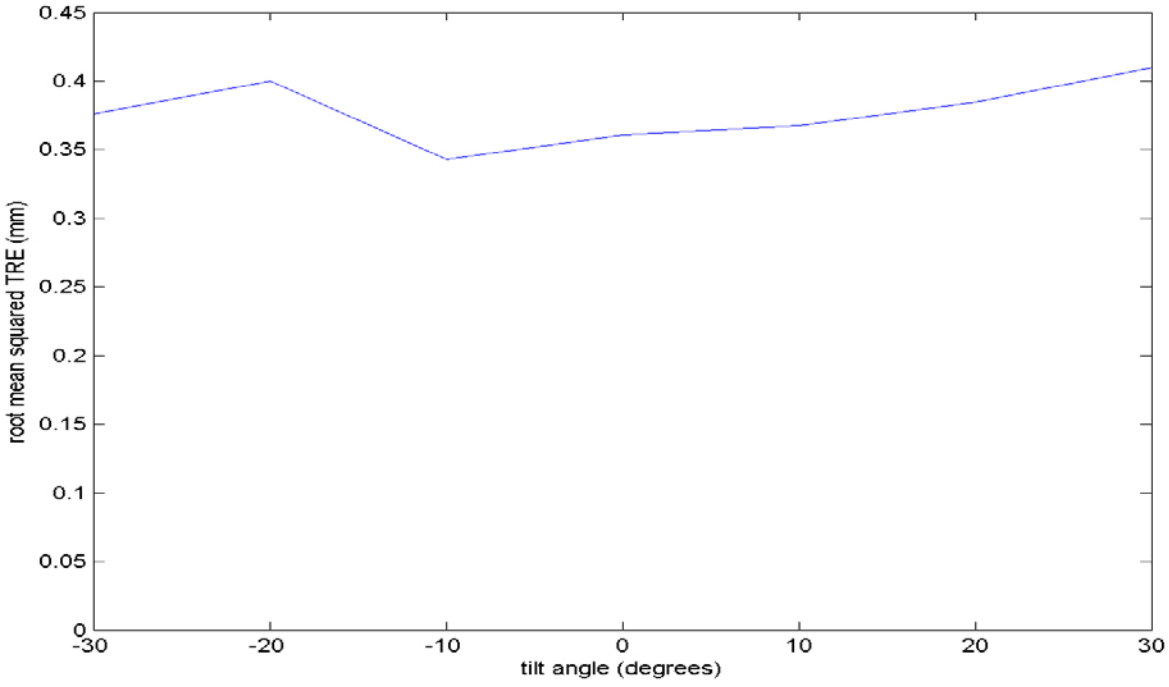

Figure 4-15: RMS TRE versus tilt angle for the T-shaped radix tool.

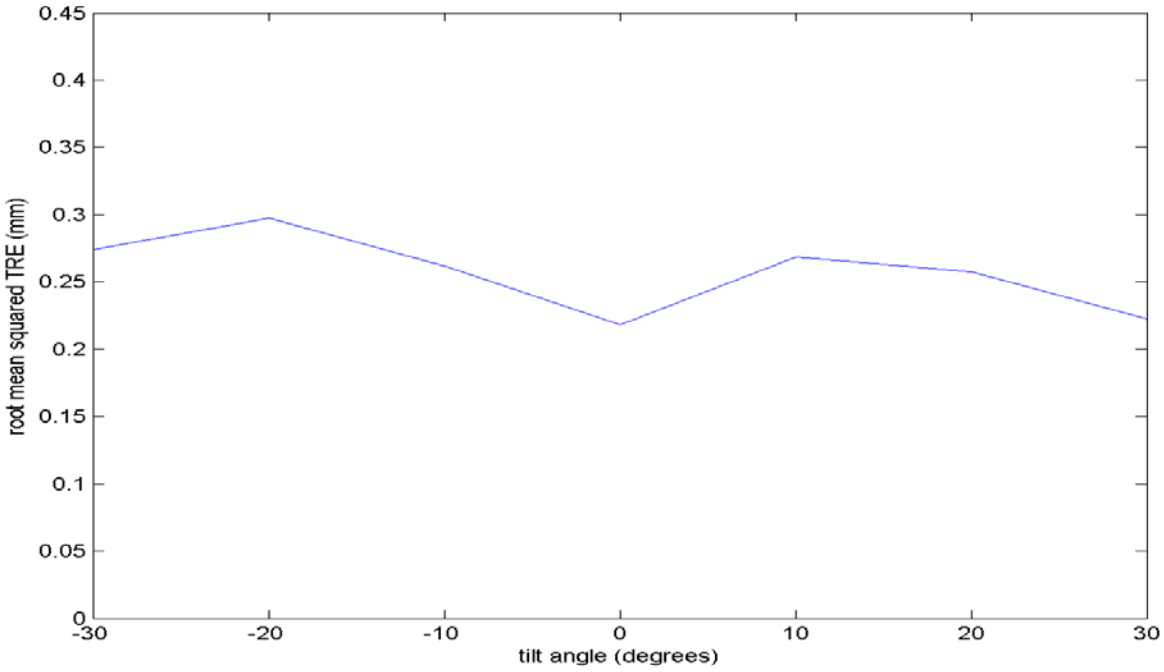

Figure 4-16: RMS TRE versus tilt angle for the V-shaped radix tool.

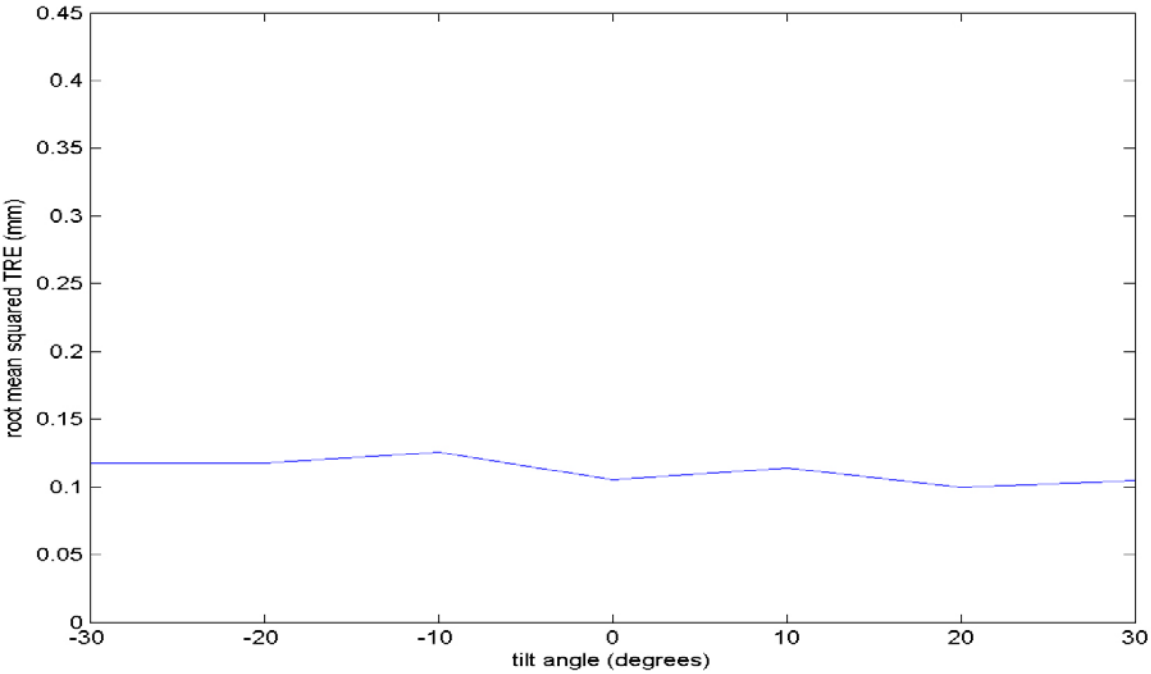

Figure 4-17: RMS TRE versus tilt angle for the T-shaped active tool.

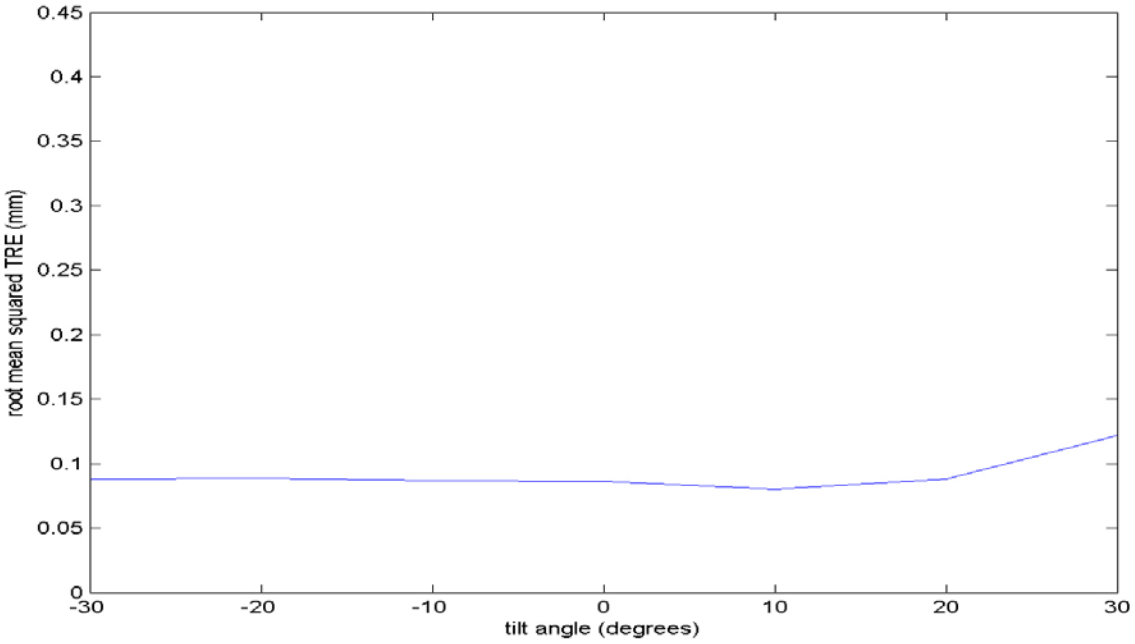

Figure 4-18: RMS TRE versus tilt angle for the V-shaped active tool.

4.4. Hybrid Configuration Experiment

In the experiments that were presented previously, we used tracking targets with the same type of markers (i.e., both tools were passive, active or radix). NDI Polaris Spectra tracking system can track different types of tools simultaneously. To study the behavior of the tracking system in the case of hybrid tracking (i.e., when different type of tools are being track at the same time), we performed the experiment described in Section 3.2.4 using T-shaped active tool and V-shaped passive tool. We had to use the tools with different configurations of markers because the tracking system was not able to track the tools with the same markers configurations even when the markers types were different.

In the following sections the plots of target location and RMS TRE for this experiment are presented. The marker locations plots can be found in the Appendix.

4.4.1 . Target Location Plots

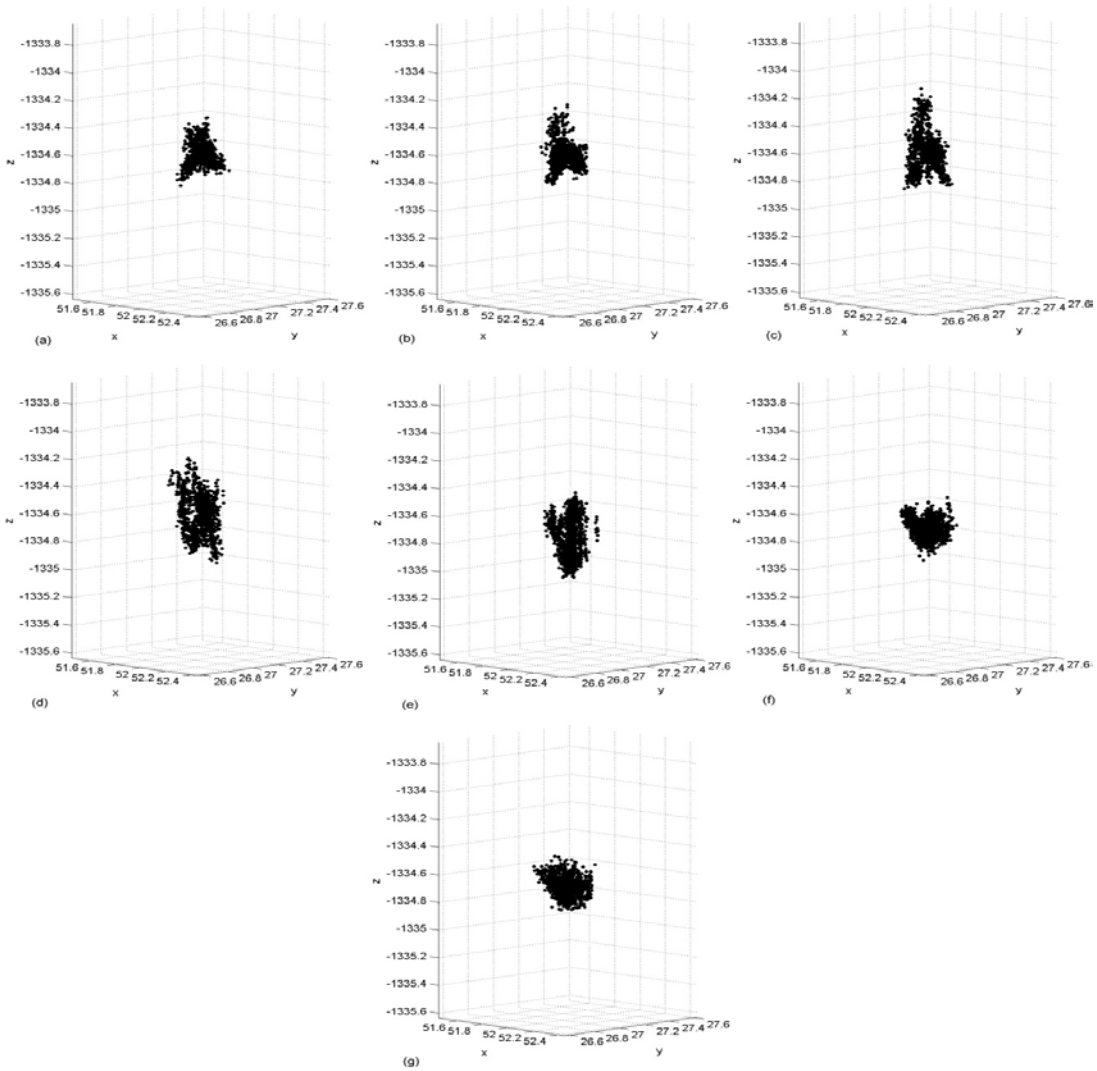

Figure 4-19: Calculated target locations of the T-shaped active tool for each tool orientation. (a) -30º tilt angle. (b) -20º tilt angle. (c) -10º tilt angle. (d) 0º tilt angle. (e) 10º tilt angle. (f) 20º tilt angle. (g) 30º tilt angle.

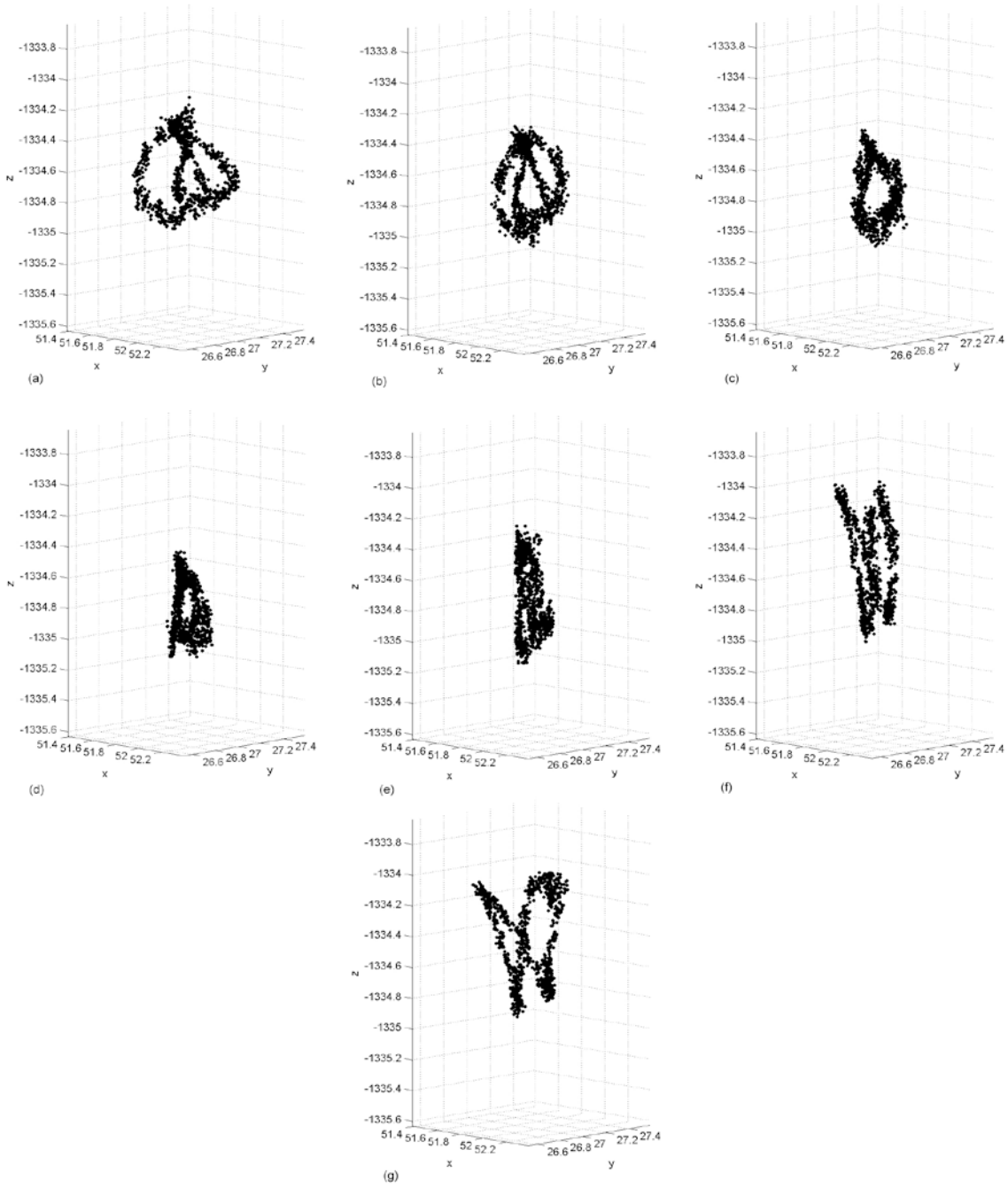

Figure 4-20: Calculated target locations of the V-shaped passive tool for each tool orientation. (a) -30º tilt angle. (b) -20º tilt angle. (c) -10º tilt angle. (d) 0º tilt angle. (e) 10º tilt angle. (f) 20º tilt angle. (g) 30º tilt angle.

4.4.2 . Root-Mean-Squared TRE

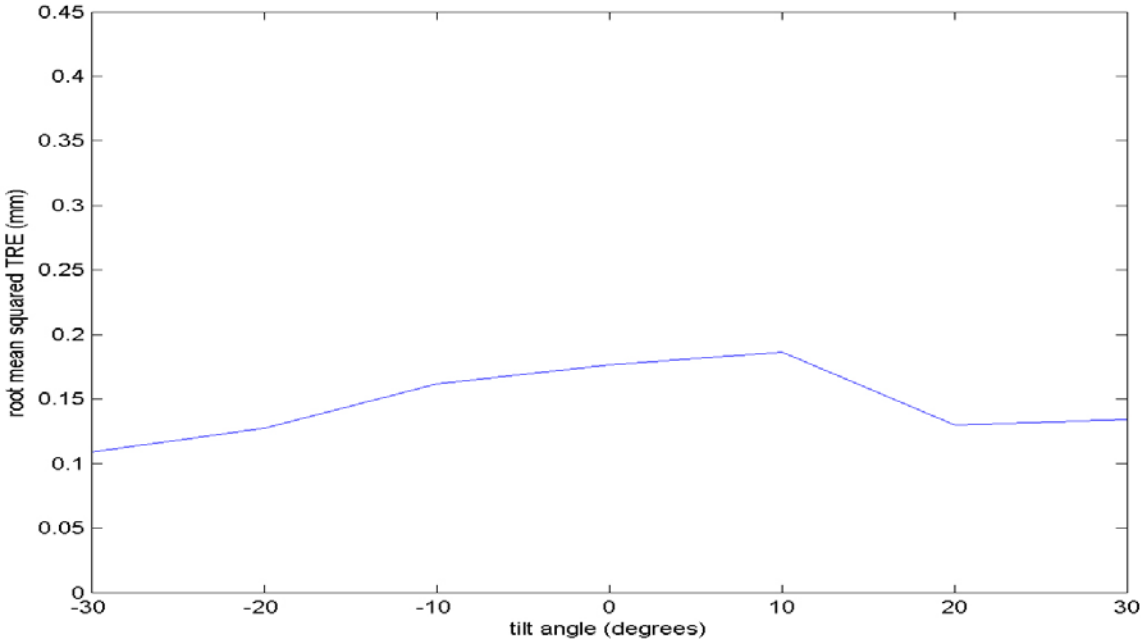

Figure 4-21: RMS TRE versus tilt angle for the T-shaped active tool.

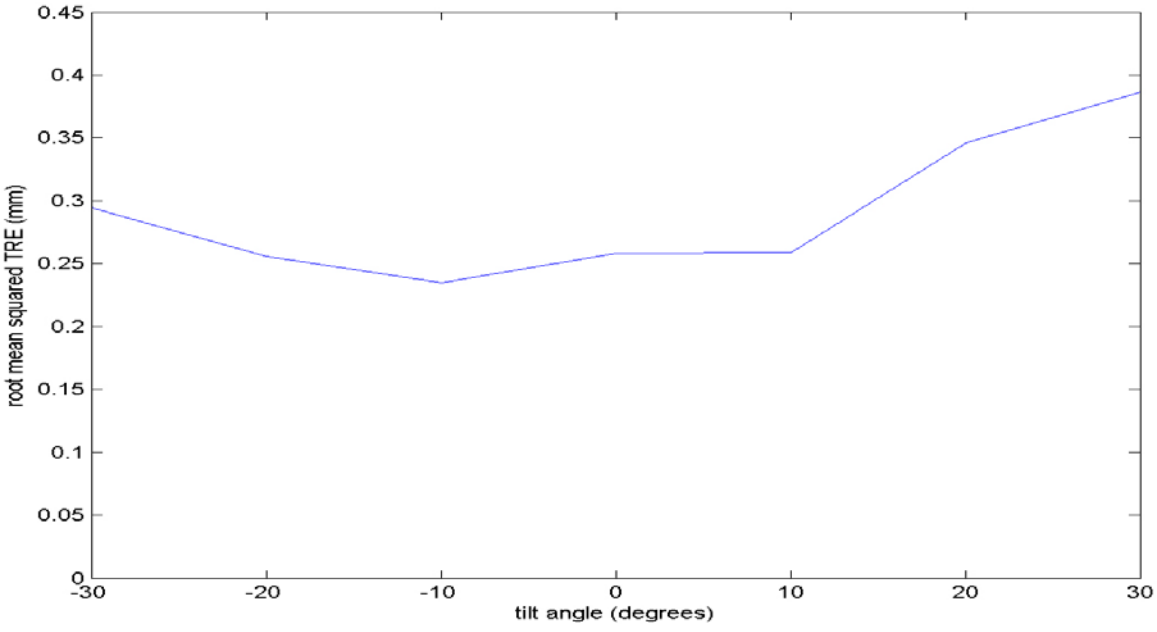

Figure 4-22: RMS TRE versus tilt angle for the V-shaped passive tool.

Chapter 5
Discussion and Conclusion

In this thesis, we studied the effect of tool orientation on the tracking accuracy of an actual optical tracking system. This is important because tracking accuracy is a major issue in the design of surgical guidance systems. Currently, most of the recommendations on best tool orientations for reliable tracking are based on the theoretical models of TRE. Knowing the real behavior of optical tracking systems in terms of tracking accuracy is beneficial in both design and application of surgical navigation systems. In this work, we empirically investigated the relation between tool orientation and TRE to understand the error behavior of an actual optical tracking system. We also compared our results with the theoretical predictions of TRE.

The first step in our work has been the design of experiments to measure TRE for different orientations of a tool. As detailed in Chapter 3, we designed and implemented an experimental setup in a way that we were confident the target location was fixed during each experiment for all tool orientations. Other studies that measure TRE, such as (Thompson, Penney, Dasgupta, & Hawkes, 2013), use a tracked and calibrated pointing stylus that is pivoted in a divot. Such a setup limits the range of motion of the stylus to a small conical volume above the divot. In comparison, our apparatus permits a range of motion of approximately ±40 degrees of tilt and a full 360 degrees of rotation about the target location. We also developed software for recording the tracking information from

the tracker. Then we collected data in a variety of experiments using different types of tools (i.e., passive, Radix and active tools) each with two different configurations of the fiducial markers.

In chapter 4, we analyzed the collected data from the experiments. First, we presented the plots of markers locations for each handle (Figures 4-1 to 4-6). These plots showed that the motion of the markers during an experiment were approximately spherical and centered at a fixed target location. Next, we calculated target location for each handle using Equation 3-8 (see Section 3.1 in Chapter 3). Then the calculated values of target location were plotted per tilt angle for each handle (Figures 4-7 to 4-12).

Figures 4-7, 4-8, 4-10, and 4-11 show the estimated target location for the passive marker type tools (spherical passive markers and Radix markers). The error in the estimated target locations in these plots is not randomly distributed; instead, there is clear evidence of structure in the target location that depends on the tool orientation. In all cases, the structure in the target location error becomes more apparent as the magnitude of the tilt angle increases. The structure is least apparent when the tilt angle of the tool is 0º (tool is directly facing the tracking system camera unit).

Figures 4-9 and 4-12 show the estimated target location for the active marker tools. The errors in the estimated target locations in these plots are dramatically different in comparison with those for the passive marker tools. At the scale used in the plots, there is less evidence of structure in the target location and there are no obvious trends that depend on the tool tilt angle. The errors are much smaller compared to the passive and

Radix markers. Despite their superior precision, active markers are not commonly used in surgical applications because active marker tools require a power source. Electrically powered targets are more difficult to construct to withstand sterilization processes. If the tool is powered via a wired connection, the tethering effect of the wire can compromise the ergonomics of the tool.

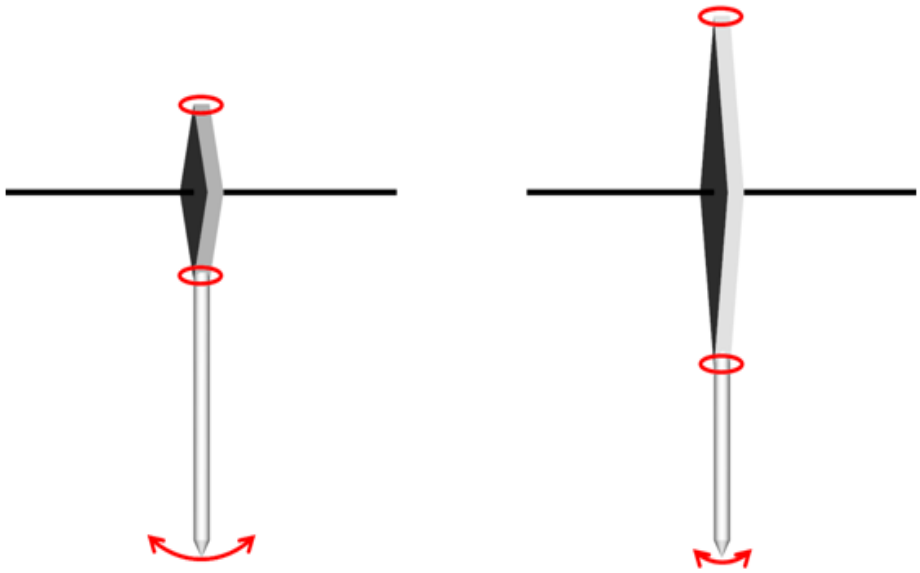

Figure 5-1: A short target (left) produces a larger TRE (red arrows) at the stylus tip compared to a long target (right) for a given FLE (red ellipses). Both targets are directly pointing along the z axis (horizontal black line) of the tracking system reference frame. The rotational error induced by the FLE is smaller for the long target, which in turn, leads to smaller TRE at the stylus tip.

The arrangement of markers on a tool also affects the behaviour of TRE. For each marker type, the RMS TRE is lower for the V-shaped tool compared to the T-shaped tool. This can be explained by the fact that the arrangement of markers on the V-shaped target is significantly longer than the T-shaped target. A long target produces lower TRE for a given FLE because the FLE induces a smaller rotational error in the longer target (see Figure 5-1). The situation is analogous to fitting a straight line between two noisy points; the variance in the slope of the estimated line decreases as the distance between points increases. It should be noted that the length of a target is defined as the distance between the centroid of the markers and the target location. This is different from the length of the tool, which is the distance between the tip of a tool and the farthest marker from the tool tip.

One of the assumptions made in all of the theoretical models of TRE is that FLE in a single marker can be modelled as a zero-mean Gaussian random variable; furthermore, the models assume that FLE is independent between markers. Given zero-mean, independent Gaussian noise in the measured marker locations, we would not expect to observe the strong patterns in the estimated target locations shown in Figures 4-7, 4-8, 4-10, and 4-11. From these observations, we can conclude that FLE in the Spectra tracking system is either biased (with the bias varying as a function of tilt and rotation angle), not independent (correlated), or both biased and correlated. Similar observations

of bias were described by (Thompson, Penney, Dasgupta, & Hawkes, 2013) for a different and supposedly more accurate tracking system.

We can compare our results for RMS TRE using the passive marker tools to the values predicted by models of TRE[1]. The predicted values of RMS TRE as a function of tilt angle for the T-shaped and V-shaped tools are shown in Figure 5-2; these values were obtained using the spatial-stiffness model of Ma et al. (Ma, Moghari, Ellis, & Abolmaesumi, Estimation of optimal fiducial target registration error in the presence of heteroscedastic noise, 2010) and the FLE covariance matrix for passive markers reported by Simpson et al. (Simpson, Dillon, Miga, & Ma, 2013). Comparing Figure 5-2 to Figures 4-12 and 4-13, we see that the patterns of the measured RMS TRE values do not match the predicted values. In particular, the measured values do not peak at zero degrees of tilt angle as occurs with the predicted values. The mismatch between measured and predicted TRE is not surprising given the observed bias/correlation in FLE.

A potential criticism of our work is that we have relied on a manufacturer's stated tolerance for the sphericity of the ball bearings in our experimental apparatus. If the shape of the main ball bearing was not close to spherical then that could partially explain the patterns we observed in the estimated target location; however, we would expect to

[1] We were not able to compute the predicted values of RMS TRE for the Radix and active marker tools because the FLE for these types of markers are not known. We were not able to measure the FLE for these types of markers using the techniques reported by Simpson et al. (Simpson, 2013) because we did not have easy access to a programmable, high precision robotic arm with a spherical wrist.

see such patterns for all of the marker types, and we did not observe strong patterns in the active marker tools.

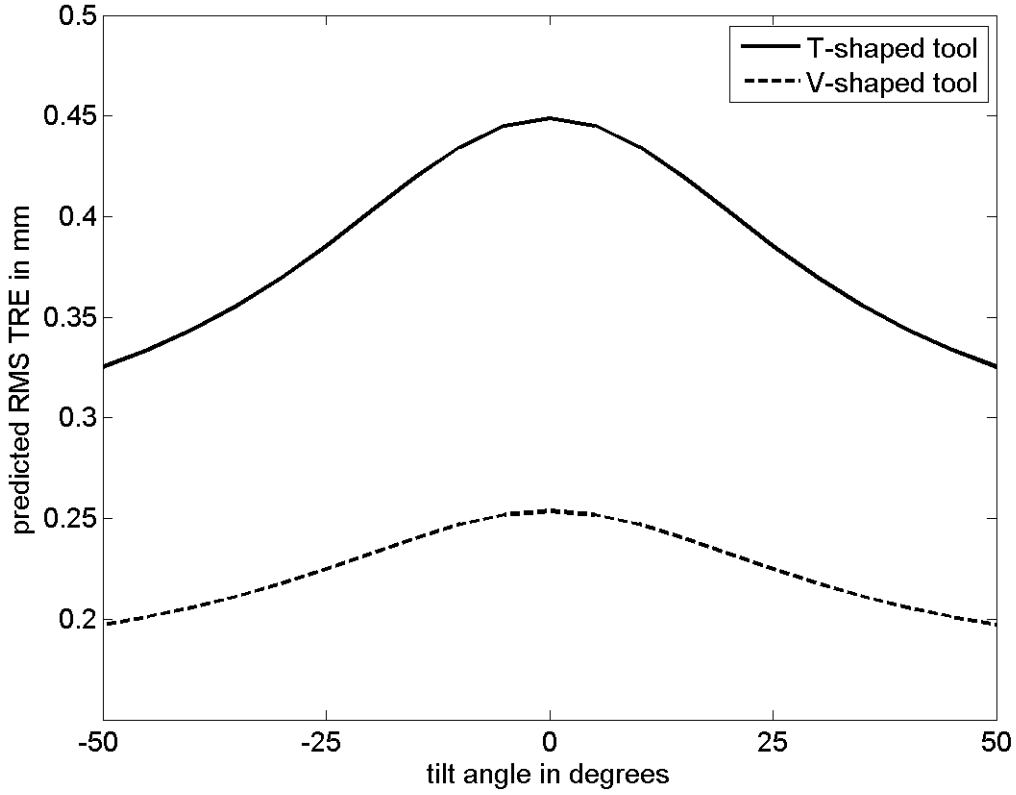

Figure 5-2: Predicted RMS TRE using the spatial-stiffness model of Ma et al. (Ma, Moghari, Ellis, & Abolmaesumi, Estimation of optimal fiducial target registration error in the presence of heteroscedastic noise, 2010)for the T-shaped and V-shaped passive marker tools. The model predicts peak values of TRE at 0 degrees of tilt angle.

Another factor that might have affected our measurements is the design of the active tools. As it can be seen in figure 3-6, we used insulating tape to fix the wires on the tools. Although unlikely, the tape might have reduced the amount of spurious infrared

light reflected from the body of the tool compared to the passive tools which had no tape on them. The reduction in spurious reflections might have contributed to the better performance of the active tools. This could easily be confirmed by wrapping the passive tools in the same tape.

5.1 Future Work

While we have brought our study to fruition, research is a continuous process. Future work can be focused on studying the effect of tool design factors such as the length of a tool or the markers configuration, on measured TRE. Of particular interest is the effect of non-planar marker configurations on TRE. Simulation results have suggested that non-planar marker configurations compared to planar configurations are less sensitive to changes in orientation relative to the tracking system and to anisotropy in FLE (Ma, Moghari, Ellis, & Abolmaesumi, Estimation of optimal fiducial target registration error in the presence of heteroscedastic noise, 2010). Currently, planar targets are the most commonly used configuration of markers used in surgical navigation systems, but this could change if evidence was provided for the superiority of non-planar configurations.

We studied the TRE behaviour of a single tool in isolation. In practice, two tools are used for navigation purposes. One tool, called the reference tool, is rigidly attached to the patient's anatomy and the surgical tool or tools are tracked relative to the patient tool. Relative tracking is used so that motion of the patient does not affect the tracking accuracy. An extension of our current work would be to study the behaviour of TRE when relative tracking is used. At first glance, our current data sets seem to contain

exactly the measurements we would require (two tools both rotating about the same center point); unfortunately, both tools remain stationary relative to each other in our current apparatus. Ideally, we would be able to rotate both tools independently about a common center point, which would require a redesign and rebuild of our apparatus.

Another area that can be investigated is measuring the tracking accuracy when multiple tools with different type of markers are being tracked at the same time (e.g., tracking active and passive tools simultaneously). This kind of work may shed light on some of the less studied underlying factors behind the accuracy of optical tracking systems and help us to design and use these systems with more confidence.

There are features of our apparatus that could be further improved. We could use a central ball bearing with sphericity traceable to an official standard to eliminate the possibility that we were using a non-spherical bearing. We could increase the range of tilt angle by redesigning the mount that attaches the tools to the central ball bearing. A more substantial undertaking would be to redesign the apparatus so that the tilt and rotation angles could be controlled by computer so that we would not have to manually manipulate the apparatus; this would remove the tedium of data collection, and possible speed up the rate of data collection.

5.2 Conclusion

In conclusion, we investigated how tool orientation affects the tracking accuracy of an optical tracking system. For this purpose, we designed and built an experimental setup and developed software which enabled us to obtain the markers locations and

transformations of a tool in different orientations. The key design feature of our apparatus is that it allowed tools to be rotated about a stationary center point through almost ±40 degrees of tilt and a full 360 degrees of rotation. Through a variety of experiments, we measured the target locations of the tools and calculated TRE for different tool orientations. Based on our results, active tools had the smallest spread of measured target locations in each experiment. This means that the tracking system can track tools with active markers more precisely than other types of markers. On the other hand, Radix tools were shown to have the widest spread of measured target locations in each experiment which means that they are the least precise type of tools. The precision in tracking the passive tools were somewhere in between the other two types of tools. We also calculated RMS TRE for each tilt angle. We concluded that unlike theoretical predictions of TRE, the actual measured TRE is the smallest when a tool is parallel to the tracking system's camera plane and it increases as the tool tilted from this orientation. This conclusion was true for all three different types of tools. We believe that our findings can be of great use in design and application of optical tracking systems in general and more specifically for improving the accuracy of clinical guidance applications.

Bibliography

Balachandran, R., Fitzpatrick, M., & Labadie, R. F. (2005). Fiducial registration for tracking systems that employ coordinate reference frames. *SPIE Medical Imaging: Visualization, Image-Guided, and Display, 5744*, pp. 126-138. San Diego, CA.

Barnett, G. H., Kormos, D. W., Steiner, C. P., & Weisenberger, J. (19930). Intraoperative localization using an armless, frameless stereotactic wand. *Journal of Neurosurgery , 78* (3), 510-514.

Bejek, Z., Sólyom, L., & Szendrõi, M. (2007). Experiences with computer navigated total knee arthroplasty. *International orthopaedics, 31*(5), 617-622.

Chassat, F., & Lavallee, S. (1998). Experimental protocol of accuracy evaluation of 6-D localizers for computer-integrated surgery: Application to four optical localizers. *Medical Image Computing and Computer-Assisted Interventation — MICCAI'98* (pp. 277-284). Cambridge, MA, USA: Springer Berlin Heidelberg.

Danilchenko, A., & Fitzpatrick, J. M. (2010). General approach to error prediction in point registration. *IEEE Transactions on Medical Imaging , 30* (3), 679-693.

Fitzpatrick, J. M. (2009). Fiducial registration error and target registration error are uncorrelated. *SPIE Medical Imaging: Visualization, Image-Guided Procedures, and Modeling. 7261*. Lake Buena Vista, FL: SPIE.

Fitzpatrick, M., & West, J. B. (2001). The distribution of target registration error in rigid-body point-based registration. *IEEE Transactions on Medical Imaging , 20* (9), 917-927.

Fitzpatrick, M., West, J. B., & Maurer, C. R. (1998). Predicting error in rigid-body point-based registration. *IEEE Transactions on Medical Imaging , 17* (5), 694-702.

Friets, E. M., Strohbehn, J. W., Hatch, J. F., & Roberts, D. W. (1989). A frameless stereotaxic operating microscope for neurosurgery. *IEEE Transactions on Biomedical Engineering , 36* (6), 608-617.

Galloway, R. L., Edwards, C. A., Lewis, J. T., & Maciumas, R. J. (1993). Image display and surgical visualization in interactive image-guided neurosurgery. *Optical Engineering , 32* (9), 1955-1962.

Hill, D. L., Hawkes, D. J., Gleeson, M. J., Cox, T. C., Strong, A. J., Wong, W. L., et al. (1994). Accurate frameless registration of MR and CT images of the head: applications in planning surgery and radiation therapy. *Radiology* , 447-454.

Hoff, W., & Vincent, T. (2000). Analysis of head pose accuracy in augmented reality. *IEEE Transactions on Visualization and Computer Graphics , 6* (4), 319-334.

Horn, B. K. (1987). Closed-form solution of absolute orientation using unit quaternions. *Journal of Optical Society of America* , 1127-1135.

Horsley, V., & Clarke, R. (1908). The structure and functions of the cerebellum examined by a new method. *Brain , 130* (6), 1449-1452.

Hounsfield, G. (1973). Computerized transverse axial scanning (tomography): Part 1. Description of system. *The British Journal of Radiology , 46* (552), 1016-1022.

Khadem, R., Yeh, C., Sadeghi-Tehrani, M., Bax, M., Johnson, J., Welch, J. N., et al. (2000). Comparative tracking error analysis of five different optical tracking systems. *Computer Aided Surgery , 5* (2), 98-107.

Kosugi, Y., Watanabe, E., Goto, J., Watanabe, T., Yoshimoto, S., Takakura, K., et al. (1988). An articulated neurosurgical navigation system using MRI and CT images. *IEEE Transactions on Biomedical Engineering , 35* (2), 147-152.

Ma, B., & Ellis, R. E. (2003). A spatial-stiffness analysis of fiducial registration accuracy. *Medical Image Computing and Computer-Assisted Intervention. (MICCAI 2003). 2878*, pp. 359-366. Montréal, Canada: Springer Berlin Heidelberg.

Ma, B., & Ellis, R. E. (2006). Analytic expressions for fiducial and surface target registration error. *Medical Image Computing and Computer-Assisted Intervention. (MICCAI 2006). 4191*, pp. 637-644. Copenhagen, Denmark: Springer Berlin Heidelberg.

Ma, B., & Ellis, R. E. (2004). Spatial-stiffness analysis of surface-based registration. *Medical Image Computing and Computer-Assisted Intervention. (MICCAI 2004). 3216*, pp. 623-630. Saint-Malo, France: Springer Berlin Heidelberg.

Ma, B., Moghari, M. H., Ellis, R. E., & Abolmaesumi, P. (2010). Estimation of optimal fiducial target registration error in the presence of heteroscedastic noise. *IEEE Transactions on Medical Imaging , 29* (3), 708-723.

Ma, B., Moghari, M. H., Ellis, R. E., & Abolmaesumi, P. (2007). On fiducial target registration error in the presence of anisotropic noise. *Medical Image Computing and Computer-Assisted Intervention. (MICCAI 2007). 4792*, pp. 628-635. Brisbane, Australia: Springer Berlin Heidelberg.

Matei, B., & Meer, P. (1999). Optimal rigid motion estimation and performance evaluation with bootstrap. *IEEE Computer Society Conference on Computer Vision and Pattern Recognition.* Fort Collins, CO: IEEE.

Maurer, C. R., Aboutanos, G. B., Dawant, B. M., Maciunas, R. J., & Fitzpatrick, M. (1996). Registration of 3-D images using weighted geometrical features. *IEEE Transactions on Medical Imaging , 15* (6), 836-849.

Maurer, C. R., Fitzpatrick, M., Wang, M., Galloway, R. L., Maciunas, R. J., & Allen, G. S. (1997). Registration of head volume images using implantable fiducial markers. *IEEE Transactions on Medical Imaging* , 447-462.

Maurer, C. R., McCrory, J. J., & Fitzpatrick, J. M. (1993). Estimation of accuracy in localizing externally attached markers in multimodal volume head images. *Medical Imaging 1993: Image Processing* (pp. 43-54). SPIE.

Mogahri, M. H., & Abolmaesumi, P. (2009). Distribution of target registration error for anisotropic and inhomogeneous fiducial localization error. *IEEE Transactions on Medical Imaging , 28* (6), 799-813.

Moghari, M. H., & Abolmaesumi, P. (2006). A high-order solution for the distribution of target registration error in rigid-body point-based registration. *Medical Image*

Computing and Computer-Assisted Intervention. (MICCAI 2006). 4191, pp. 603-611. Copenhagen, Denmark: Springer Berlin Heidelberg.

Moghari, M. H., & Abolmaesumi, P. (2008). Maximum likelihood estimation of the distribution of target registration error. *SPIE Medical Imaging: Visualization, Image-guided Procedures, and Modeling, 6918.* San Diego, CA.

Ohta, N., & Kanatani, K. (1998). Optimal estimation of three-dimensional rotation and reliability evaluation. *European Conference on Computer Vision. (ECCV 98). 1406*, pp. 175-187. Freiburg, Germany: Springer Berlin Heidelberg.

Peters, T., & Clearly, K. (2008). *Image-Guided Interventions: Technology and Applications.* New York: Springer.

Reinhardt, H. F., Horstmann, G. A., & Gratzl, O. (1993). Sonic stereometry in microsurgical procedures for deep-seated brain tumors and vascular malformations. *Neurosurgert , 32* (1), 51-57.

Roberts, D. W., Strohbehn, J. W., Hatch, J. F., Murray, W., & Kettenberger, H. (1986). A frameless stereotaxic integration of computerized tomographic imaging and the operating microscope. *Journal of Neurosurgery* , 545-549.

Shamir, R. R., Joskowicz, L., & Shoshan, Y. (2012). Fiducial optimization for minimal target registration error in image-guided neurosurgery. *IEEE Transactions on Medical Imaging , 31* (3), 725-737.

Sibson, R. (1979). Studies in the robustness of multidimensional scaling: Perturbational analysis of classical scaling. *Journal of the Royal Statistical Society* , 217-229.

Sielhorst, T., Bauer, M., Wenisch, O., Klinker, G., & Navab, N. (2007). Online estimation of the target registration error for n-ocular optical tracking systems. *Medical Image Computing and Computer-Assisted Intervention – MICCAI 2007* (pp. 652-659). Brisbane, Australia: Springer Berlin Heidelberg.

Simpson, A. L., Dillon, N. P., Miga, M. L., & Ma, B. (2013). A framework for measuring TRE at the tip of an optically tracked pointing stylus. *Image-Guided Procedures, Robotic Interventions, and Modeling* .

Steinmeier, R., Rachinger, J., Kaus, M., Ganslandt, O., Huk, W., & Fahlbusch, R. (2000). Factors influencing the application accuracy of neuronavigation systems. *Stereotactic and Functional Neurosurgery , 75* (4), 188-202.

Sugano, N. (2013). Computer-assisted orthopaedic surgery and robotic surgery in total hip arthroplasty. *Clinics in orthopedic surgery, 5*(1), 1-9.

Thompson, S., Penney, G., Dasgupta, P., & Hawkes, D. (2013). Improved modelling of tool tracking errors by modelling dependent marker errors. *IEEE Transactions on Medical Imaging , 32* (2), 165-177.

West, J. B., & Maurer, C. R. (2004). Designing optically tracked instruments for image-guided surgery. *IEEE Transactions on Medical Imaging* (pp. 533-545). Sunnyvale: IEEE.

West, J. B., Fitzpatrick, M., Toms, S. A., Maurer, C. R., & Maciunas, R. J. (2001). Fiducial point placement and the accuracy of point-based, rigid body registration. *Neurosurgery , 48* (4), 810-816.

West, J., Fitzpatrick, M., Wang, M. Y., Dawant, B. M., Maurer, C. R., Kessler, R. M., et al. (1999). Retrospective intermodality registration techniques for images of the head: surface-based versus volume-based. *IEEE Transactions on Medical Imaging , 18* (2), 144-150.

Wiles, A. D., Likholyot, A., Frantz, D. D., & Peters, T. M. (2008). A statistical model for point-based target registration error with anisotropic fiducial localizer error. *IEEE Transactions on Medical Imaging , 27* (3), 378-390.

Woerdeman, P. A., Willems, P. W., Noordmans, H. J., Tulleken, C. A., & van der Sprenkel, J. W. (2007). Application accuracy in frameless image-guided neurosurgery: a comparison study of three patient-to-image registration methods. *Journal of Neurosurgery , 106* (6), 1012-1016.

Appendix
Results of the Other Experiments

In this appendix, we present the results of the other performed experiments, which were not included in chapter 5. As described in chapter 4, in our experiments we collected data when the apparatus was located in three different positions within the tracking volume of the optical tracking system. In chapter 5, we presented the results and analysis for the experiments in which the apparatus was located directly in front of the tracking system's camera (i.e., middle position). This appendix presents the results and analysis for the other experiments in which the apparatus was moved from the original middle position and located to the right and left of the middle location.

We analyzed the results of the experiments in the left and right positions in the same way as the middle position experiments. In the following section, the plots for the experiments in the left position are presented. Next, the results of the experiments in the right position are provided. The plots in this chapter are presented in the same other as chapter 5.

A.1 Results of Left Position Experiments

A.1.1 Marker Locations Plots

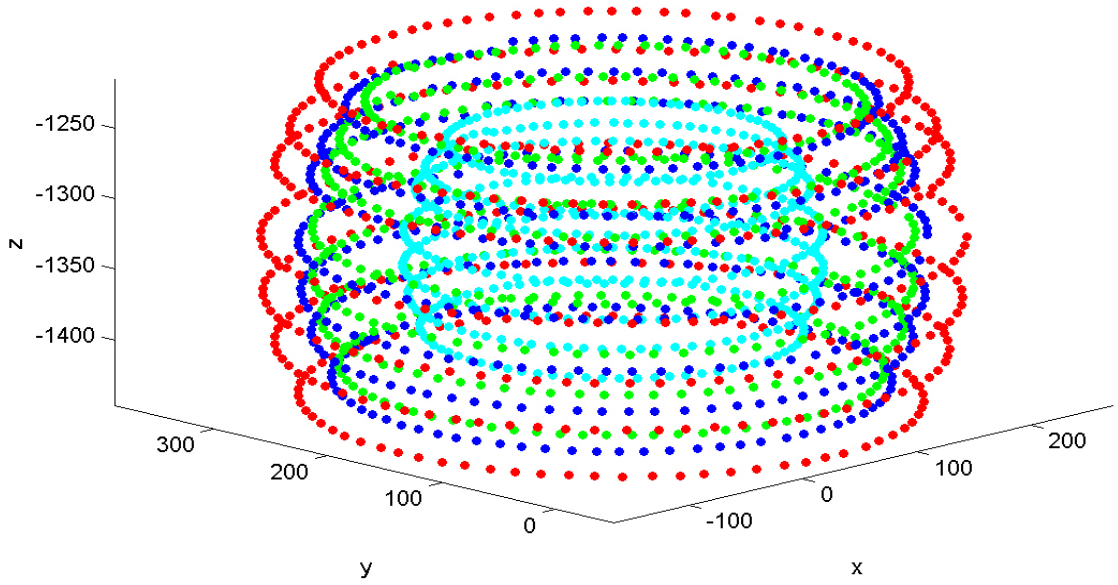

Figure A- 1: Markers locations of the T-shaped passive tool.

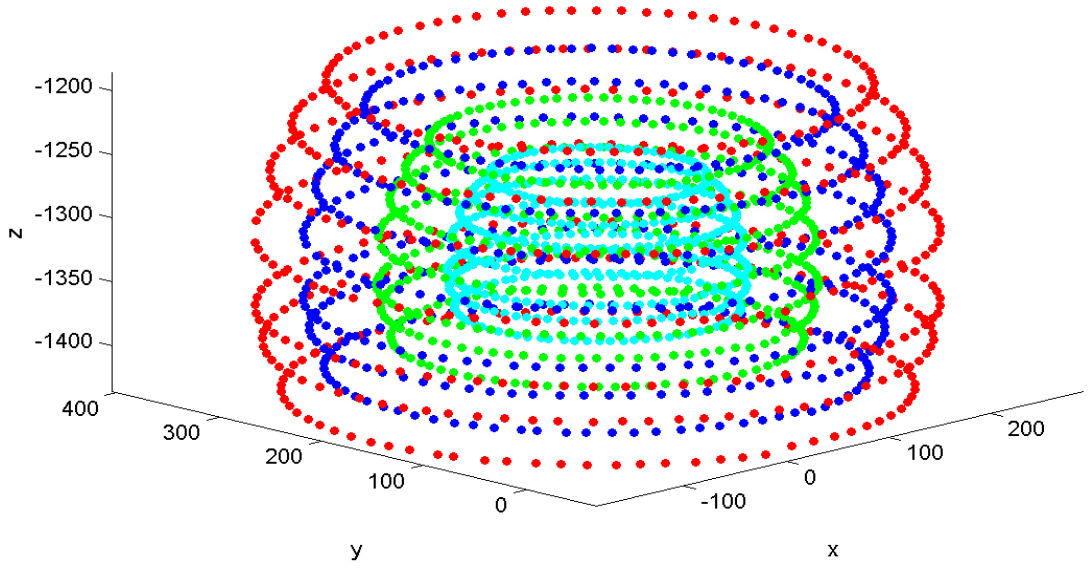

Figure A- 2: Markers locations of the V-shaped passive tool.

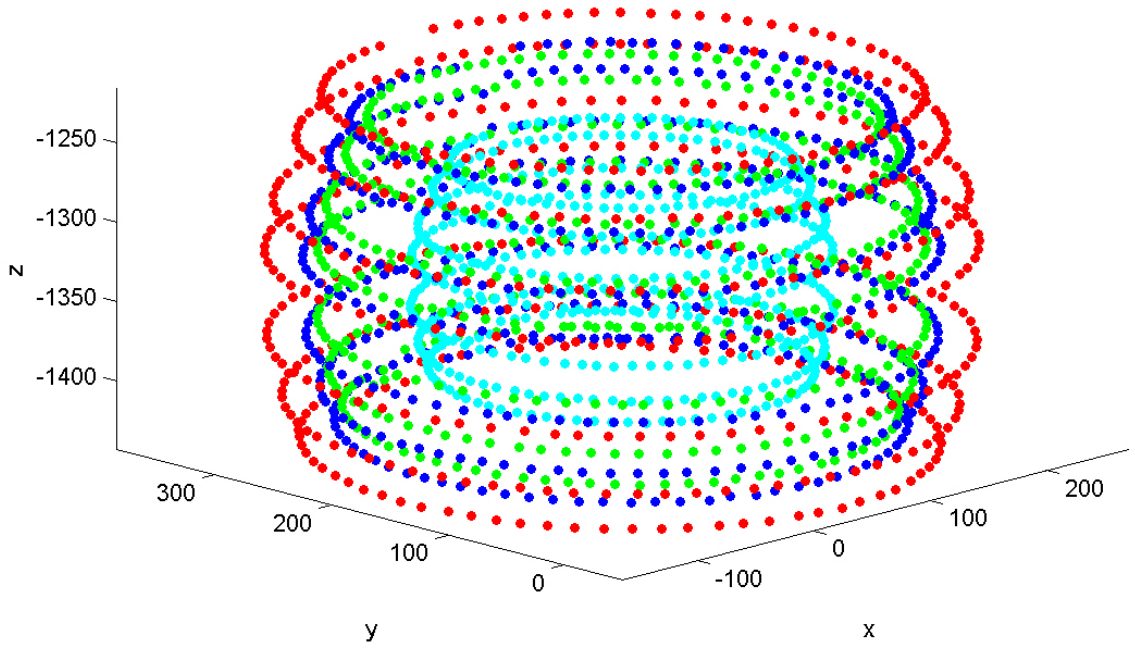

Figure A- 3: Markers locations of the T-shaped radix tool.

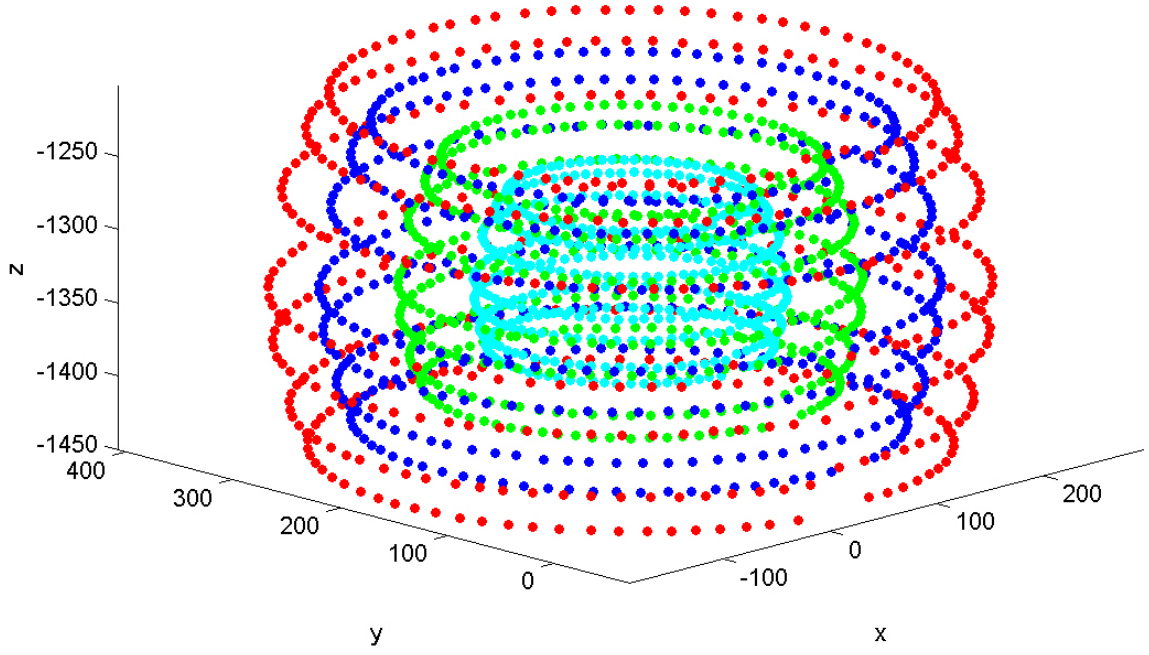

Figure A- 4: Markers locations of the V-shaped radix tool.

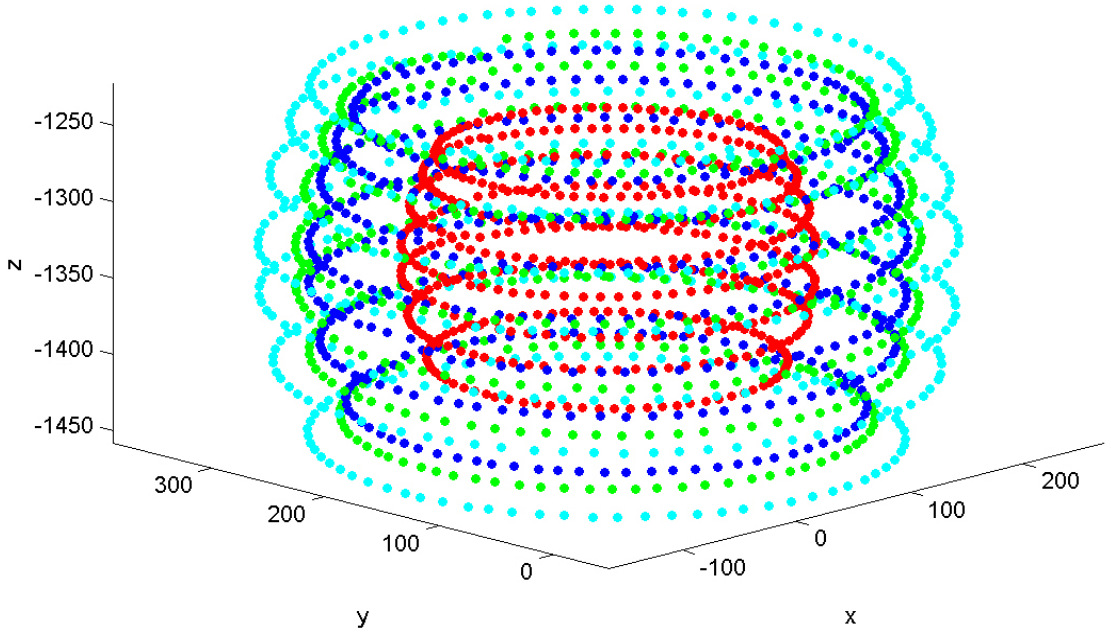

Figure A- 5: Markers locations of the T-shaped active tool.

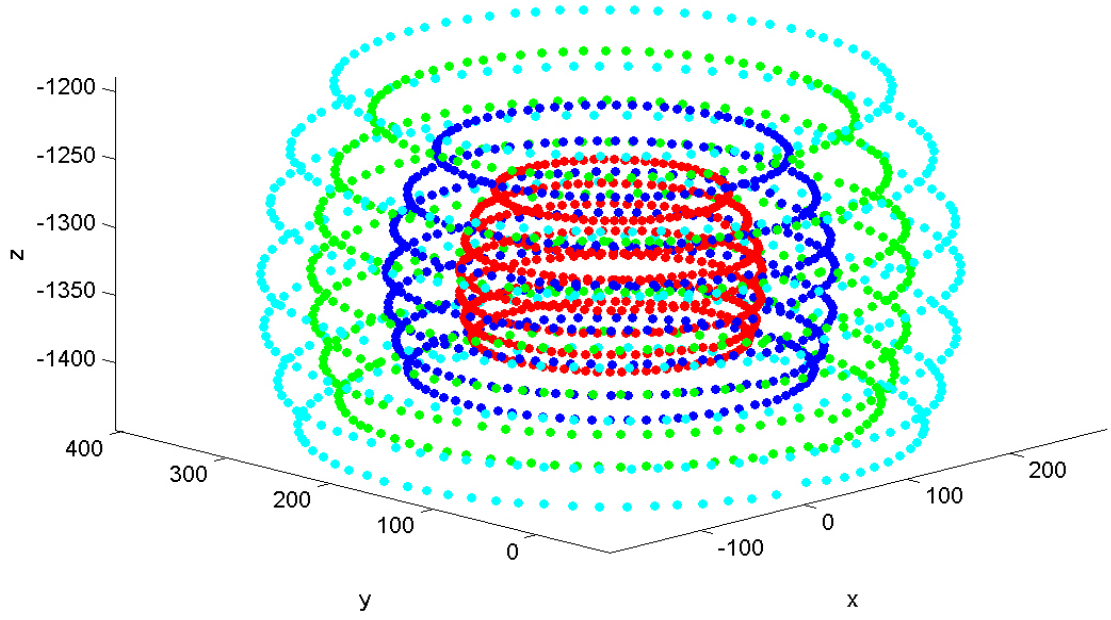

Figure A- 6: Markers locations of the V-shaped active tool.

A.1.2 Target Location Plots

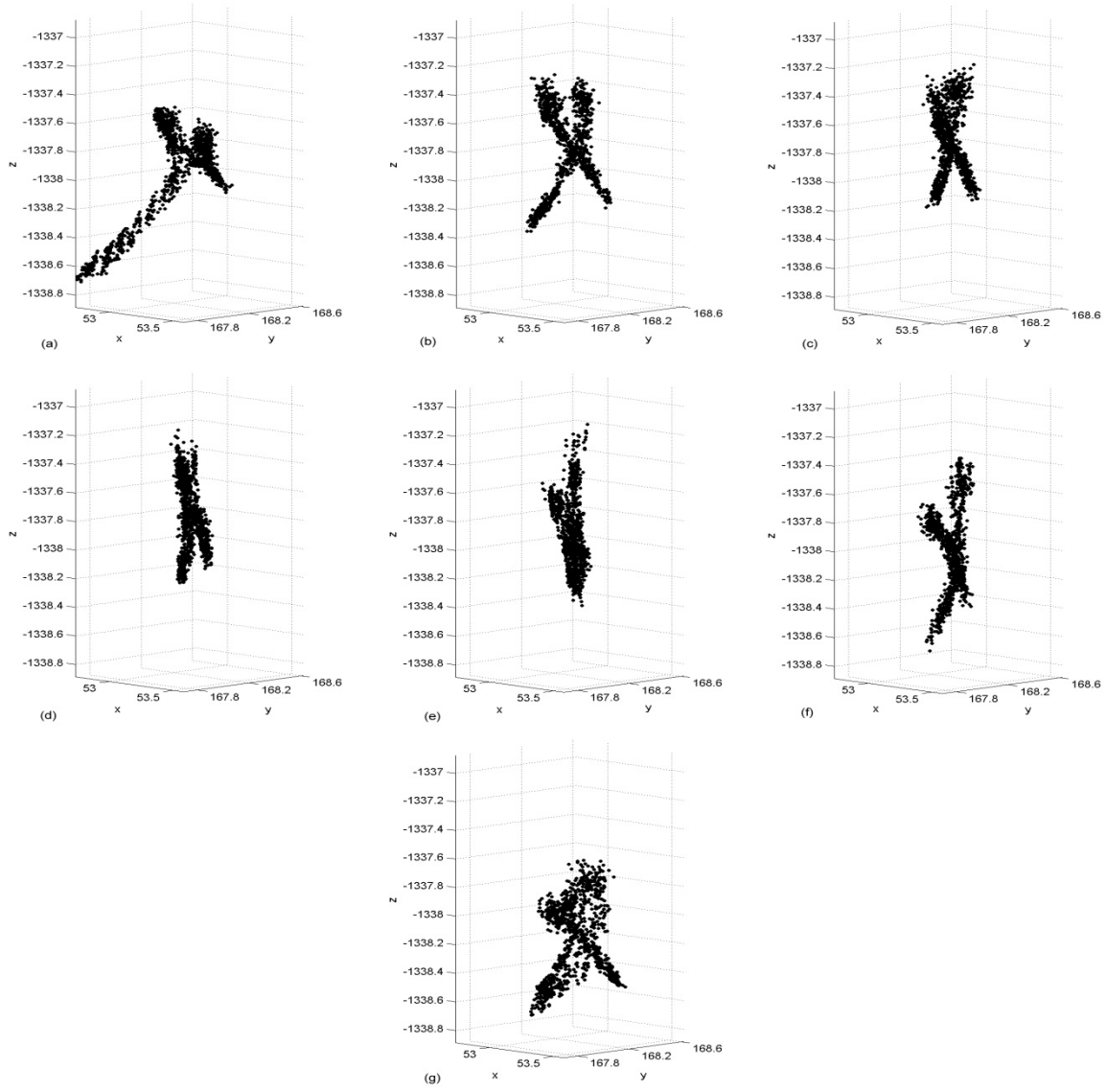

Figure A- 7: Calculated target locations of the T-shaped passive tool for each tool orientation. (a) -30º tilt angle. (b) -20º tilt angle. (c) -10º tilt angle. (d) 0º tilt angle. (e) 10º tilt angle. (f) 20º tilt angle. (g) 30º tilt angle.

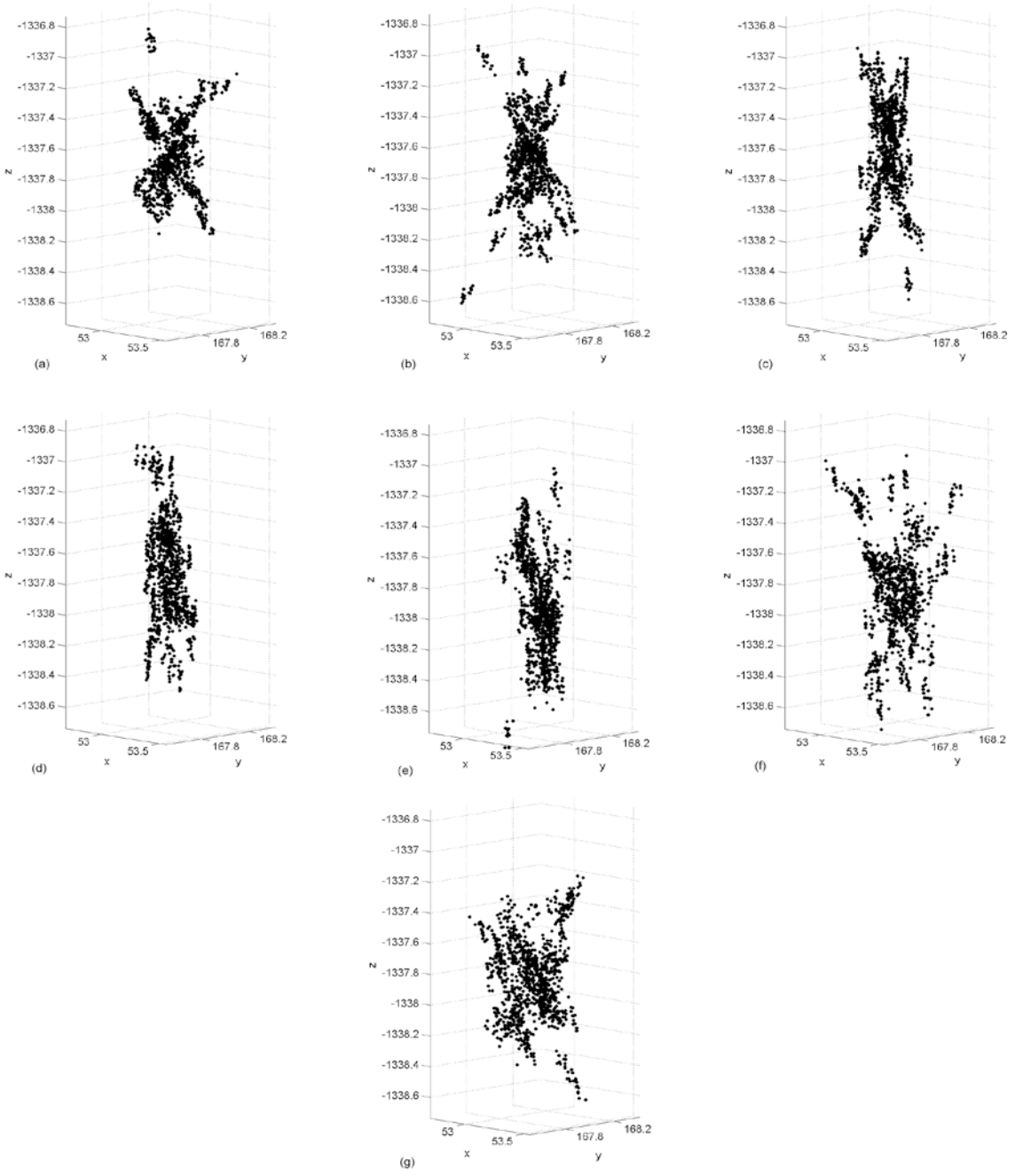

Figure A- 8: Calculated target locations of the T-shaped radix tool for each tool orientation. (a) -30º tilt angle. (b) -20º tilt angle. (c) -10º tilt angle. (d) 0º tilt angle. (e) 10º tilt angle. (f) 20º tilt angle. (g) 30º tilt angle.

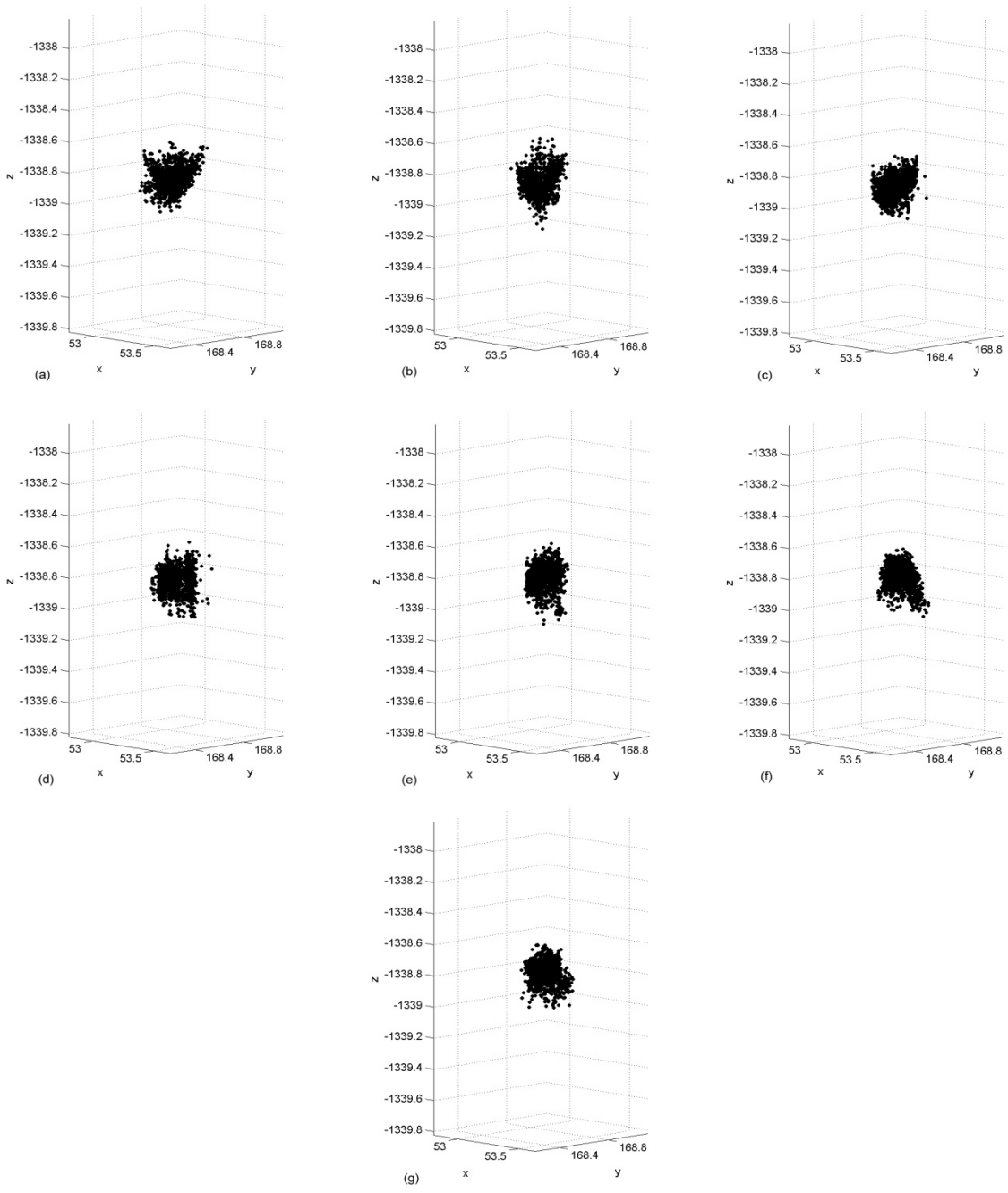

Figure A- 9: Calculated target locations of the T-shaped active tool for each tool orientation. (a) -30º tilt angle. (b) -20º tilt angle. (c) -10º tilt angle. (d) 0º tilt angle. (e) 10º tilt angle. (f) 20º tilt angle. (g) 30º tilt angle.

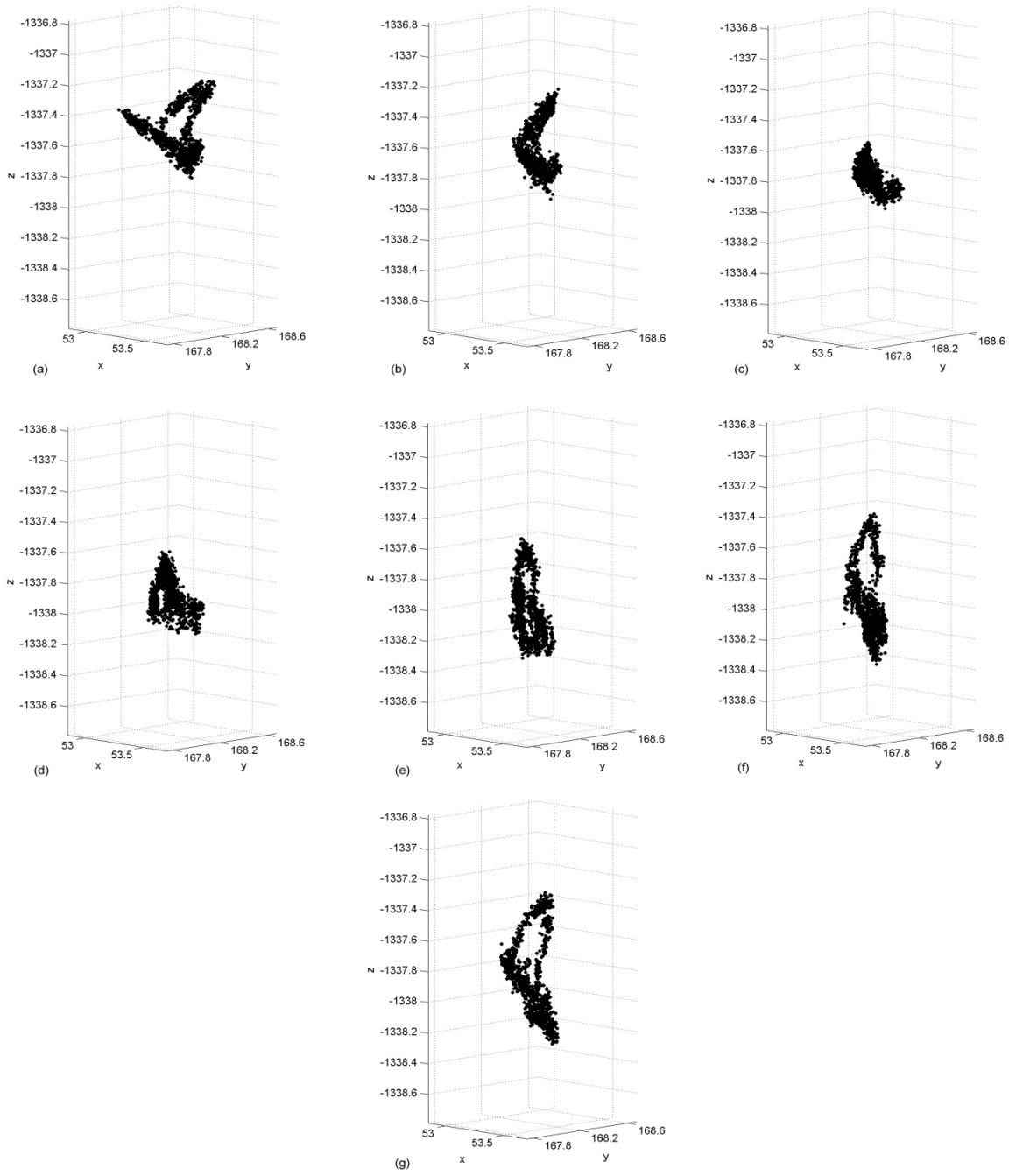

Figure A- 10: Calculated target locations of the V-shaped passive tool for each tool orientation. (a) -30º tilt angle. (b) -20º tilt angle. (c) -10º tilt angle. (d) 0º tilt angle. (e) 10º tilt angle. (f) 20º tilt angle. (g) 30º tilt angle.

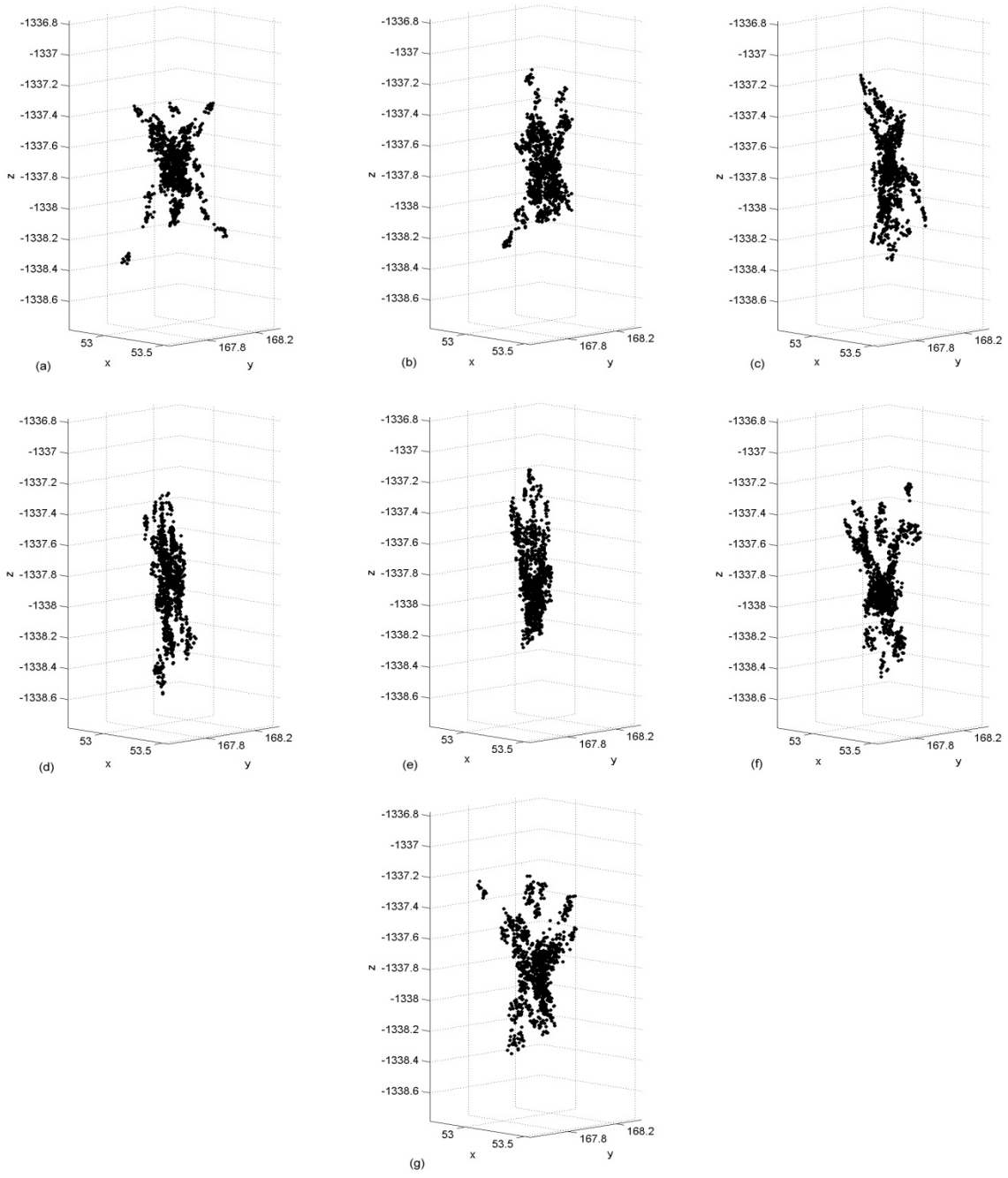

Figure A- 11: Calculated target locations of the V-shaped radix tool for each tool orientation. (a) -30º tilt angle. (b) -20º tilt angle. (c) -10º tilt angle. (d) 0º tilt angle. (e) 10º tilt angle. (f) 20º tilt angle. (g) 30º tilt angle.

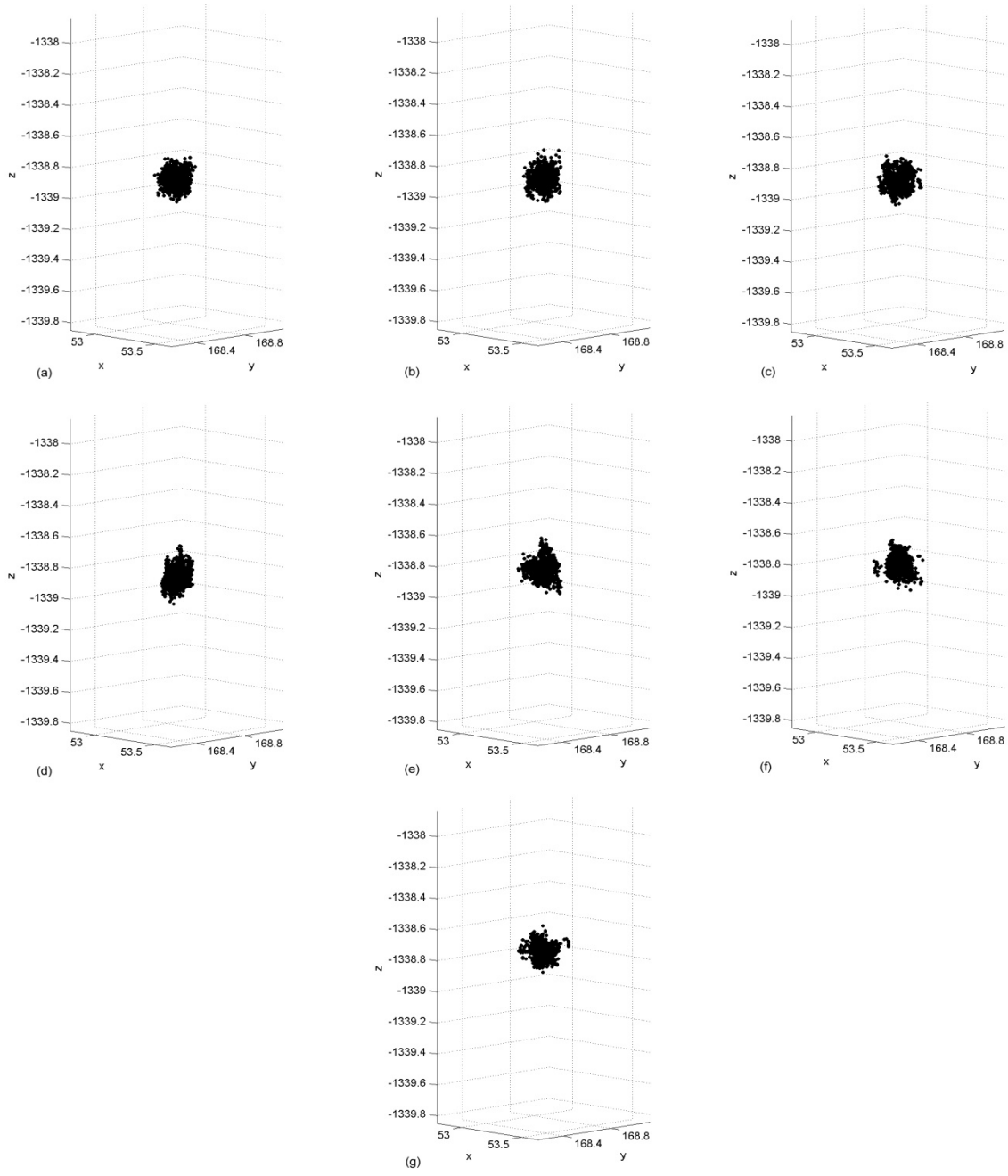

Figure A- 12: Calculated target locations of the V-shaped active tool for each tool orientation. (a) -30º tilt angle. (b) -20º tilt angle. (c) -10º tilt angle. (d) 0º tilt angle. (e) 10º tilt angle. (f) 20º tilt angle. (g) 30º tilt angle.

A.1.3 Root-Mean-Squared TRE

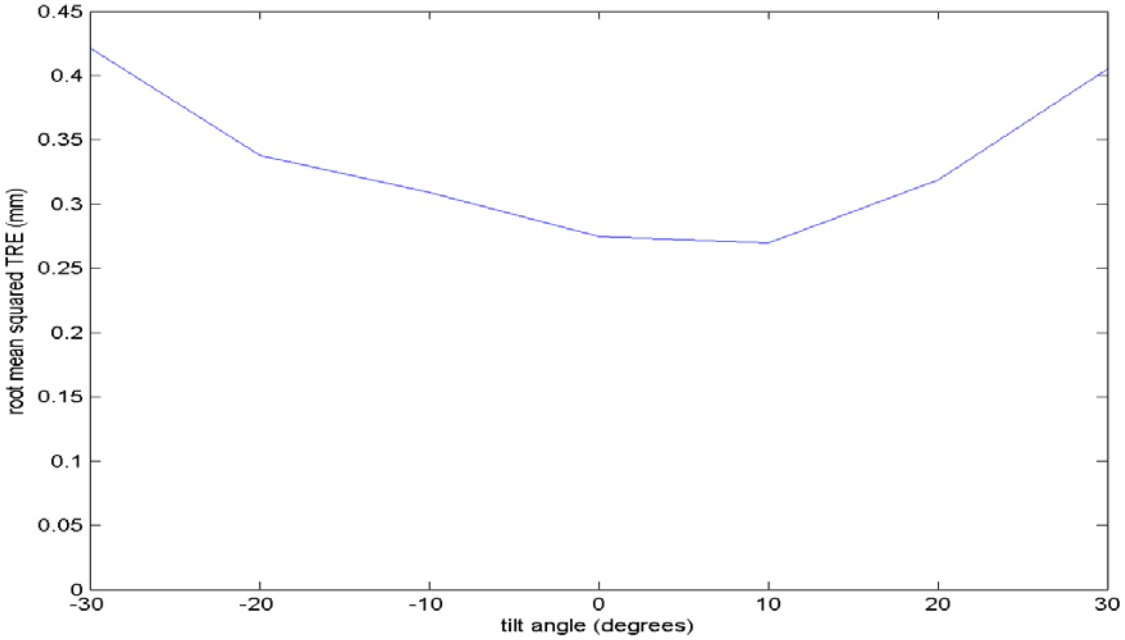

Figure A- 13: RMS TRE versus tilt angle for the T-shaped passive tool.

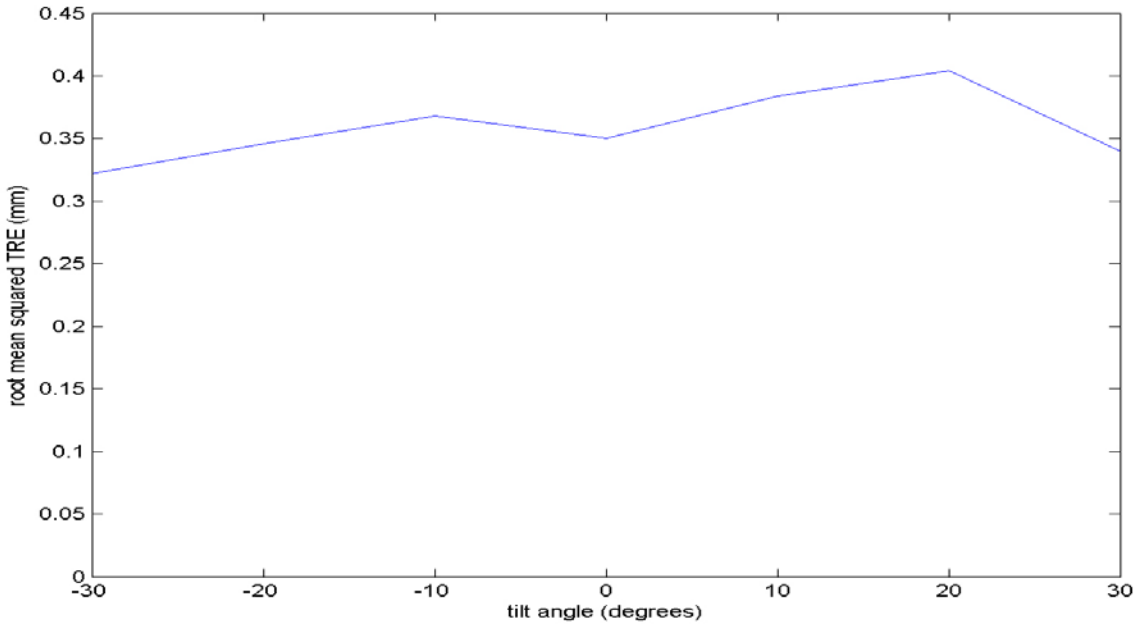

Figure A- 14: RMS TRE versus tilt angle for the T-shaped radix tool.

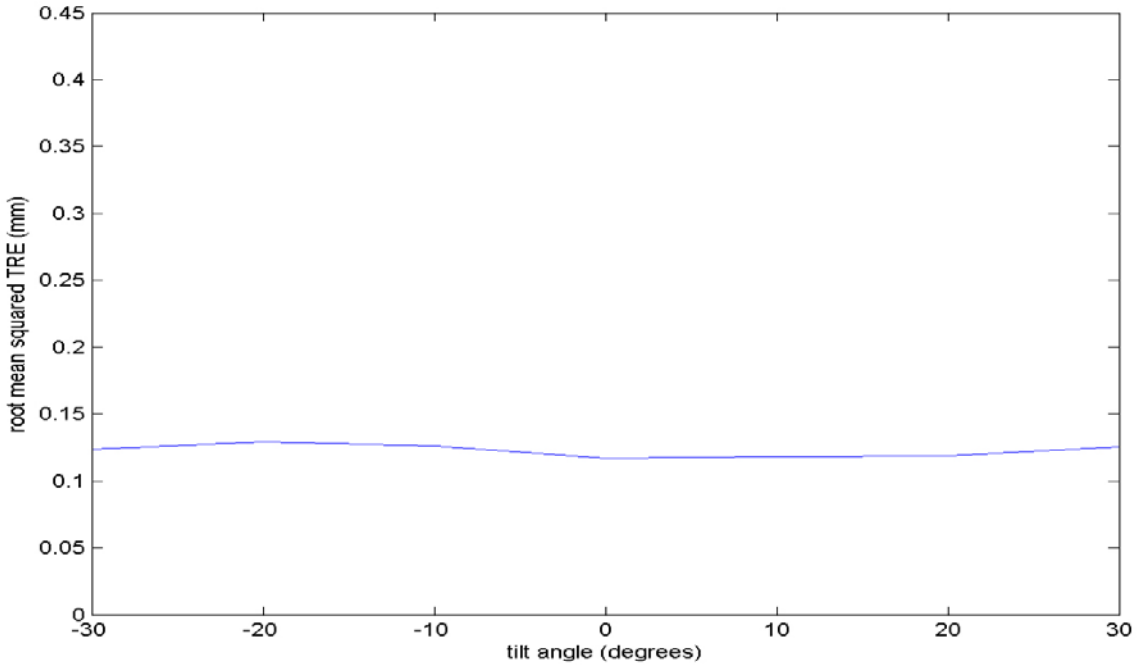

Figure A- 15: RMS TRE versus tilt angle for the T-shaped active tool.

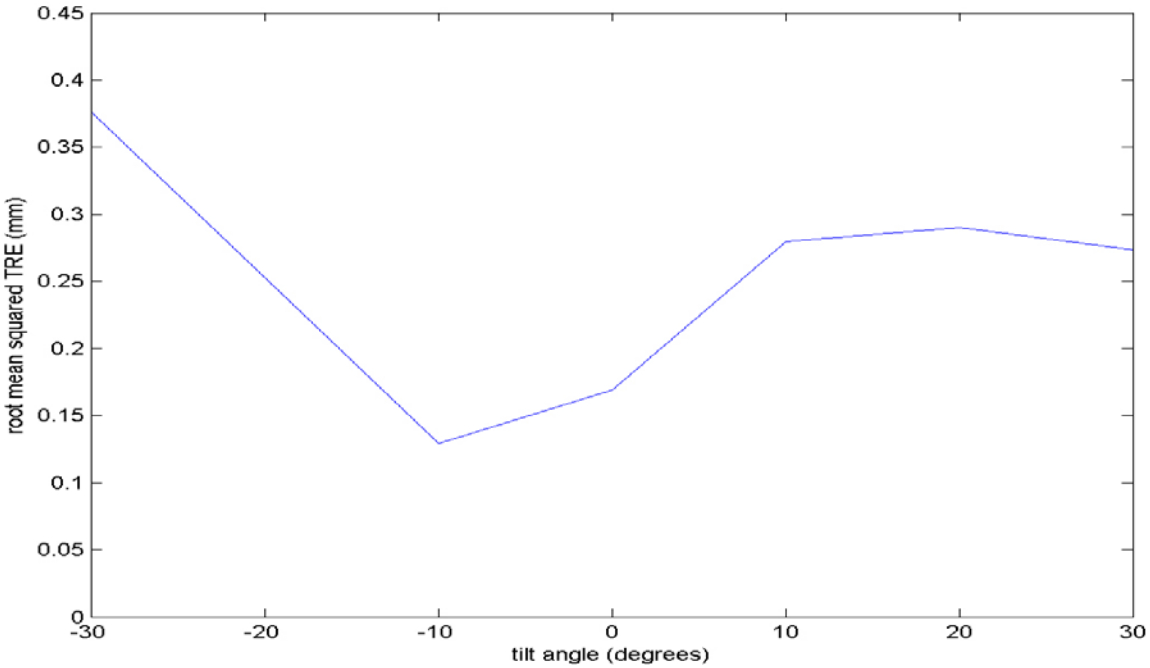

Figure A- 16: RMS TRE versus tilt angle for the V-shaped passive tool.

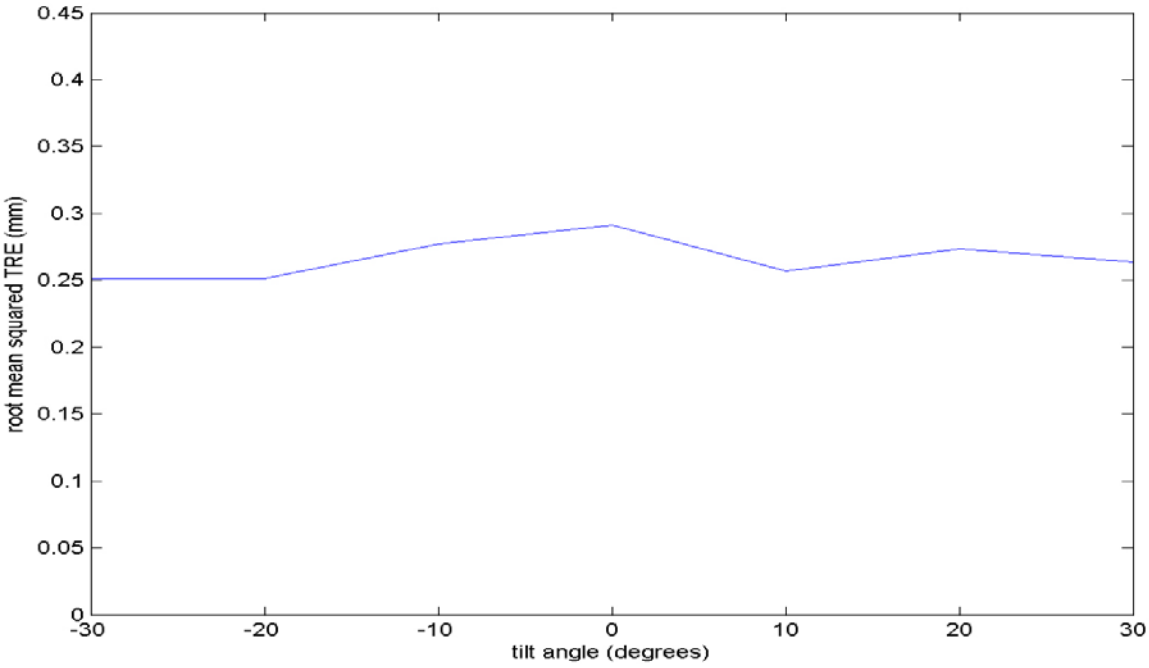

Figure A- 17: RMS TRE versus tilt angle for the V-shaped radix tool.

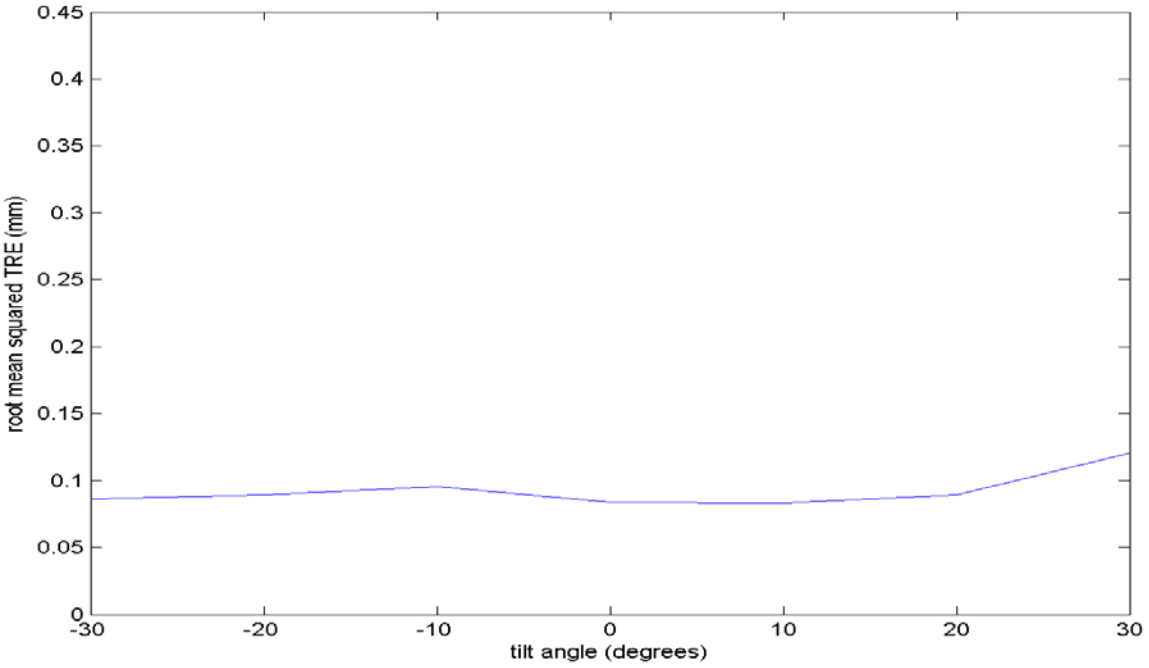

Figure A- 18: RMS TRE versus tilt angle for the V-shaped active tool.

A.2 Results of Right Position Experiments

A.2.1 Marker Locations Plots

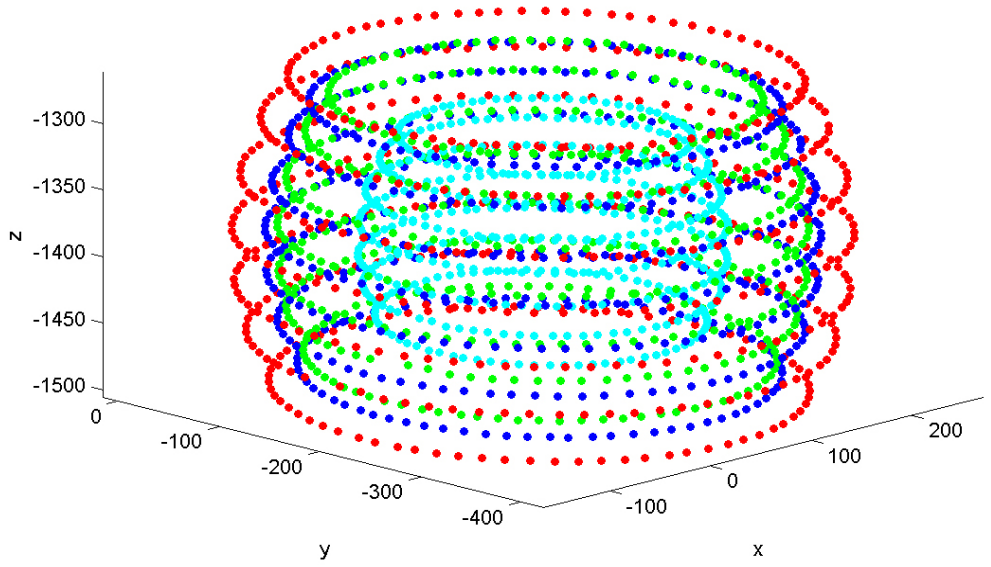

Figure A- 19: Markers locations of the T-shaped passive tool.

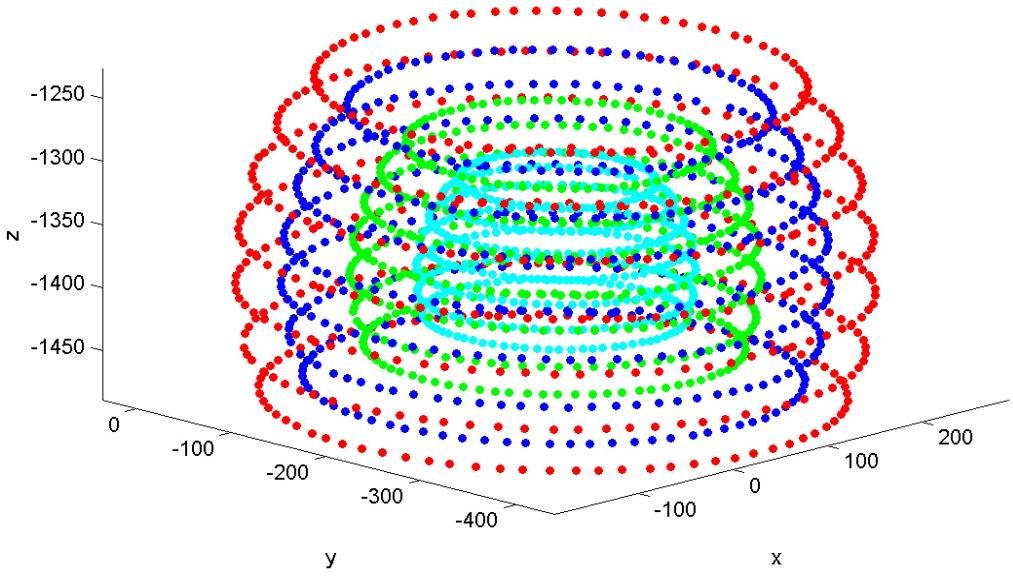

Figure A- 20: Markers locations of the V-shaped passive tool.

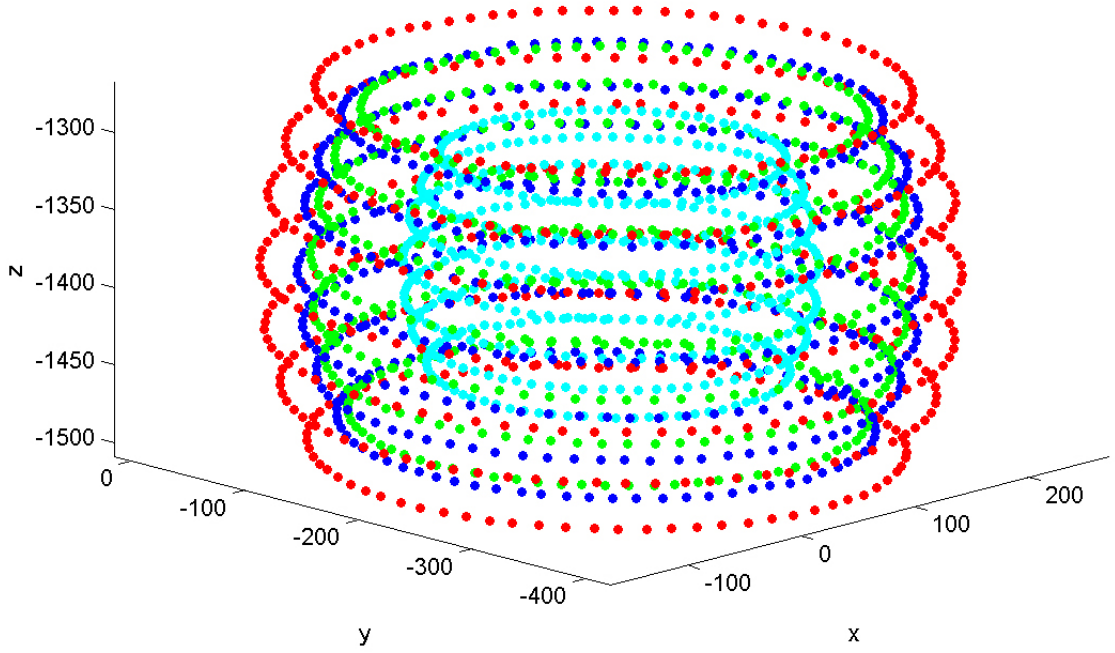

Figure A- 21: Markers locations of the T-shaped radix tool.

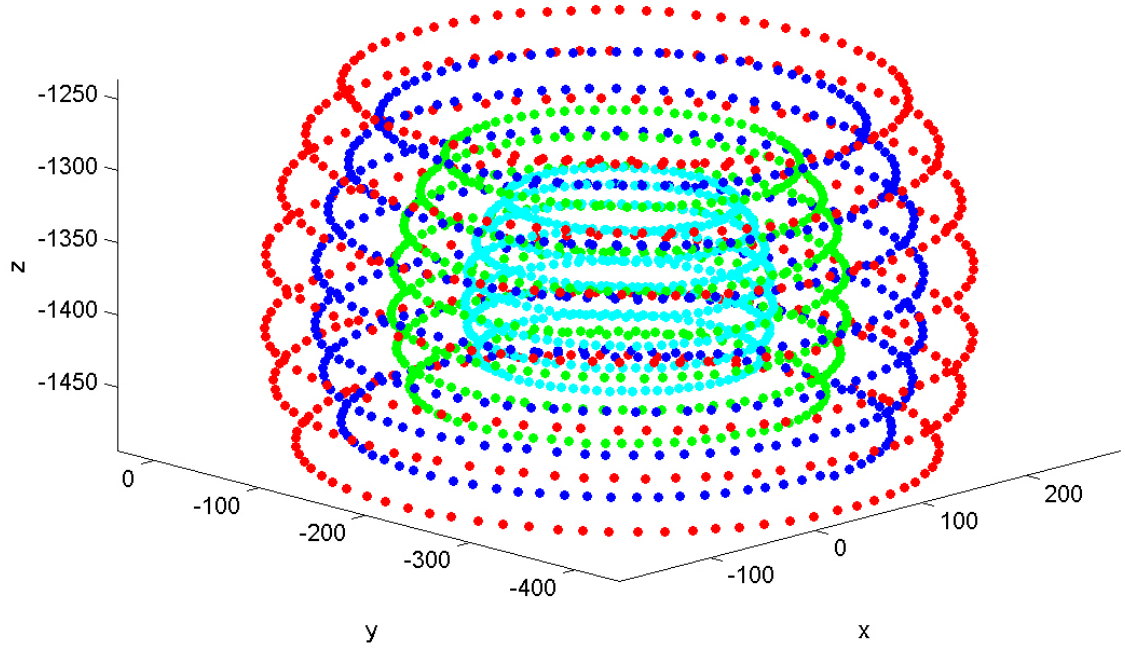

Figure A- 22: Markers locations of the V-shaped radix tool.

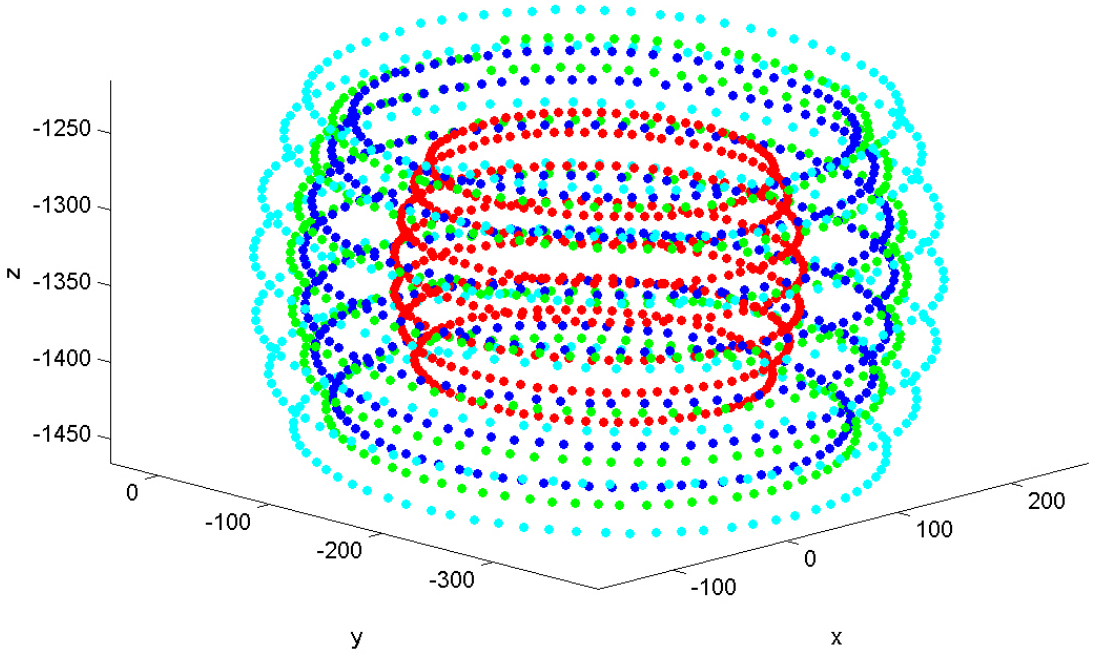

Figure A- 23: Markers locations of the T-shaped active tool.

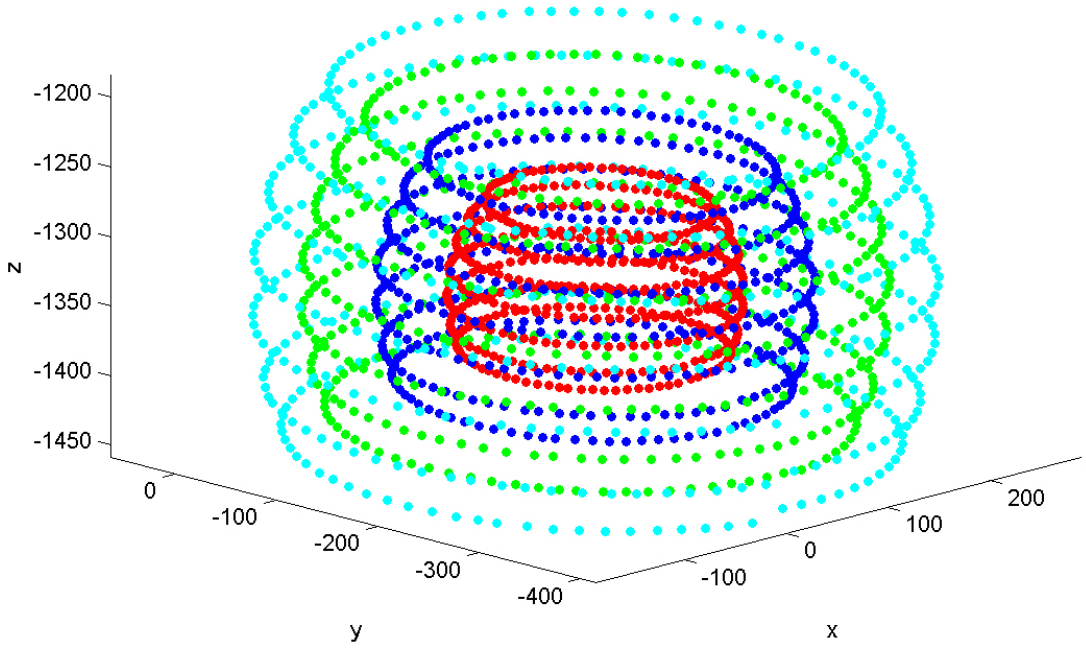

Figure A- 24: Markers locations of the V-shaped active tool.

A.2.2 Target Location Plots

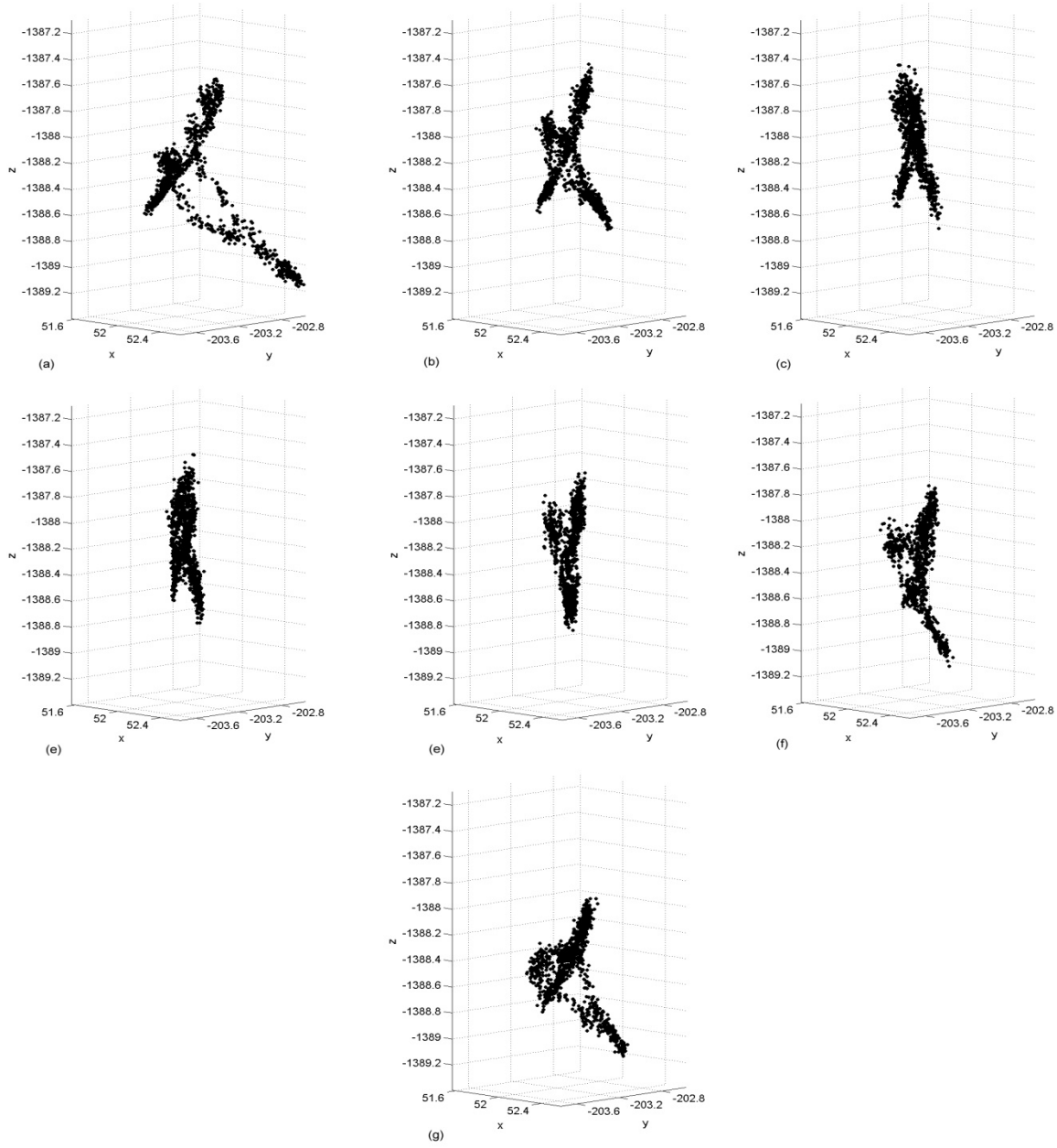

Figure A- 25: Calculated target locations of the T-shaped passive tool for each tool orientation. (a) -30º tilt angle. (b) -20º tilt angle. (c) -10º tilt angle. (d) 0º tilt angle. (e) 10º tilt angle. (f) 20º tilt angle. (g) 30º tilt angle.

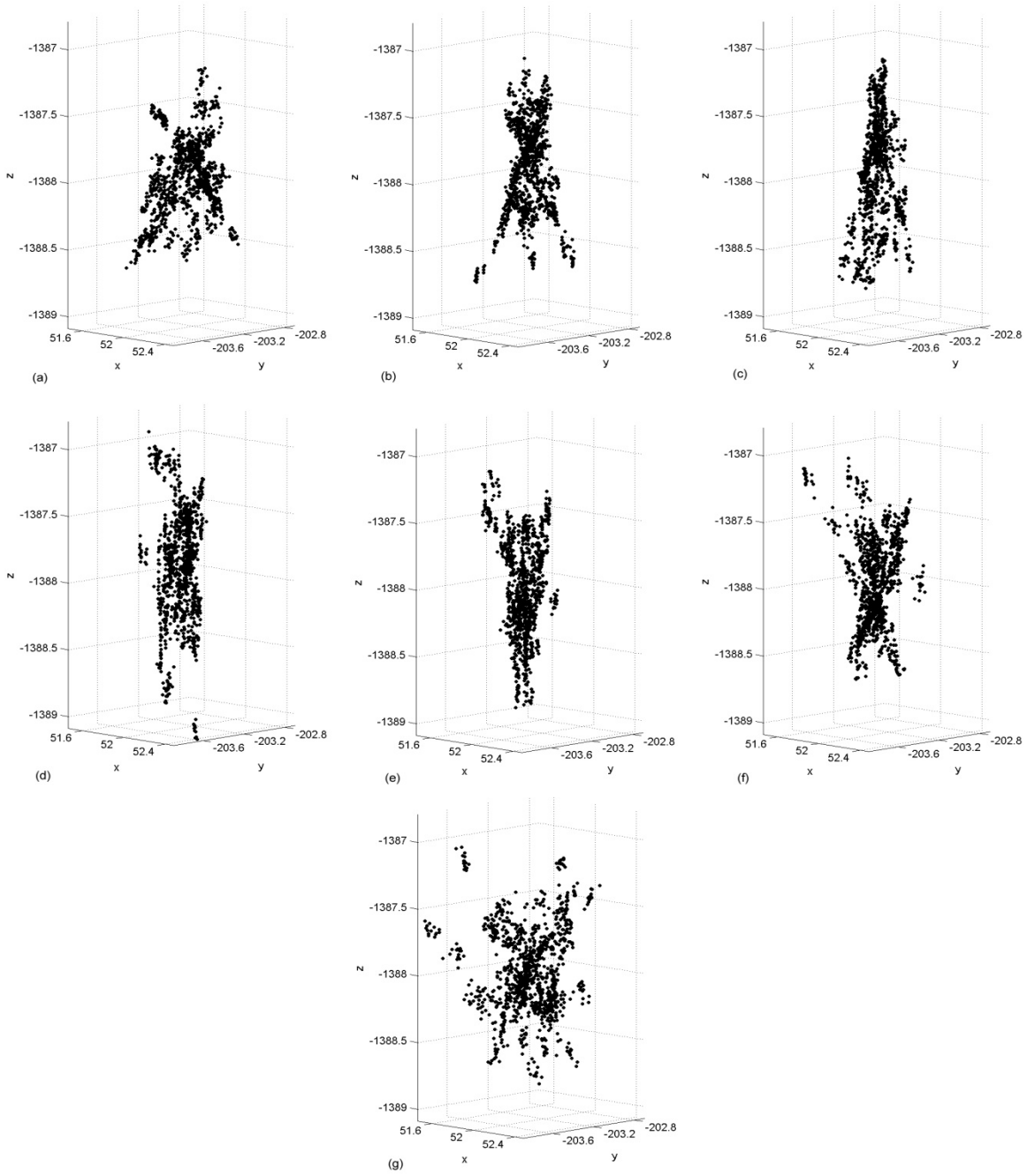

Figure A- 26: Calculated target locations of the T-shaped radix tool for each tool orientation. (a) -30º tilt angle. (b) -20º tilt angle. (c) -10º tilt angle. (d) 0º tilt angle. (e) 10º tilt angle. (f) 20º tilt angle. (g) 30º tilt angle.

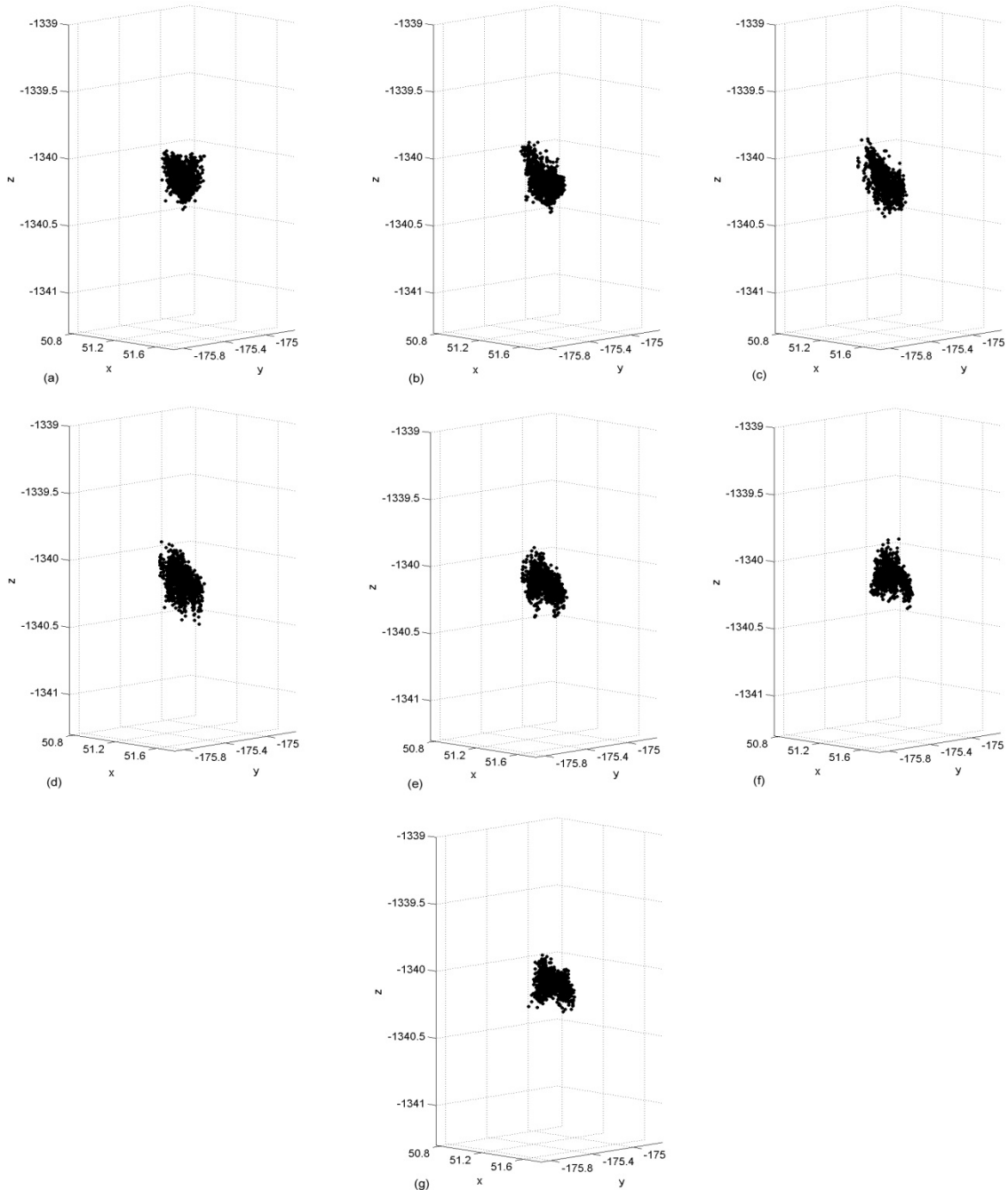

Figure A- 27: Calculated target locations of the T-shaped active tool for each tool orientation. (a) -30º tilt angle. (b) -20º tilt angle. (c) -10º tilt angle. (d) 0º tilt angle. (e) 10º tilt angle. (f) 20º tilt angle. (g) 30º tilt angle.

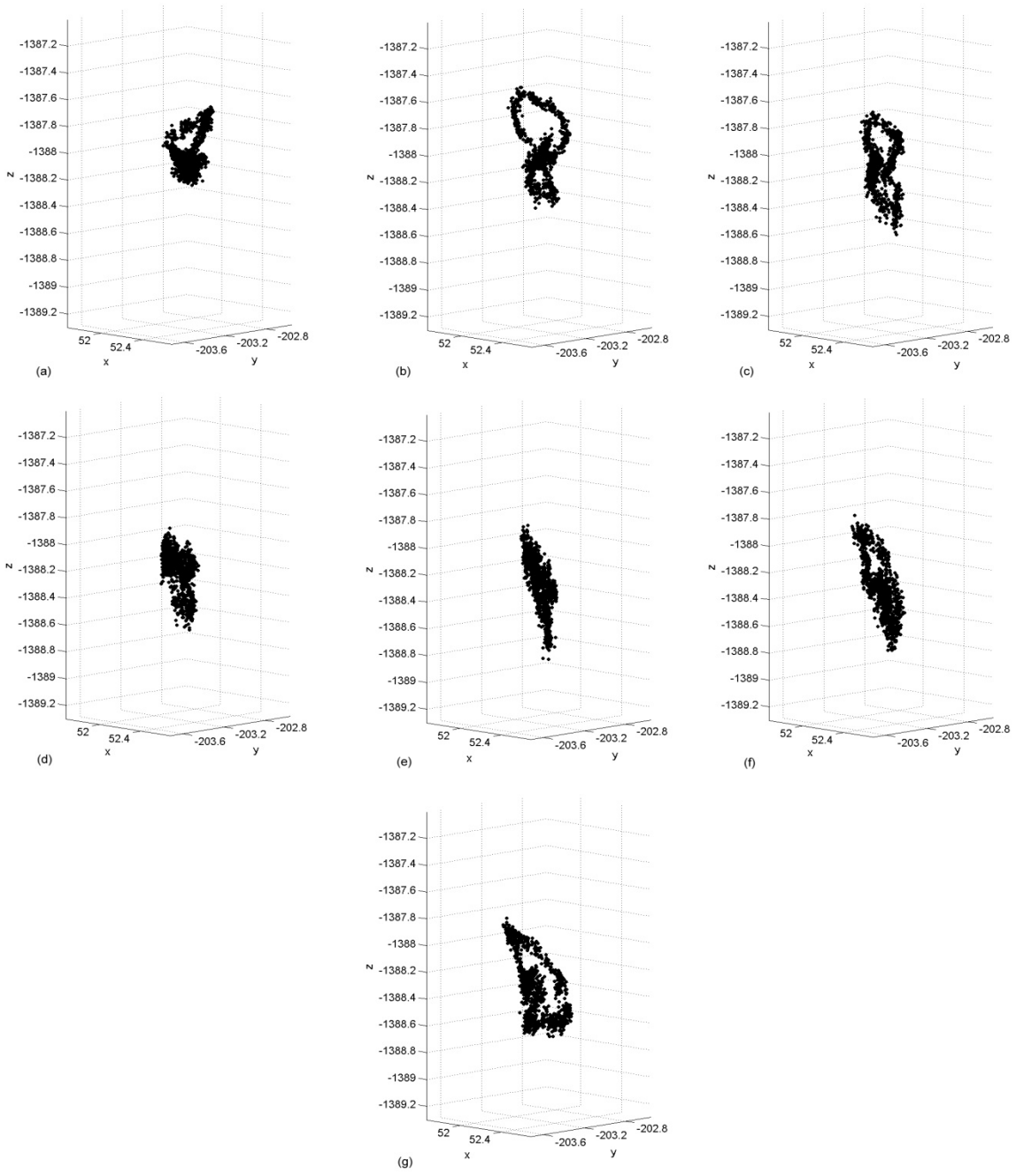

Figure A- 28: Calculated target locations of the V-shaped passive tool for each tool orientation. (a) -30º tilt angle. (b) -20º tilt angle. (c) -10º tilt angle. (d) 0º tilt angle. (e) 10º tilt angle. (f) 20º tilt angle. (g) 30º tilt angle.

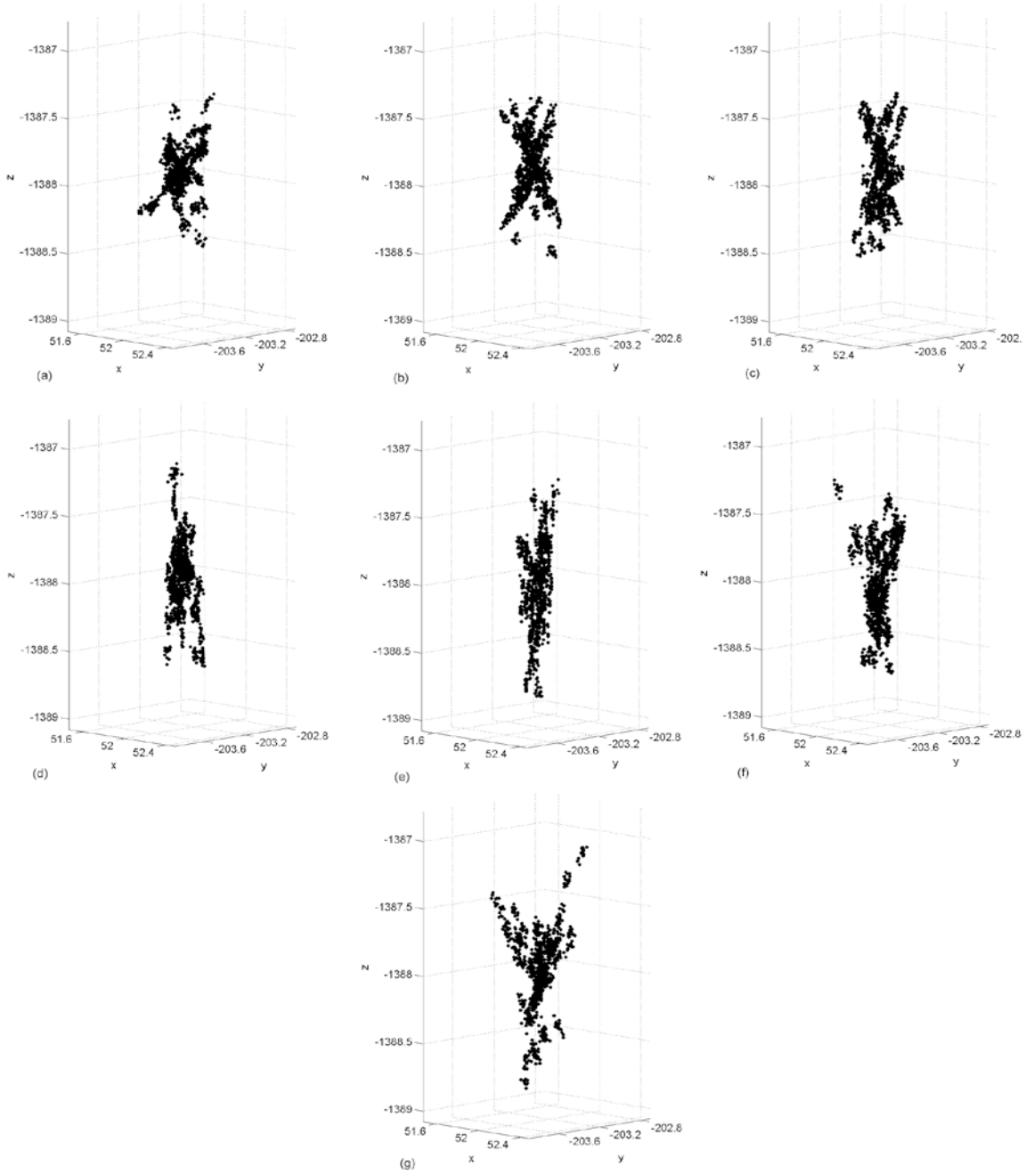

Figure A- 29: Calculated target locations of the V-shaped radix tool for each tool orientation. (a) -30º tilt angle. (b) -20º tilt angle. (c) -10º tilt angle. (d) 0º tilt angle. (e) 10º tilt angle. (f) 20º tilt angle. (g) 30º tilt angle.

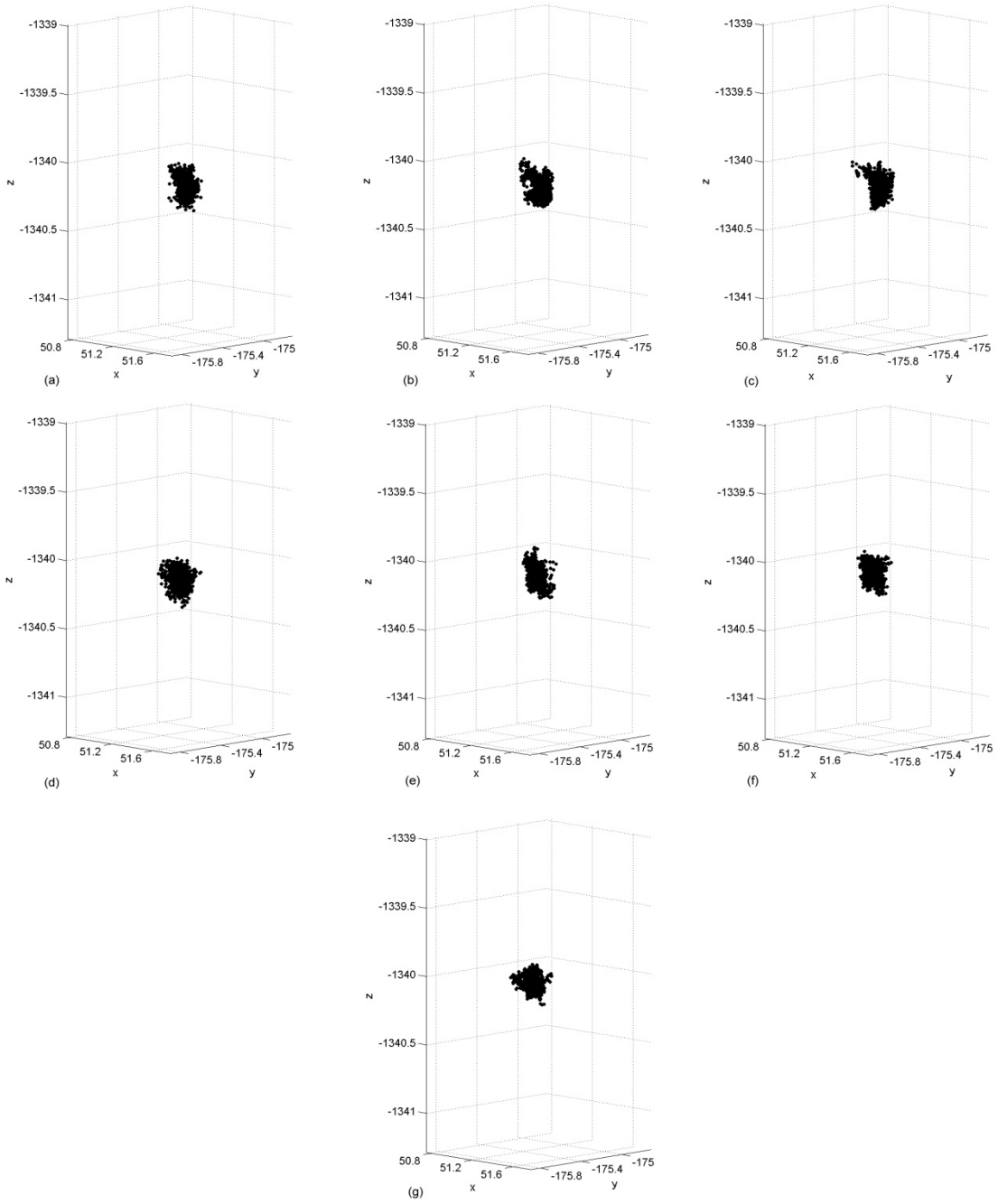

Figure A- 30: Calculated target locations of the V-shaped active tool for each tool orientation. (a) -30º tilt angle. (b) -20º tilt angle. (c) -10º tilt angle. (d) 0º tilt angle. (e) 10º tilt angle. (f) 20º tilt angle. (g) 30º tilt angle.

A.2.3 Root-Mean-Squared TRE

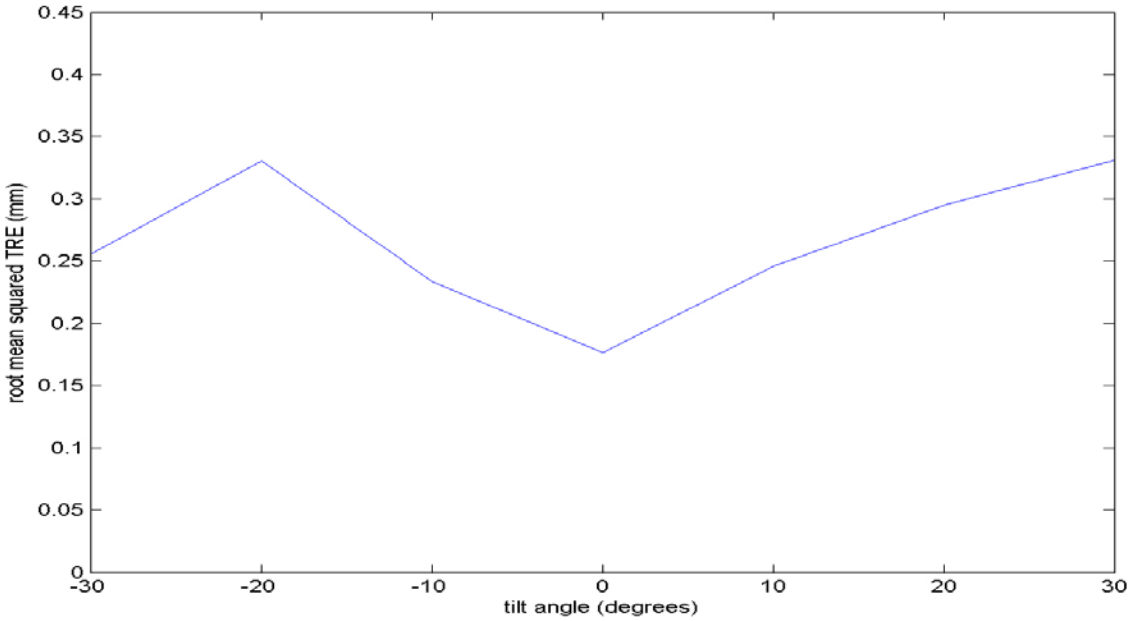

Figure A- 31: RMS TRE versus tilt angle for the T-shaped passive tool.

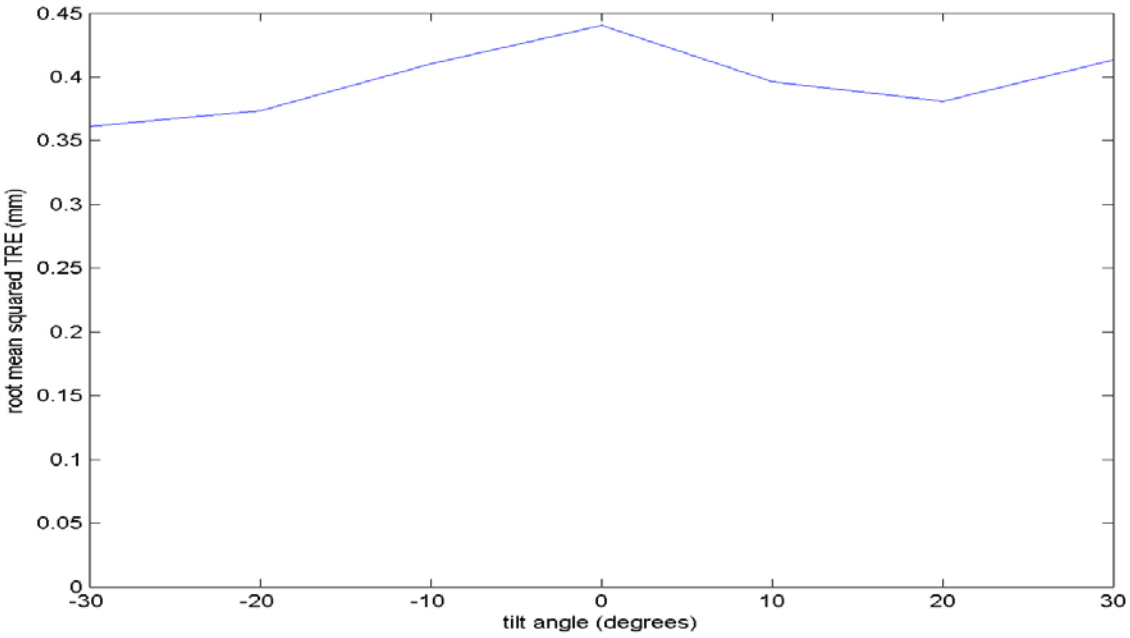

Figure A- 32: RMS TRE versus tilt angle for the T-shaped radix tool.

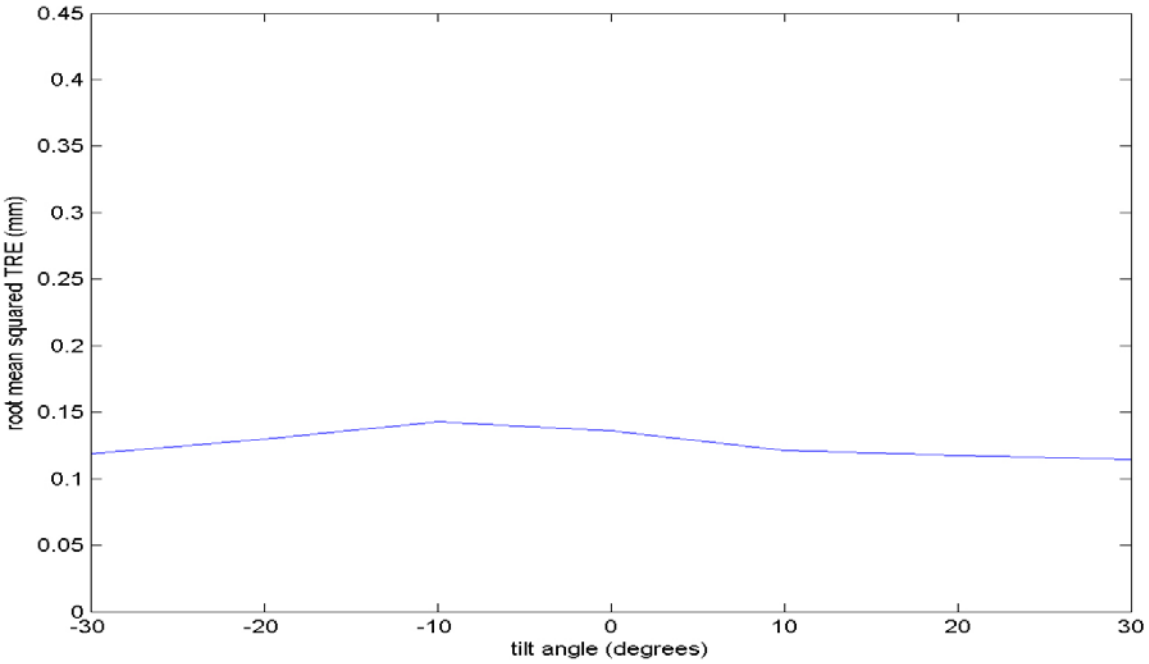

Figure A- 33: RMS TRE versus tilt angle for the T-shaped active tool.

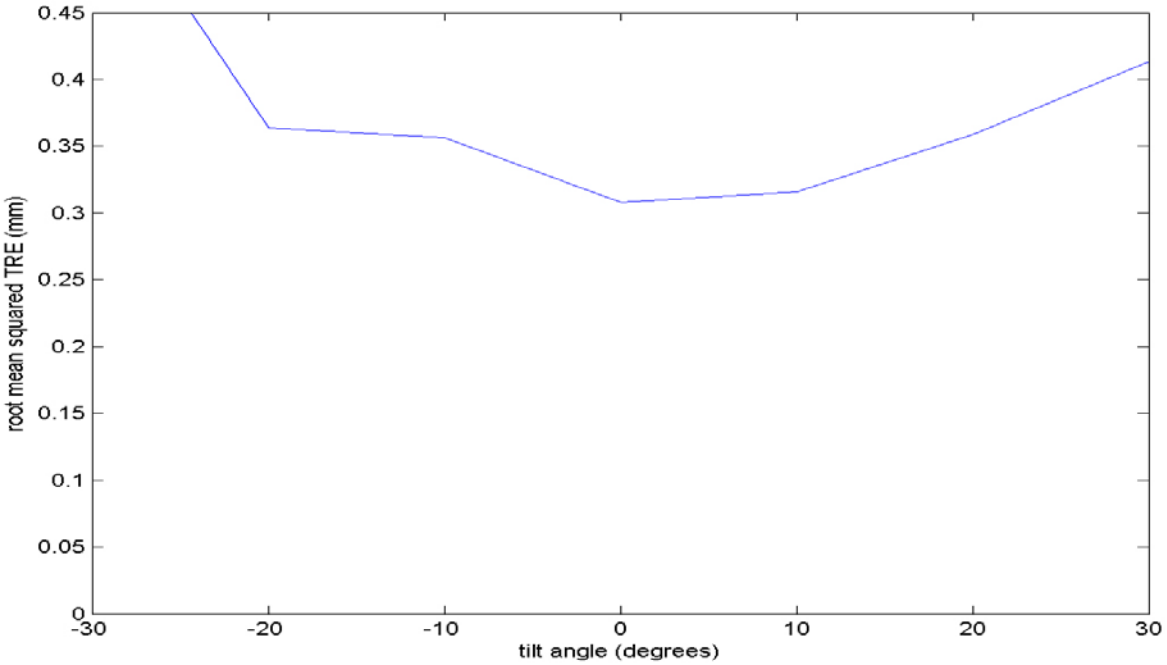

Figure A- 34: RMS TRE versus tilt angle for the V-shaped passive tool.

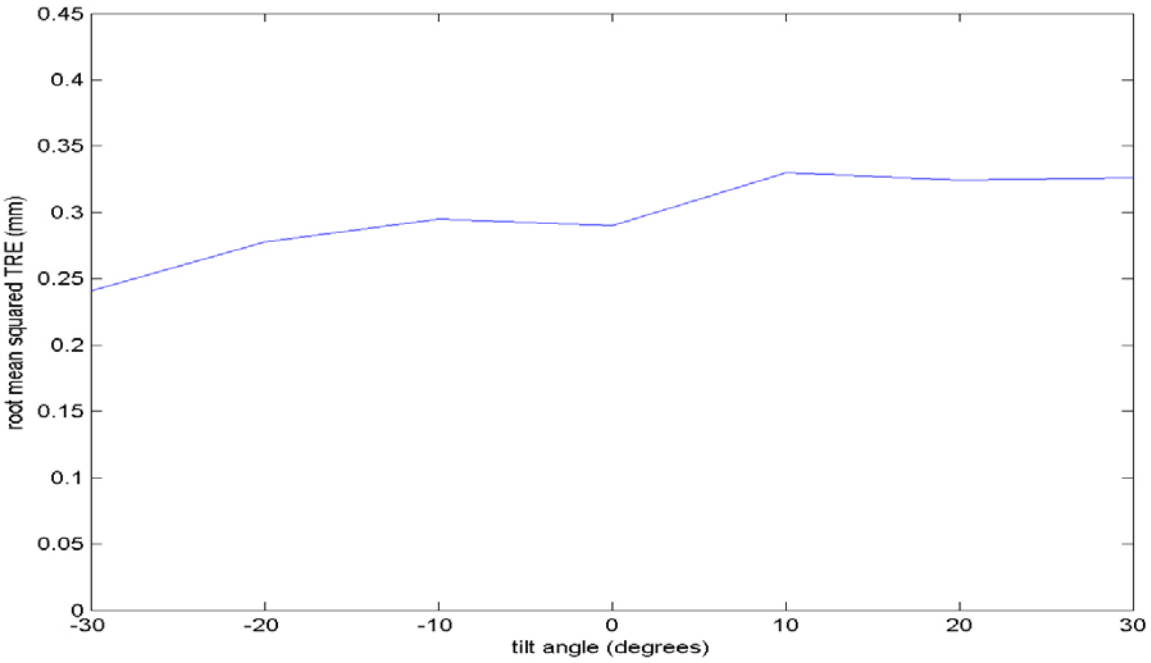

Figure A- 35: RMS TRE versus tilt angle for the V-shaped radix tool.

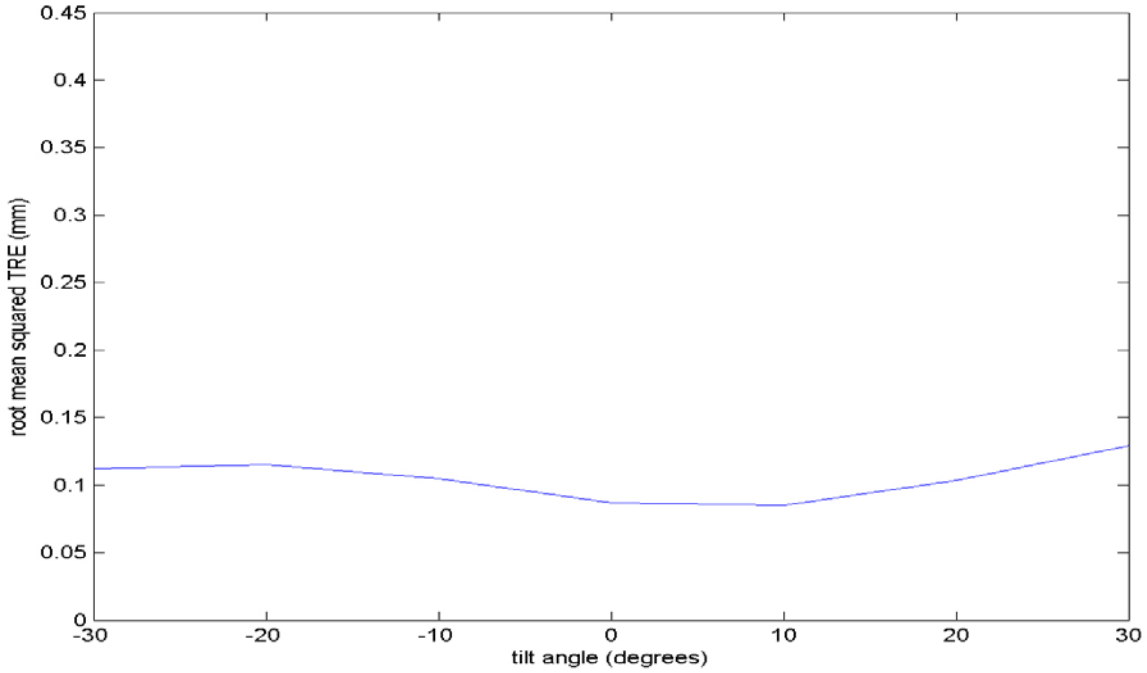

Figure A- 36: RMS TRE versus tilt angle for the V-shaped active tool.

A.3 Results of Hybrid Configuration Experiment

A.2.4 Marker Locations Plots

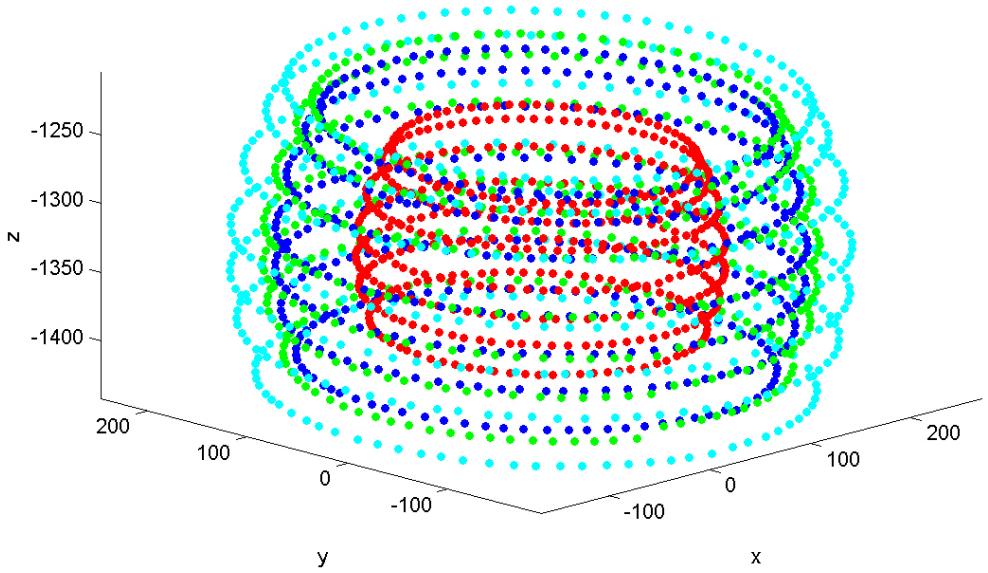

Figure A- 37: Markers locations of the T-shaped active tool.

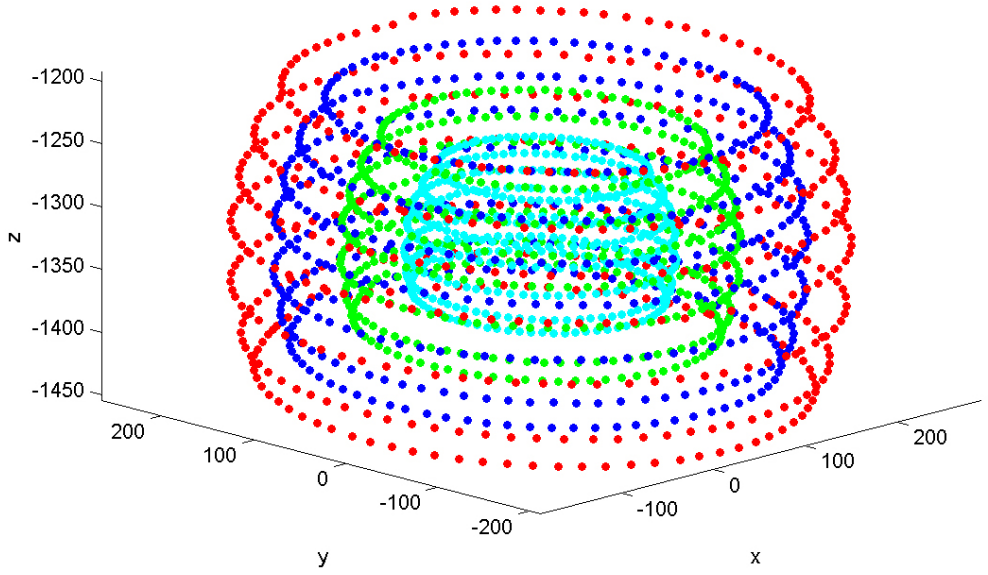

Figure A- 38: Markers locations of the V-shaped passive tool.

Glossary

Active marker: An infrared light emitting diode (IRED) that is mounted on a ceramic base.

CT (Computer Tomography): A type of medical imaging that uses computer-processed x-rays to produce three-dimensional images of an internal structure of the body.

Fiducial marker or **Fiducial:** An object placed in the field of view of an optical tracking system which appears in the image produced, for use as a point of reference or a measure.

FRE (Fiducial Registration Error): the root-mean-squared distance between the measured position of a fiducial marker in one coordinate system and its corresponding position in the other system after the registration process.

FLE (Fiducial Localization Error): The distance between the true position of a fiducial marker and its measured position.

Passive marker: A sphere with a retro-reflective coating that reflects IR.

Radix marker: A lens with a retro-reflective coating, which reflects IR, on the back and a plastic surface on the front.

RMS (Root-Mean-Squared): The square root of the arithmetic mean of the squares.

TRE (Target Registration Error): The distance between corresponding points other than fiducial points after registration.